VARIABLE-COMPLEXITY RESPONSE SURFACE APPROXIMATIONS FOR AERODYNAMIC PARAMETERS IN HSCT OPTIMIZATION

By

Oleg B. Golovidov

a thesis submitted to the faculty of

virginia polytechnic institute and state university

in partial fulfillment of the requirements for the degree of

master of science

in

Aerospace Engineering

William H. Mason, Chairman

Bernard Grossman

Layne T. Watson

June 1997

Blacksburg, Virginia

VARIABLE-COMPLEXITY RESPONSE SURFACE APPROXIMATIONS
FOR AERODYNAMIC PARAMETERS IN HSCT OPTIMIZATION

by

Oleg B. Golovidov

Committee Chair: William H. Mason
Aerospace Engineering

(ABSTRACT)

A procedure for generating and using polynomial approximations to the range or to the cruise drag components in terms of 29 design variables for the High Speed Civil Transport (HSCT) configuration and performance design is presented. Response surface model methodology is used to fit quadratic polynomials to data gathered from a series of numerical analyses of different HSCT designs. Several techniques are employed to minimize the number of required analyses and to maintain accuracy. Approximate analysis techniques are used to find regions of the design space where reasonable HSCT designs could occur and response surface models are built using higher fidelity analysis results of the designs in this "reasonable" region. Regression analysis and analysis of variance are then used to reduce the number of polynomial terms in the response surface model functions. Optimizations of the HSCT are then carried out both with and without the response surface models, and the effect of the use of the response surface models is discussed. Results of the work showed that considerable reduction of the amount of numerical noise in optimization is achieved with response surface models and the convergence rate was slightly improved. Careful attention was required to keep the accuracy of the models at an acceptable level.

Acknowledgements

This work has been supported by NASA Grant NAG1-1160 with Mr. P. Coen as contract monitor.

I want to thank my advisor, Dr. William H. Mason, for helping me and guiding my work. I would like also to thank Dr. Bernard Grossman, Dr. Raphael T. Haftka, and Dr. Layne Watson for their support and help during our weekly project meetings.

While working on my research, I received a significant amount of help from other graduate students. In particular, a big thanks goes to Anthony Giunta, Vladimir Balabanov, and Duane Knill.

Contents

List of Tables

List of Figures

List of Symbols

$C_{D_{fric}}$	friction drag coefficient
$C_{D_{wave}}$	wave drag cofficient
C_{L_α}	lift curve slope
C_L	lift coefficient
C_T	leading edge suction coefficient
C_T/C_L^2	leading edge suction term
LES_{att}	attainable leading edge suction parameter
$\mathbf{X}$	least squares matrix
$\mathbf{x}$	vector of design variables
$\mathbf{x}_c$	vector of design variables for the central design
$(\mathbf{X}^T\mathbf{X})^{-1}$	variance-covariance matrix
I	the leading edge radius parameter
τ_{TE}	the trailing edge half angle
r_t	the leading edge radius-to-chord ratio
α	independent parameter in α-plots
β	independend parameter in bisection search
p	number of design variables
y	modeled response
x_i	design variable
x_i'	scaled design variable
c_i, c_{ij}	coefficients of the polynomial
m	number of observations
n	number of terms in the polynomial

Υ	coefficient of variation
$\mathrm{Var}(\epsilon)$	variance in the measured response function values
σ_k	standard deviation
a, b	scaling factors for design variables

Acronyms

ANOVA	**An**alysis **o**f **V**ariance
AOA	**A**ngle **o**f **A**ttack
BFL	**B**alanced **F**ield **L**ength
CFD	**C**omputational **F**luid **D**ynamics
DACE	**D**esign and **A**nalysis of **C**omputer **E**xperiments
DV	**D**esign **V**ariables
FE	**F**inite **E**lement
FLOPS	**FL**ight **OP**timization **S**ystem
HSCT	**H**igh-**S**peed **C**ivil **T**ransport
LE	**L**eading **E**dge
MAC	**M**ean **A**erodynamic **C**hord
MDO	**M**ultidisciplinary **D**esign **O**ptimization
PBIB	**P**artially **B**alanced **I**ncomplete **B**lock design of experiments
RS	**R**esponse **S**urface
RSG	**R**esponse **S**urface **G**eneration code
RSM	**R**esponse **S**urface **M**ethodology
TOGW	**T**ake **O**ff **G**ross **W**eight
VCM	**V**ariable-**C**omplexity **M**odeling
VLM	**V**ortex **L**attice **M**ethod

Chapter 1

Introduction

Multidisciplinary Design Optimization (MDO) is emerging as a critical component of conceptual level aircraft design. For extremely demanding missions, creation of a successful and profitable aircraft design, or even a feasible aircraft design, is often impossible without fully integrating the key engineering disciplines. At the same time each discipline has to be accurately represented to obtain meaningful results. Numerous MDO methods have evolved in recent years with a broad range of applications, as described by Haftka and Sobieszczanski-Sobieski [1]. Our research group at Virginia Tech has long been developing and applying MDO methodology to the design and optimization of a High-Speed Civil Transport (HSCT), starting with an HSCT wing [2, 3] and then adding the fuselage [4], and including numerous trim, control, and performance constraints into the optimization [5, 6].

One of the inherent and distinguishing features of the MDO methodology is the possibility to explicitly address the interactions between different disciplines. For design of complex systems with difficult mission requirements, such as the HSCT, MDO is an empowering technology and the key to achieving the design goals. But the advantages of MDO come at a price. The intrinsic coupling of disciplines in the MDO process increases the complexity of the problem enormously. The number of design variables grows rapidly with each additional discipline. The computational cost of optimization increases at a superlinear rate with the number of design variables and optimization constraints, so the MDO process requires more computational

resources than the several single discipline optimizations represented in the MDO. As a result, as soon as more detailed numerical simulations are considered in MDO, it becomes very difficult to keep the computational cost at a reasonable level. Modern single disciplinary optimization studies typically use high fidelity models, both in structures and aerodynamics. Although several MDO packages exist (e.g. FLOPS [7], ACSYNT [8]), they primarily use simple algebraic models for aircraft analysis. Because of the high computational cost associated with using detailed analysis methods, such as three-dimensional non-linear aerodynamic models based on Euler equations, or large finite-element structural models, MDO is not feasible. *Hundreds* or even *thousands* of design analyses are required in each optimization cycle.

One of the approaches to overcoming this cost is the *variable-complexity modeling* concept (a version of the well-known mathematical concept of *scale*) which has been applied by our research group to various aspects of the HSCT optimization process [2, 3, 4, 9]. The variable-complexity modeling (VCM) approach is based on using a variety of analysis models of varying fidelity. We combine a large number of low fidelity computationally cheap analyses with a low number of expensive, high fidelity analyses to improve the accuracy of the analysis used throughout the optimization. A typical MDO process is divided into a sequence of optimization cycles and detailed analyses are performed at the beginning of each cycle. Scaling factors are then calculated for the optimization cycle and applied together with the simple analysis methods for current design evaluation. The VCM approach proved to be efficient in reducing the computational cost of the MDO process.

Another problem arises when one tries to use gradient-based optimization methods with high fidelity analysis methods, previously developed for disciplinary analyses. This problem is numerical noise, often present in different computational models as a result of round-off errors and discretization of continuous physical processes (e.g., CFD or finite-element grids). The numerical noise typically shows up in the form of high frequency oscillations of the resulting output (e.g., drag coefficients) as a function of the design variables. The amplitude of these oscillations is usually very low and is well within the accuracy of the computational models. However, the presence of this noise has a strong negative effect on the convergence of the optimization process,

creating numerous artificial local optima and diverting gradient-based optimizers from the best search direction. The VCM approach described earlier does not eliminate the problems associated with numerical noise of the detailed analyses and still inherits most of the convergence difficulties of a general multidisciplinary design optimization.

One way of addressing problems of computational cost and numerical noise in optimization is based on *response surface methodology* (RSM) [10, 11, 12]. RSM methods use simple mathematical models (e.g., low-order polynomials or other simple basis functions) to approximate the *response* of a computationally expensive detailed analysis during the optimization process. Such response surface models are created using a limited number of analyses at a set of statistically selected points in the design space. Selection of designs for creating RS models using *design of experiments theory* [13] attempts to achieve maximum accuracy using a minimal number of designs. The result of using RSM in MDO is an extremely fast design evaluation, which shortens the optimization process and filters out numerical noise of the detailed analysis tools. With smooth response function models and no artificial local optima (due to noise), it is not only easier to obtain an optimum design, it becomes possible to search for the global optimum. This is practically impossible using MDO without RS models.

In recent years considerable interest has been shown in the use of RSM methods in MDO problems. Some examples of such studies are given in the works by Tai, *et al.* [14] and Engelund, *et al.* [15]. For the HSCT design problem, RSM methods have been used by Giunta, *et al.* [16, 17] to construct approximations to aerodynamic drag in two, five, and ten design variables. A summary of results of RSM studies by Giunta can also be found in Ref. [18], along with the description of a new approach to building approximations for the results of computer simulations, called DACE (Design and Analysis of Computer Experiments). Kauffman, *et al.* [19] and Balabanov, *et al.* [20, 21] developed methods for creating and using RSM approximations to the wing bending material weight in twenty five design variables, and applied them to the HSCT optimization problem. Crisafulli, *et al.* [22] used the RSM approach to incorporate pitch-up effects in an HSCT optimization using eight design variables for RS modeling.

This thesis describes the work that is one part of the continuous effort of our

research group in the development and implementation of RSM in multidisciplinary design optimization of a High-Speed Civil Transport. One important feature of this work is that aerodynamic RS models in very high-dimensional space are generated, and their application is studied. Twenty five design variable space is used in the first part of the work and twenty nine design variables are used in the second part. The results presented here describe our work to construct RSM approximations to some of the *expensive* aerodynamic constraints for the HSCT. Out of 68 constraints currently employed in our *HSCT* optimization code, 16 constraints involve aerodynamic calculations requiring a considerable amount of CPU time. The idea was to substitute RSM approximations for all or some of the constraints, thus reducing the time to find an optimum design and improving convergence of the optimization. RSM approximations were constructed for 7 constraints. Since the range constraint is one of the most critical constraints in the HSCT design, the response surface model for the range constraint was used in the trial optimization runs. These runs showed big discrepancies between actual and modeled range values. Response surface models for drag components were then constructed in an attempt to improve the progress of optimization. The issues of the *reasonable design space* and complexity of the parameter being modeled are addressed here as possible reasons for the unsuccessful RSM implementation. The process was then repeated to create the response surface models for the range and the drag components using a new, *valid* reasonable design space, and optimizations of the HSCT were performed using these RSM approximations.

Chapter 2 describes the HSCT design problem to which RSM is applied in this work. In Chapter 3 the process of creating response surface models is described in some detail. In Chapter 4 results of response surface model creation for *expensive* constraints are presented. Chapter 5 describes the latest results from implementing response surface models for range and drag components in an HSCT optimization. Conclusions are discussed in Chapter 6.

Chapter 2

The HSCT Design Problem, Methods, and Optimization Approach

The HSCT design problem [5, 6] is to optimize an aircraft configuration to minimize TOGW for a range of 5500 n.mi., and 251 passengers. The aircraft's mission is a supersonic cruise-climb at Mach 2.4 with a maximum altitude of 70,000 *ft*.

TOGW was chosen as the merit function due to its direct relation to the aerodynamic, structural and propulsion efficiency of the aircraft. Structural design of the aircraft dictates its empty weight, while aerodynamic performance affects the required amount of fuel weight. Both components contribute to the TOGW and determine the required engine size.

2.1 Design Variables

To perform the numerical optimization of an HSCT configuration, the latter has to be completely and uniquely described by a set of design variables. The cost of optimization directly depends on the number of design variables, thus it is desirable to keep their number to a minimum. A typical number of design variables in an MDO problem usually does not exceed 100. In our problem, an HSCT configuration has

been parametrized by 29 design variables uniquely describing the aircraft's geometry, propulsion system, and mission.

The variables can be divided into seven categories: wing planform, airfoil, nacelle placement, engine thrust, fuselage shape, mission performance variables, and tail areas. Table 2.1 presents the set of design variables.

The wing planform is described using the root and tip chord lengths, the wing span, and by blending linear line segments at the leading and trailing-edges. The eight design parameters used to define the planform are shown in Fig. 2.1. The airfoil sections have round leading edges. The thickness distribution is defined by four parameters: the thickness-to-chord ratio t/c, the leading-edge radius parameter I, the chordwise location of maximum thickness m, and the trailing-edge half angle τ_{TE}. They are shown in Fig. 2.2. The thickness distribution at any spanwise station is then defined using the following rules:

1. The wing thickness-to-chord ratio is specified at the wing root, the leading-edge break, and the wing tip. The wing thickness varies linearly between these control points.

2. The chordwise location of the maximum airfoil thickness is constant across the span.

3. The airfoil leading-edge radius parameter is constant across the wing span. The leading edge radius-to-chord ratio r_t is defined by $r_t = 1.1019\left[(t/c)\,(I/6)\right]^2$.

4. The trailing-edge half-angle of the airfoil section varies with the thickness-to-chord ratio according to $\tau_{TE} = 3.03125(t/c) - 0.044188$. This relationship is fixed throughout the design.

The spanwise nacelle locations are defined by the two design variables. Axial location of the nacelles in relation to the wing's trailing edge is fixed at 25% overhang. This is done to keep the rotating parts of the engine behind the rear wing spar to avoid the "rotor burst" problem, so that an engine failure will not cause the wing to fail.

Table 2.1: HSCT baseline design variables (central design 1).

#	Value used in the code	Multiplier*	Description
1	1.814780	100	Wing root chord (ft)
2	1.559070	100	LE Break, x (ft)
3	4.923480	10	LE Break, y (ft)
4	1.816030	100	TE Break, x (ft)
5	6.424340	10	TE Break, y (ft)
6	1.695730	100	LE of wing tip, x (ft)
7	0.700360	10	Tip chord (ft)
8	7.590870	10	Wing semi-span (ft)
9	4.019410	0.10	Chordwise location of max. t/c
10	3.692140	1	Airfoil LE radius parameter, r_t
11	2.578860	0.01	Airfoil t/c at root
12	2.159350	0.01	Airfoil t/c at LE break
13	1.803900	0.01	Airfoil t/c at tip
14	0.021960	100	Fuselage restraint 1, x (ft)
15	0.106100	10	Fuselage restraint 1, r (ft)
16	0.122000	100	Fuselage restraint 2, x (ft)
17	0.349610	10	Fuselage restraint 2, r (ft)
18	1.324630	100	Fuselage restraint 3, x (ft)
19	0.534100	10	Fuselage restraint 3, r (ft)
20	2.486680	100	Fuselage restraint 4, x (ft)
21	0.466610	10	Fuselage restraint 4, r (ft)
22	2.623010	10	Nacelle 1, y (ft)
23	3.238760	10	Nacelle 2, y (ft)
24	3.226170	100000	Mission fuel (lbs)
25	6.479430	10000	Starting cruise altitude (ft)
26	0.338980	100	Cruise climb rate (ft/min)
27	6.978540	100	Vertical tail area (ft^2)
28	7.130590	100	Horizontal tail area (ft^2)

*The scaling factor for each design variable,
e.g., Wing root chord = 1.814780 x 100 = 181.478 (ft).

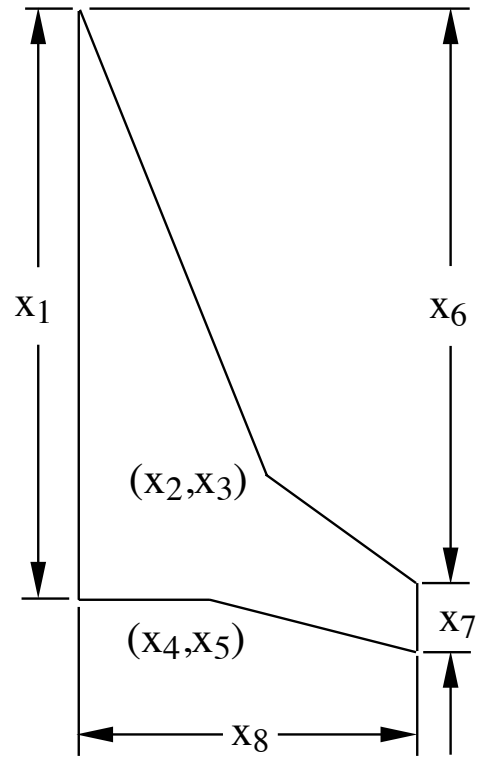

Figure 2.1: HSCT wing planform parameters.

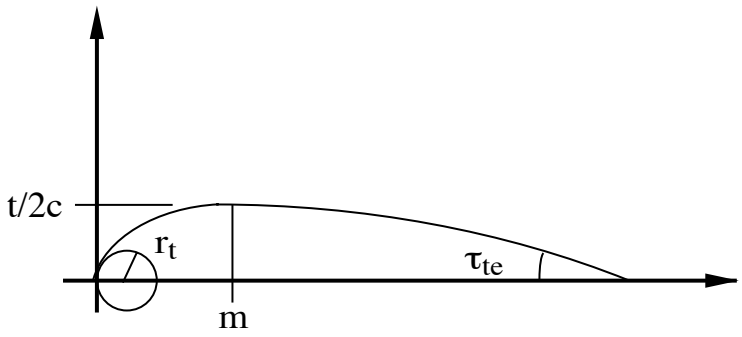

Figure 2.2: HSCT airfoil parameters.

Another design variable specifies the maximum engine thrust. The nacelle diameter and length are scaled by the square root of the ratio of current thrust to the baseline thrust. The weight of the engine is also a function of this ratio.

The axisymmetric fuselage requires eight variables to specify both the axial positions and radii of the four fuselage restraint locations. We define the shape of the fuselage between these restraints by requiring that it be a minimum wave-drag body for the specified length and volume. The vertical tail and horizontal tail are trapezoidal planforms. For each of these control surfaces, the aspect ratio, taper ratio, and quarter-chord sweep are specified, and the surface area is the design variable.

The idealized cruise mission is defined by three design variables, one of which is the mission fuel weight and the other two describe the simplified flight profile in terms of the initial supersonic cruise altitude and the constant climb rate. The resulting aircraft range is calculated using the fuel weight design variable, assuming that 85% of the mission fuel is used in cruise and the remaining 15% is the reserve fuel.

In this study, a baseline HSCT design is used to provide a point near the interior of the feasible design space. The baseline geometry is from an HSCT configuration previously thought to be optimal by Dudley, *et al.* [23] (Table 2.1). Because of modifications and improvements to the analysis methods, this geometry no longer satisfies all of the performance constraints; however, more recent optimal designs exhibit similar characteristics [5].

2.2 Constraints

The constraints used in the problem fall into three categories: constraints implicit in the analysis, performance/aerodynamic constraints, and geometric constraints. The implicit constraints are not handled by the optimization program, but rather are part of the analysis or geometry:

1. The maximum altitude, 70,000 *ft*, is enforced in the range calculation.

2. The fuselage volume is fixed at 23,270 ft^3 and the fuselage length is fixed at 300 *ft*.

3. The axial location of the wing's MAC quarter chord is adjusted to match the value found on the baseline configuration (147.3 *ft* aft of the aircraft nose).

4. The nacelles are fixed axially as noted in Section 2.1 above.

Aside from these implicit constraints we also use up to 68 explicit constraints, summarized in Table 2.2. The range is constrained to be 5500 *n.mi.* or more. The C_L at landing speed must be less than 1, the C_ℓ for each of the 18 wing sections must be less than 2 (an elliptic load distribution is used), and the landing angle of attack is constrained to be less than or equal to 12°. Typically, the landing angle-of-attack is a critical constraint. The mission fuel must not require more space than the available fuel volume, which we assume to be 50% of the total wing volume.

Another group of constraints is designed to keep the optimizer from developing geometrically impossible or implausible designs. For example, a constraint is used to prevent the design of a wing which is highly swept back into a spiked shape, since this may lead to geometries which can not be accurately analysed by the used methods. In this category are the thickness-to-chord constraints, without which the optimizer could attempt to create a wing with negative thickness. The constraint numbered 51 forces the wing's trailing edge to end before the horizontal tail's leading edge begins. Constraints 64 and 65 require nacelle 1 to be outboard of the fuselage and inboard of nacelle 2. Constraint 66 requires that the aircraft be trimmed with two engines inoperative.

Trim and control considerations require 11 constraints: numbers 42–50, 53 and 66 in Table 2.2, most of which are related to landing. The landing constraints are enforced for assumed emergency conditions, i.e., a landing altitude of 5,000 *ft* with an outside temperature of 90° F, and with the aircraft carrying 50% fuel. The vertical tail is sized based on either the requirement that the aircraft be capable of trimmed flight with two engines on the same side inoperative or to meet the 20 *knot* crosswind landing requirement. The pilot must have sufficient control authority to trim the aircraft in these situations, as well as to be able to perform necessary maneuvers safely. Therefore, we require the aircraft be trimmed directionally using no more than 75% of the available control authority and limit the bank angle to 5°. For the

Table 2.2: Optimization constraints.

#	Formula used in the code*	Description
1	$g = 20(PV/LL - 1)$	Range $\geq$ 5,500 *n.mi.*
2	$g = UL/PV - 1$	Required C_L at landing speed ≤ 1
3-20	$g = UL/PV - 1$	Section $C_\ell \leq 2$
21	$g = 1 - PV/UL$	Landing angle of attack $\leq 12^\circ$
22	$g = UL/PV - 1$	Fuel volume $\leq$ half of wing volume
23	$g = PV/LL - 1$	Spike prevention
24-41	$g = PV/LL - 1$	Wing chord $\geq$ 7.0 *ft.*
42-43	$g = -PV/5$	No engine scrape at landing angle-of-attack
44-45	$g = -PV/5$	No engine scrape at landing angle-of-attack, with 5° roll
46	$g = -PV/5$	No wing tip scrape at landing
47	$g = UL/PV - 1$	Rudder deflection for crosswind landing $\leq 22.5^\circ$
48	$g = UL/PV - 1$	Bank angle for crosswind landing $\leq 5^\circ$
49	$g = 1 - PV/UL$	Takeoff rotation to occur ≤ 5 *sec*
50	$g = UL/\|PV\| - 1$	Tail deflection for approach trim $\leq 22.5^\circ$
51	$g = UL/PV - 1$	Wing root T.E. $\leq$ horiz. tail L.E.
52	$g = UL/PV - 1$	Balanced field length $\leq 11,000$ *ft*
53	$g = -PV/5$	T.E. break scrape at landing with 5° roll
54	$g = UL/PV - 1$	L.E. break $\leq$ semispan
55	$g = UL/PV - 1$	T.E. break $\leq$ semispan
56-58	$g = PV/LL - 1$	Root, break, tip $t/c \geq 1.5\%$
59	$g = PV/LL - 1$	Fuselage: $x_{rest_1} \geq 5ft$
60	$g = UL/PV - 1$	Fuselage: $x_{rest_1} + 10\text{ft} \leq x_{rest_2}$
61	$g = UL/PV - 1$	Fuselage: $x_{rest_2} + 10\text{ft} \leq x_{rest_3}$
62	$g = UL/PV - 1$	Fuselage: $x_{rest_3} + 10\text{ft} \leq x_{rest_4}$
63	$g = UL/PV - 1$	Fuselage: $x_{rest_4} + 10\text{ft} \leq 300\text{ft}$
64	$g = PV/LL - 1$	Nacelle 1, $y \geq$ side-of-body
65	$g = PV/LL - 1$	Nacelle 1, $y \leq$ nacelle 2, y
66	$g = UL/PV - 1$	Engine-out limit with vertical tail design; otherwise 50%
67-68	$g = 10(PV/LL - 1)$	Maximum thrust required $\leq$ available thrust

*The letters in the formulae are: PV - physical value of a parameter, UL - upper limit, LL - lower limit.

engine-out condition these constraints are implicit in the analysis. For the crosswind landing requirements these are explicit in constraints 47 and 48.

The engine nacelle strike constraint requires that the nacelles not strike the runway during landing, which limits the allowable spanwise engine location. This is checked at main gear touch down, with the aircraft at the landing angle of attack and 5° bank, the typical certification requirement. This constraint not only limits the spanwise engine location, but effectively limits the allowable trailing edge sweep, because the nacelles are mounted at the trailing edge, with 25% overhang. Another constraint checks wing tip strike under the same conditions. During the crosswind landing, the aileron and rudder deflections are limited to 75% of maximum, or 22.5°, and the bank must be less than 5°. In our design, the landing gear length is fixed, although it can be adjusted parametrically.

Constraints on take-off rotation time (no. 49), balanced field length (no. 52) and approach trim (no. 50) determine the size of the horizontal tail. We require the aircraft rotate to lift-off attitude in less than 5 *seconds*. For the approach trim, the aircraft must trim at the approach attitude with a horizontal tail deflection of less than 22.5°.

The constraint on the balanced field length insures that the aircraft can operate from existing airports. The final two constraints require the maximum thrust required in each segment of the mission be less than the thrust that is actually available at the given flight condition.

2.3 Optimization Approach

A complete design optimization is composed of a sequence of optimization cycles. In our so-called "standard" MDO procedure without use of RS models, detailed analysis methods are employed at the beginning of each cycle, while simple analyses, scaled to match the initial detailed results, are performed in subsequent calculations during each cycle [24, 23]. A typical HSCT design requires approximately 40–50 cycles until an optimal configuration is identified. The optimizer NEWSUMT-A [25], which employs an extended interior penalty function method, is used for this work.

NEWSUMT-A utilizes constraints based on both the simple and detailed analyses along with constraints that limit the movement of the design variables. Move limits are imposed on the design variables on each optimization cycle, so that the optimizer is always in the region of the design space where the scaling factors are valid. Typical values of the move limits are 5-15% and they have to be reduced if the "approximations" are far from the "exact" values, i.e., an "approximate" range value differs from the "exact" one by more than a hundred nautical miles. A typical convergence plot is presented on Figure 2.3.

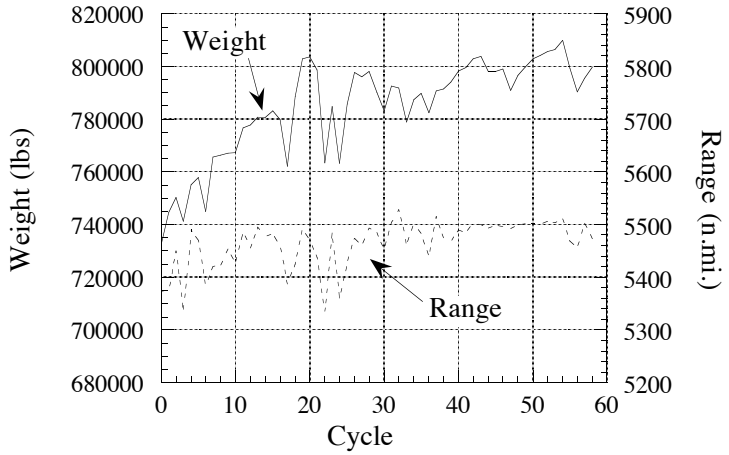

Figure 2.3: Typical HSCT convergence plot.

2.4 Analysis Methods

We use the aerodynamic drag analysis methods and representation of the wing structure using weight equations as described in Refs. [2, 3, 4]. The so-called "exact" or high fidelity aerodynamics calculations used in this work are based on the vortex lattice method [26], the Mach box method [27, 28], and the Harris wave drag code [29]. A simple strip boundary layer skin friction estimate is implemented as in Ref. [3].

The simplified or "approximate" methods of aerodynamic analysis used in this work include wave drag estimation using a classical far-field slender body formulation due to Hutchison [30], with the oblique cross-section calculations replaced by the use

of normal areas to reduce the computational time. A simplified calculation of the drag due to lift is based on the cranked delta wing method as described in [4]; analytical solutions for these wings have been given in the work by Cohen and Friedman [31].

To analyze trim and control conditions it is necessary to obtain information not normally used in initial sizing programs. This includes the location of the center of gravity (*cg*), the inertias, and the stability and control derivatives. These are estimated for a given geometry and flight condition.

During the cruise and landing approach we assume the *cg* position to be at the center of pressure of the aircraft, which is achieved by fuel transfer. During take-off the *cg* position is estimated using expressions given by Roskam [32]. The inertias of the aircraft are estimated using a routine from FLOPS which is based on a modified DATCOM [33] method.

We use two techniques to estimate the stability and control derivatives: (1) empirical algebraic relations from the U.S.A.F. Stability and Control DATCOM [33], as interpreted by J. Roskam [32], and (2) a VLM code developed by Kay, *et al.* [34]. The DATCOM methods rely on simple theories and some experimental data, and do not handle unusual configurations well. The VLM code is better able to handle different configurations, but is more expensive computationally. A detailed description of these techniques is given in Ref. [5].

Chapter 3

Response Surface Model Generation Process

The RSM approach used in this work is based primarily on the work done by Kaufman [35], who developed the algorithms and used RSM to incorporate the results of structural optimizations of the wing bending material weight into the HSCT optimization process [19]. In this chapter the most important aspects of the process are presented for better understanding, and the process itself is outlined in detail as it was actually used here.

As mentioned previously, RSM uses simple, smooth function approximations to replace the actual function. Quadratic polynomials are widely used for RSM applications since they are easy to implement and provide the capability of modeling curvature of the actual function. Quadratic response surface models are also used in this work, so that response of the function is modeled in the form:

$$y = c_0 + \sum_{1 \le i \le p} c_i x_i + \sum_{1 \le i \le j \le p} c_{ij} x_i x_j \,, \tag{3.1}$$

where the x_i are the design variables, the c_i, c_{ij} are the polynomial coefficients, and y is the modeled response. For p design variables, Eq. (3.1) has $n = (p+1)(p+2)/2$ terms. In such a model the polynomial coefficients may be estimated using the method of least squares. For the 25 design variable problem, described in Chapter 4, Eq. (3.1) gives 351 terms in the approximating polynomial. For the 29 design variables used

in the second part of this work (Chapter 5), this yields a quadratic polynomial with 465 terms.

The process of response surface model generation used in this work can be divided into several stages: 1) creating a *central (baseline)* design, 2) generating the initial design space, 3) reducing the design space down to a *reasonable design space*, 4) choosing a limited number of points for response surface model generation, 5) analyses at the selected design points, 6) response surface model generation using the high fidelity analysis results, and 7) reduction of the model size using analysis of variance (ANOVA). In the next few sections each of these stages is described in more detail, including the problems that arose in each step of the process and the approaches taken to overcome them. Figure 3.1 shows a flow chart of the procedure along with the names of the codes used in the process. The flow chart includes the optimization of an HSCT using response surface models as a final step.

3.1 Creating a Central Design

The *central* (or *baseline*) design is that reference point in the multivariable design space around which a *reasonable design space* will be created. Thus, the importance of choosing the right central design may be much greater than it may seem at first glance. By the reasonable designs here we mean those designs having similar characteristics to the feasible designs even though some of the aerodynamic and performance constraints may be violated. More details on the criteria of the reasonable design space are given in section 3.3. The central design, thus, has to be a reasonable one, and preferably a feasible one.

A distinguishing feature of the optimization in a high dimensional design space is that finding a feasible design by itself is not a trivial task. The feasible design space is restricted by numerous geometric and aerodynamic constraints, is extremely irregular (nonconvex), and its volume is several orders of magnitude smaller than the volume of the reasonable design space. This means that simply assuming reasonable values for the design variables and then tweaking them to bring the design into the feasible domain will hardly ever produce the desired result. One of the solutions

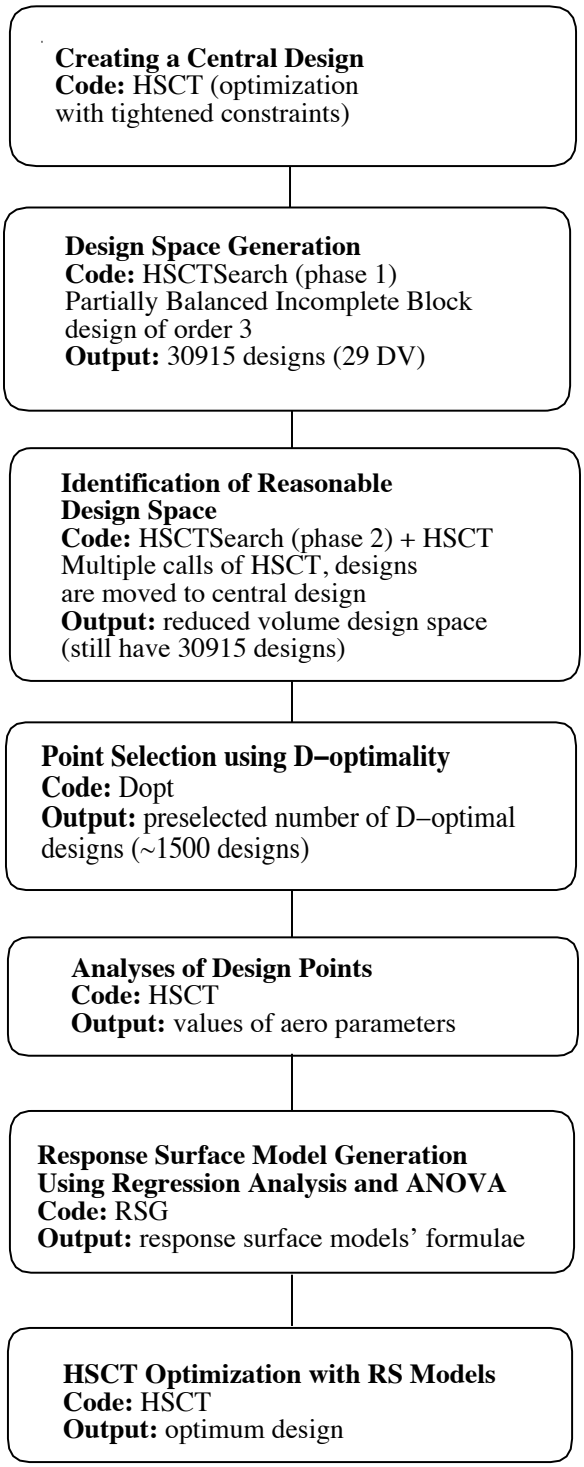

Figure 3.1: Flow chart of the response surface model generation and implementation process.

to the problem is to use gradients of the constraints to find the direction required to move towards the feasible design space. The tool for implementing this process already exists: it is an optimizer capable of working in the infeasible domain. Thus, the simplest way to get a suitable central design is to take one of the final designs from previous optimization runs, or to perform a new optimization, possibly incomplete, if no existing optimum designs are available. If the cost of optimization is too high to make a full optimization run, incomplete optimization may provide a design close enough to the feasible domain, so that a reasonable design space may be constructed around it. For the first part of this work the same central design was used as in the work of Kaufman, *et al.* [19], which was an optimum design for one of the previous optimization studies of HSCT. Figure 3.2 shows the planform of the design. Design variables for this design are listed in Table 2.1.

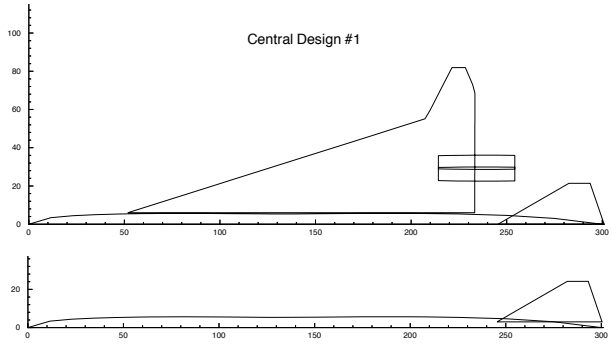

Figure 3.2: Central HSCT design used in the first part of the work.

To ensure that a large part of the design space used for creating RS models lies in the feasible domain, it's preferable to have the central design *inside* the feasible domain. The method of obtaining a baseline design using standard optimization described above provides at best a design on the border of the feasible design space. To get a design inside the feasible space it's necessary to continue *pushing* it inside past the border of the feasible domain. This may be accomplished by performing optimization with *tightened* constraints. This approach was used in the second part of this work. Optimization was started from one of the previous optimum designs using a modified HSCT code, where most of the performance and aerodynamic constraints

(i.e., range, landing angle of attack, maximum lift coefficient, etc.) and also some of the geometric constraints (i.e., fuel volume, nacelle spacing, minimum chord, etc.) were *tightened* by 1–2% of their nominal value, meaning that the level of requirements was raised (e.g., the range requirement was changed from 5500 to 5555 n.mi). This change in constraint values may seem to be a very small one, but one has to remember that the sensitivity of the take-off gross weight (TOGW) and the configuration of HSCT to small changes in constraints is very big (see Refs. [5, 6] for results of some sensitivity studies). Any bigger changes in the constraint values will not only result in a completely different configuration, but will also make the optimization process much more difficult. Making the constraints too severe reduces the feasible space and also typically greatly increases the size of the HSCT. If the constraints are too severe, the feasible region will vanish, and no solution will be possible.

When optimizing the HSCT using this approach, the weight and geometrical size of the aircraft had to be increased to satisfy the new constraints, which led to difficulties in satisfying the engine nacelle scrape constraints. With a 1-2% artificial increase in the values of constraints the size of the aircraft became too big for the given landing gear length. Thus, the length of the gear was increased by 1 ft, from 19.75 ft to 20.75 ft for the main legs and from 18.75 ft to 19.75 ft for the nose leg. With this change a new design was found satisfying most of the tightened constraints (the increased range, engine scrape and rotation time constraints were still violated) and all of the standard ones (with the nominal values). Figure 3.3 shows the configuration and Table 3.1 contains design variables of the new baseline design.

Table 3.1: Design variables of HSCT central design 2.

#	Value used in the code	Multiplier*	Description
1	1.781470	100	Wing root chord (ft)
2	1.141291	100	LE Break, x (ft)
3	4.070442	10	LE Break, y (ft)
4	1.734057	100	TE Break, x (ft)
5	1.222726	10	TE Break, y (ft)
6	1.463565	100	LE of wing tip, x (ft)
7	0.920425	10	Tip chord (ft)
8	8.260918	10	Wing semi-span (ft)
9	5.114403	0.10	Chordwise location of max. t/c
10	2.525195	1	Airfoil LE radius parameter, r_t
11	2.818364	0.01	Airfoil t/c at root
12	1.900977	0.01	Airfoil t/c at LE break
13	1.704753	0.01	Airfoil t/c at tip
14	0.026108	100	Fuselage restraint 1, x (ft)
15	0.046578	10	Fuselage restraint 1, r (ft)
16	0.132450	100	Fuselage restraint 2, x (ft)
17	0.249456	10	Fuselage restraint 2, r (ft)
18	1.116824	100	Fuselage restraint 3, x (ft)
19	0.532127	10	Fuselage restraint 3, r (ft)
20	1.869078	100	Fuselage restraint 4, x (ft)
21	0.534270	10	Fuselage restraint 4, r (ft)
22	1.149741	10	Nacelle 1, x_9 (ft)
23	2.837171	10	Nacelle 2, x_{10} (ft)
24	4.647425	100000	Mission fuel (lbs)
25	5.840310	10000	Starting cruise altitude (ft)
26	0.379744	100	Cruise climb rate (ft/min)
27	9.211897	100	Vertical tail area (ft^2)
28	9.866076	100	Horizontal tail area (ft^2)
29	5.727139	10000	Thrust per engine (lbs)

*The scaling factor for each design variable,
e.g., Wing root chord = 1.781470 x 100 = 178.147 (ft).

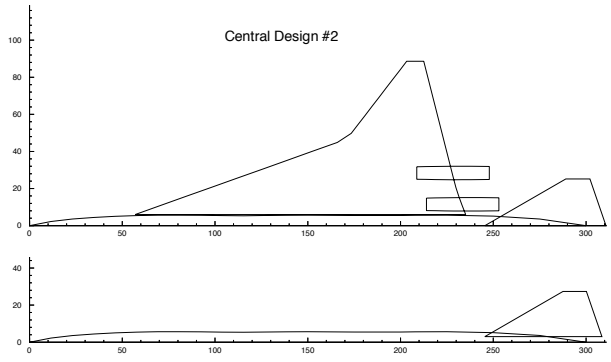

Figure 3.3: Central HSCT design used in the second part of the work.

3.2 Initial Design Space Generation

The next step of the response surface model creation process was the generation of a large number of candidate designs covering that portion of the design space where the models are expected to be valid. The most general approach to the problem is to assume the initial design space to have the shape of a p-dimensional hypercube (here p is the number of design variables) with the design variables scaled so that the hypercube is centered at the origin and the design variables are allowed to have values between -1 and $+1$.

Ideally, we would like to have design samples distributed everywhere inside the hypercube so that every possible combination of the design variables is represented in the data set, with enough detail to find all nonlinear variations. Such design space sampling quickly leads to a large number of designs, all of which can not be evaluated in any reasonable time frame using high fidelity analysis methods. Thus, statistical methods for creating *experimental designs* with a smaller number of design variable combinations, where each combination of design variables is called an *experiment*, must be adopted. Note, that the statistical sense of the word "design" is different from an aircraft "design" used here.

The *full factorial* method of experimental design assumes that every design variable is allowed to take a certain number of values in the range $\{-1, 1\}$ determined by the *level* of the system. Full factorial design of level three, where design variables can

take values $\{-1, 0, +1\}$, for twenty five design variables will require $3^{25} \approx 8.5 \times 10^{11}$ design points. For twenty nine design variables, used in the second part of the work, this number would be $3^{29} \approx 6.9 \times 10^{13}$. For a level two system these numbers reduce to $2^{25} \approx 3.4 \times 10^{7}$ and $2^{29} \approx 5.4 \times 10^{8}$ respectively. Clearly, even for the system of level two the number of evaluations required is too high.

The approach used in this work is based on the partially balanced incomplete block design (PBIB) [36] of order three. In this algorithm, implemented in the *HSCTSearch* code by Kauffman, up to three design variables per design point are allowed to take values $\{-1, +1\}$, while the rest of the variables are held constant at the third level 0. This produces three blocks of design points with one, two, and three design variables perturbed from the level 0 value. Every block is included into the system, as well as the center point (0,...,0). For p design variables this algorithm requires

$$n = 1 + \sum_{i=1}^{3} 2^i \frac{p!}{i!\,(p-i)!} \tag{3.2}$$

design points. For twenty five design variables this gives 19,651 points. For twenty nine design variables this number increases to 30,915 points. The *HSCTSearch* code written by Kauffman was used for generating candidate designs in both parts of the work. The first part of the work was based on the set of design points developed previously for creation of RS models for structural weight of the HSCT wing, and used by Balabanov, *et al.* [21]. Only 25 design variables out of 29 were allowed to vary. The initial deviation from the central design was set to $\pm 80\%$ of the value for each design variable except for the fuel weight, for which only a $\pm 25\%$ variation was allowed due to its strong effect on the aircraft range. In the second part of the work all 29 variables were varied by the amount of $\pm 20\%$ of the value of the central design. Reduced allowable variation was expected to decrease the volume of the design space covered by the response surface models and to improve its accuracy.

3.3 Identification of the Reasonable Design Space

Generation of the initial design space was followed by the reduction of its volume down to the size of the reasonable design space, containing reasonable HSCT configurations, to exclude from consideration unrealistic designs. By reasonable we mean those configurations having similar characteristics to the feasible designs, but allowed to have some aerodynamic/performance constraints violated. The elimination of unreasonable designs was not possible, since this would lead to removing most of the designs in the already very sparsely covered design space. Instead, each unreasonable design was moved towards the baseline design using the same approach as in previous studies [35, 21]. Each unreasonable design $\mathbf{x}$ was moved linearly towards the baseline design $\mathbf{x}_c$ until it met a certain set of criteria shown in the Table 3.2. The set of parameters, used to determine whether a design is reasonable or not, includes 34 standard geometric constraints for HSCT, several additional geometric constraints and some aerodynamic constraints which use "approximate" methods for design analysis and are therefore inexpensive to evaluate. This procedure brings an unreasonable design $\mathbf{x}$ to the border of the reasonable design space. The design variables were changed linearly with a parameter β between the initial unreasonable design $\mathbf{x}$ and the central design $\mathbf{x}_c$:

$$\mathbf{x}' = \beta\,(\mathbf{x} - \mathbf{x}_c) + \mathbf{x}_c\,. \tag{3.3}$$

The parameter β, $0 \leq \beta \leq 1$, was found for each design using bisection with tolerance 0.01.

Each design is evaluated using the routines of the *HSCT* code, and if the constraints (Table 3.2) are violated the design is moved closer to the baseline. The criteria are applied in two phases, with computationally inexpensive geometric and weight constraints coming first, and more expensive aerodynamic evaluations used in the second phase. This assures minimum computational expense, since after applying the geometric criteria the majority of the designs (approximately 80-90%) have been moved into the reasonable design space, and aerodynamic criteria are not satisfied for only a small number of the designs.

The requirement for the wing bending material weight W_{b_F} to be between

Table 3.2: Criteria for reasonable designs.

#	Description
1-34	HSCT geometric constraints
35-36	20,000 lbs $< W_{b_F} <$ 120,000 lbs
37-58	Minimum fuselage radius
59	Inboard $\Lambda_{le} >$ Outboard Λ_{le}
60	$\Lambda_{le} > 0$
61-62	5,000 ft^2 $< S_w <$ 15,000 ft^2
63-64	$1.0 < AR < 3.2$
65	Inboard $\Lambda_{te} < 40^\circ$
65-83	$c_{y_{i+1}}/c_{y_i} < 1.0$
84	Approximate range > 5,000 n. mi.
85-86	0.8*Thrust required < Thrust available (approximate analysis)

20,000 lbs and 120,000 lbs was introduced into the procedure when structural RS models were being developed [19, 21]. It was decided to keep the requirement among the reasonable design criteria, since it helps to eliminate some unrealistic designs. The wing bending material weight being too high may indicate that design has a very large TOGW and grossly inferior aerodynamic performance. A very low value of W_{b_F} may simply indicate a physically unrealizable design. Since results of the work by Kaufman [35] showed that more appropriate limits on W_{b_F} would be between 15,000 and 60,000 lbs, these values were used in the second part of this work (the 29 design variable problem).

The design space in the first part of this work (the 25 design variable problem), used for structural RS models by Balabanov, *et al.* [21], was generated without applying aerodynamic criteria for determining a reasonable design space, since the geometric and weight constraints were thought to be sufficient for excluding structurally unrealistic designs. In the second part of the work both phases of the design space reduction were performed, with the range and thrust constraints coming in the second phase of the process. Note that some degree of violation is allowed for the range and thrust constraints during this process (500 n.mi. deficiency for range and 20% for thrust). The reason for this is that approximate methods are used for

analyzing designs at this step. Also, reasonable designs are allowed to have the range and thrust constraints slightly violated, as this does not invalidate the aerodynamic similarity of the reasonable and feasible designs.

3.4 Selection of D-optimal Designs

Even though we limited the reasonable design space to a much smaller number of designs than a full factorial system would have had, the computational expense of performing high fidelity HSCT analyses on each reasonable design is still enormous, and so is the expense of doing a regression analysis on the full set of 30915 designs. A subset of the designs must be used. This limits the number of designs under consideration to a small fraction of the pool of the available reasonable designs. Thus, the task is to choose an affordable number of designs, out of 19,651 designs for the 25 design variable problem and out of 30,915 designs for the 29 design variable problem, at which to perform the high fidelity analyses. The results of these analyses are then used in response surface model generation. The size of the set of designs should be adequate for providing sufficient information for fitting all coefficients in the modeling polynomial. Previous experience [35] indicated that the ratio of the number of designs to the number of coefficients in the model should be at least 3 for a high number of design variables (25-29) to reliably fit a quadratic polynomial to the analysis results.

The *D*-optimality criterion [37] was chosen as one rational means for selecting such a subset of designs from the large number of candidate HSCT designs in previous studies by Giunta, *et al.* [16, 17, 38] and Kaufman, *et al.* [19]. A *D*-optimal experimental design is a set of points with the minimum value of the determinant of the variance-covariance matrix $(\mathbf{X}^T\mathbf{X})^{-1}$. This decreases the volume of the confidence region on the regression coefficients, i.e., increases the validity of the computed coefficient values. The *D*-optimality criterion was thus used in this work. For both the 25 and 29 design variable problems of this work the *Dopt* code written by D. Haim was used. This code utilizes the "*k*-exchange" method of Mitchell [39] for selection of the *D*-optimal set of designs.

As mentioned before, for the 25 design variable problem a previously obtained

set of designs was used. The 2490 HSCT designs were selected using *Dopt* from the 19,651 reasonable designs for constructing structural RS models in previous works of Balabanov, *et al.* [21]; this provided a sufficiently large ratio of the number of designs to the number of polynomial coefficients (365) required for fitting two structural RS models. These data were also used here in the 25 design variable problem. These 2490 designs were then divided randomly into two sets: one for generating RS models and the other one for checking accuracy of the models.

For the 29 design variable problem it was decided to choose 1500 designs for generating the RS models (set A) and 1500 designs for checking the accuracy of the models (set B). Due to the enormous computational expense a complete *D*-optimal selection could not be performed on the full 30,915 reasonable designs. For this problem the code would have taken several weeks or even months of CPU time. Thus the optimization was stopped after about 400 iterations for each set of designs, which meant that about 400 badly placed design points were replaced with better placed ones in the initial randomly selected set of designs. A badly placed point is such that removing it from the data set decreases the determinant of $(\mathbf{X}^T\mathbf{X})^{-1}$ by a greater value than removing any other point. Accordingly, a well placed point increases the determinant by a minimum amount.

Designs with a range below 4,900 *n.mi.* were discarded from data sets A and B. This procedure resulted in the 1,446 design set A, with a condition number $cond\,\mathbf{X} = 252$, and 1,426 design set B with condition number $cond\,\mathbf{X} = 113$. The low values of the condition numbers indicate that the point distribution is adequate for preventing an ill-conditioned least squares problem when solving for the polynomial coefficients.

3.5 Analyses of D-optimal Designs

D-optimal sets of designs obtained in the previous step of the process constitute coordinates of the design points in the multivariable design space and do not carry any information about aerodynamic functions of interest. Thus, to use these designs in the process of response surface model creation one needs to evaluate required aerodynamic parameters at each design point.

A special case called `ANALYZE` was set up in the *HSCT* code to allow for performing multiple analyses of designs. A set of designs to be analyzed is placed in the input file *data.in* along with the total number of designs contained in the file. Each design is then loaded into *HSCT* one at a time, aircraft geometry is modified to reflect new design variables, and aerodynamic analysis is performed. For the first part of the work (Chapter 4) the *expensive aerodynamic constraints* (e.g., see Section 4.1.1) were evaluated. For the second part of the work (Chapter 5) the case was modified so that range analysis was performed, which required calculation of cruise drag coefficients. Each time after the completion of the aerodynamic analysis, design variables were duplicated into the output file *data.out* and values of aerodynamic parameters (constraints or drag coefficients) were added to the same file. This output file then served as the main information source for response surface model generation by *RSG*. Figure 3.4 shows the flow chart of the ANALYZE routine that was installed into the *HSCT* code.

3.6 Response Surface Model Generation Using Regression Analysis and ANOVA

3.6.1 Least Squares Method and RSG code

As mentioned earlier, quadratic polynomials are used for RS models throughout this work, with the least-squares method (see [12], pp.17–27) providing the means for estimating unknown coefficients of the polynomials. To estimate the n unknown polynomial coefficients at least $m \geq n$ values of the response function must be available evaluated at m distinct design points. Denoting a vector of observations (values of the response function) as $Y = (Y_1, ..., Y_m)$, and a matrix of constants obtained from the values of design variables at each point (least squares matrix) as $\mathbf{X}$ $(m \times n)$, the problem of estimating the coefficients may be written in matrix form as $Y \approx \mathbf{X}c$. Here c is the $n \times 1$ vector of unknown polynomial coefficients, $c = (c_1, ..., c_n)$. The least squares solution to the problem is that unique vector $\tilde{c}$ (assuming $\text{rank}(\mathbf{X}) = n$), which minimizes the 2-norm $||Y - \mathbf{X}c||_2$, or the sum of squares of the components of

$Y - \mathbf{X}c$, the so called *errors*. This procedure for obtaining the polynomial coefficients is called a *regression analysis*, and the solution of the least squares problem $\tilde{c}$ used in Eq. (3.1) is called a *regression model* ([12], p.16).

The *RSG* code [35] written by Kauffman was used for creating the RS models. It provides two least squares algorithms from the LAPACK library [40]. One of the algorithms uses singular value decomposition (SVD) ([41], pp. 615) and the other uses QR factorization (QR) ([41], pp.533). Although slower, SVD is more robust and is the preferred method. Hence, SVD was used exclusively in this work. *RSG* also provides a weighted least squares algorithm, where weightings can be added to each data point before the response surface is produced.

3.6.2 Data Preprocessing

Some other useful options of *RSG* which were used in this work include data preprocessing. Several types of preprocessing can be performed by *RSG*. The simplest procedures include data clipping and replacing, which are designed to alter specific data points while leaving the rest of the data unchanged. Sometimes it is advantageous to remove specific data points from the information used in creating or evaluating RS models. Usually these design points are the ones that have a value of the response function too far from the average value. Clipping data implies excluding from consideration the designs with the value of the response function outside of the user specified range defined by the *clipping limits*. Removing these points, although resulting in a possible loss of information, may considerably improve the data fit in the region where the response function is best approximated by the model. Replacing data implies replacing the value of the response function with some predefined value if it falls outside of the lower and upper bounds imposed by the user. Data clipping was extensively used in the first part of the work, when obtaining reasonable values of the average and RMS errors was impossible when fitting aero constraint RS models to the entire data set. Data clipping and replacing (not used in this work) are also called *point procedures* [35]. Point procedures are unnecessary if robust statistical least squares estimation procedures, such as M-estimation or LMS [42, 43], are used.

Global procedures are those which change the entire data set, and include scaling and conversion to a log scale. The scaling procedure changes the design variables so that they vary between -1 and 1. HSCT design variables (Table 2.1), although scaled to have values below 10, still have very dissimilar orders of magnitude. Direct use of these design variables in the response surface model generation process may lead to ill-conditioning of the **X**-matrix, resulting in longer CPU times and reduced reliability of the coefficient values. Thus, all data for response surface model generation in this work was scaled to be between -1 and 1, based on the first data set (used for generating the response surface models), before any RS models were generated. Log scale conversion can help to reduce the effect of curvature of the response function on the RS model accuracy and requires a special preprocessing procedure to shift all data into the positive region. This feature of *RSG* wasn't used in this work.

3.6.3 Backwards Regression

Regression analysis described earlier, along with the polynomial coefficients, also provides a measure of the uncertainty in these coefficients. The matrix $(\mathbf{X}^T\mathbf{X})^{-1}$ used in the regression analysis is called the variance-covariance matrix. The n diagonal elements in this matrix are the variance values associated with the n respective coefficients [44]. The standard deviation of each coefficient is the square root of its variance.

Analysis of variance (ANOVA) ([12], p.28) involves estimating the variance of the predicted polynomial coefficients and uses the variance-covariance matrix $(\mathbf{X}^T\mathbf{X})^{-1}$. The diagonal terms ${\sigma_i}^2$ in this square matrix multiplied by the variance $\mathrm{Var}(\epsilon)$ in the measured function values Y_i are the variances of the respective coefficients c_i in the response surface polynomial model. The coefficient of variation Υ for each term in the polynomial is calculated as

$$\Upsilon = \begin{cases} \dfrac{100|\sigma_i|\sqrt{\mathrm{Var}(\epsilon)}}{|c_i|}, & c_i \neq 0, \\ 100, & c_i = 0, \end{cases} \tag{3.4}$$

where the factor of 100 expresses the coefficient of variation as a percentage. The term $\sqrt{\mathrm{Var}(\epsilon)}$ is usually estimated by the RMS error of the least squares approximation at

the p data points. For the coefficient of variation calculations given below, $\mathrm{Var}(\epsilon)$ is taken to be unity. Terms in the polynomial model having large coefficients of variation, typically over 0.10, may be dropped from the polynomial without significantly affecting the fidelity of the response surface fit.

RSG allows the user to perform a so called one-step backwards regression, where the term with the highest coefficient of variation is removed from the model function, and the process of regression analysis and ANOVA is repeated until a certain stopping criterion is reached (e.g., a minimum number of terms specified by the user). This is an essential step in the response surface model generation process, as it not only reduces the size of the model function considerably, but also improves its performance. Removing terms with high coefficients of variation, although it may seem like loosing information about the response function, in fact increases the prediction accuracy of the model as will be shown in the later sections.

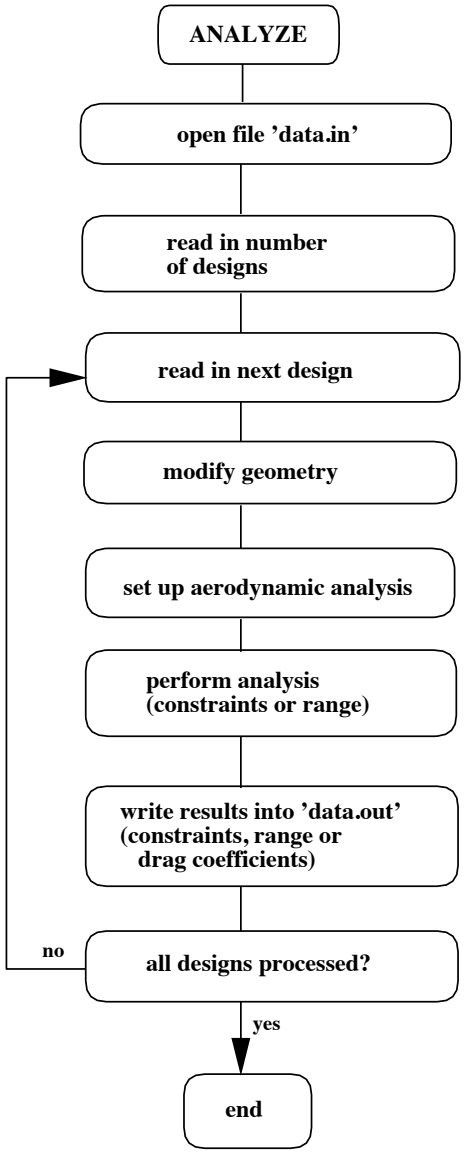

Figure 3.4: Flow chart of the `ANALYZE` routine for performing multiple analyses of HSCT designs.

Chapter 4

First Experience with Response Surface Models for Expensive Aerodynamic Constraints (25 Design Variable Problem)

4.1 Response Surface Models for "Expensive" Aerodynamic Constraints

The first part of this work described in this chapter was devoted to experiments with building response surface models to "expensive" aerodynamic constraints of the *HSCT* code. The primary purpose of this portion of the work was to get experience with models for quantities involving aerodynamic calculations in high dimensional space and examine their behavior for use in the HSCT optimization. Since the set of 2490 *D*-optimal designs was readily available from previous studies by Balabanov, *et al.* [21], it was decided to use this set of designs for aerodynamic analyses and response surface model creation. Due to the peculiarities of the mentioned work (only 25 design variables were found to affect the wing bending material weight), only 25 design variables were varied in the aforementioned set of designs. This limited consideration

of the RSM approach to only 25 of the 29 HSCT design variables. Design variables 10 (LE radius parameter), 25 (starting cruise altitude), 26 (cruise climb rate), and 29 (engine thrust) were held constant for the 25 design variable RSM work.

4.1.1 Expensive Aerodynamic Constraints

The term *"expensive" aerodynamic constraints* refers to those out of the full list of 68 constraints that require performing any aerodynamic calculations for obtaining the degree of violation/satisfaction of the constraint. Sixteen constraints that can be considered expensive in the HSCT problem are shown in Table 4.1. The primary aerodynamic analysis is the calculation of drag at cruise, which includes contributions from volumetric wave drag, drag due to lift, and friction drag. Results of drag calculations directly affect values of range (constraint 1) and required thrust at cruise (constraints 67-68). Both high fidelity ("exact") and low fidelity ("approximate") methods are used for wave drag and drag due to lift calculations, with "exact" methods providing scaling factors and "approximate" methods being used during optimization (see Section 2.4 for description of the methods and Section 2.3 for description of the optimization approach). The "exact" models require a considerable amount of CPU time for calculation and introduce noise into the optimization, thus representing good candidates for being replaced by response surface models. Other aerodynamic constraints, although not so computationally expensive, still require considerable CPU time and involve relatively complex aerodynamic analyses, such as VLM calculations for determining the lift curve slope and stability and control derivatives needed for trim and control constraints. All these constraints also provide good candidates for applying the RSM approach. Note that results of multiple VLM calculations have already been used by Crisafulli, *et al.* [22] who applied the RSM approach for incorporating pitch-up effects into the HSCT optimization.

Of these 16 aerodynamic constraints, 6 scrape constraints (42-46 and 53) use information about landing angle of attack for calculating their values. Once the latter is known, these constraints become simply geometric and do not require any additional expensive analyses. Hence they were excluded from consideration for applying the RSM approach.

Table 4.1: Expensive HSCT constraints.

# of constraint	Description
1	Range $\geq$ 5,500 *n.mi.*
21	Landing angle of attack $\leq 12^\circ$
42-43	No engine scrape at landing angle-of-attack
44-45	No engine scrape at landing angle-of-attack, with 5° roll
46	No wing tip scrape at landing
47	Rudder deflection for crosswind landing $\leq 22.5^\circ$
48	Bank angle for crosswind landing $\leq 5^\circ$
49	Takeoff rotation to occur ≤ 5 *sec*
50	Tail deflection for approach trim $\leq 22.5^\circ$
52	Balanced field length $\leq 10,500$ *ft*
53	T.E. break scrape at landing with 5° roll
66	Engine-out limit with vertical tail design; otherwise 50%
67-68	Maximum thrust required $\leq$ available thrust

4.1.2 Design Space Used for RS Models

The 2490 designs from the aforementioned D-optimal set were analyzed using the *HSCT* code and the procedure described earlier (Section 3.5). The mean, minimum and maximum values of all 10 aerodynamic constraints under consideration are shown in Table 4.2. The last column of the table contains the formulae used in the *HSCT* code for calculating the values of the constraints. The constraints were formulated so that a positive value means satisfaction of the constraint, and a negative value means violation. If the physical value (PV) of a parameter is limited from above by the upper limit (UL), the constraint formulation can be $g = 1 - PV/UL$. See the last column of the Table 4.2 for the formulation of each of the expensive aerodynamic constraints.

Several observations can be made from the values of the aerodynamic constraints presented in the table. Looking at the minimum, mean and maximum values of the constraints in Table 4.2, one may notice that many of the constraints are violated (have negative values) for the majority of the designs in the set. Only constraints 47 (rudder deflection) and 48 (bank angle) are satisfied for all of the designs. Constraints 67-68 (thrust on climb and cruise) are grossly violated for the entire set of designs.

Table 4.2: Mean, minimum and maximum values of expensive HSCT constraints.

# of constraint	Description	Min	Mean	Max	Formula*
1	Range	-9.14	-2.27	3.59	$g = 20(PV/LL - 1)$
21	Landing AOA	-0.39	0.22	0.41	$g = 1 - PV/UL$
47	Rudder deflection	1.89	1.89	1.89	$g = UL/PV - 1$
48	Bank angle	28.39	37.23	68.8	$g = UL/PV - 1$
49	Takeoff rotation	-0.13	0.18	0.33	$g = 1 - PV/UL$
50	Tail deflection	-0.90	1.48	585.3	$g = UL/\|PV\| - 1$
52	BFL	-0.43	0.08	0.58	$g = UL/PV - 1$
66	Engine-out	-1009.5	-0.91	654.4	$g = UL/PV - 1$
67	Thrust (climb)	-5.89	-3.39	-1.28	$g = 10(PV/LL - 1)$
68	Thrust (cruise)	-5.70	-3.57	-1.85	$g = 10(PV/LL - 1)$

*The letters in the formulae are: PV - physical value of a parameter, UL - upper limit, LL - lower limit

This confirms the fact that the baseline design used for generating these designs was representative of the older version (26 design variable version) of the *HSCT* code and no longer satisfies the constraints of the current code (29 design variable version). In fact, this design was found optimum without considering the thrust constraints, the trim and control constraints, and the balanced field length constraint. Thus, the design space formed by the 2490 designs in the set lies in the infeasible domain, meaning that any optimization started in that region (assuming all current constraints are included) will have to move out of this space into the feasible domain.

Several of the constraints (e.g., constraints 48, 50, and 66) were poorly formulated as functions with poles in the design space, leading to the large values even after scaling. Note also, that constraint 47 (rudder deflection for crosswind landing $\leq 22.5^{\circ}$) is constant for all of the designs in the set. This constraint, along with other control related constraints, requires estimation of control derivatives for the HSCT for obtaining their exact values, which is performed by the VLM code developed by J.Kay [45, 34]. Calculation of control derivatives takes a lot of CPU time and couldn't be afforded while performing aerodynamic analyses of the designs. It was decided to proceed with the available information and create response surface models

only for those constraints that exhibit nearly realistic behavior (change their values with design variables) and can be fitted with quadratic polynomials, since the primary purpose of this part of the study was getting experience with response surface models.

4.1.3 Generating Response Surface Models

After all 2490 designs in the data set were analyzed, response surface models for all constraints in Table 4.2 except for constraint 47 were generated using the *RSG* code. Clipping of the data points was used here extensively since acceptable levels of average and RMS errors could not be achieved by fitting polynomials to the entire data set. The procedure of response surface model generation started each time with dividing randomly the 2490 designs into two approximately equal size sets, so that two sets of about 1245 designs each were obtained. This provided two independent sources of data — one for fitting the models and the other for checking errors. Table 4.3 shows the effect of data clipping on the accuracy of the range constraint response surface model. The data is plotted in Figure 4.1. Fitting errors of the RS model reduce considerably as the limits of clipping move closer and fewer points are left in the data set. Recall that clipping limits are the values of the response function (the range constraint in this case) chosen by the user to define the allowable range of its values. The limits were placed symmetrically around the mean value of the response function.

Table 4.3: Fitting errors of the range constraint response surface model for different clipping limits (All 2490 designs used before clipping, limits are imposed on the constraint value. Errors are for the HSCT range calculated from the constraint value.)

Number of designs	Clipping limits	Average error, n.mi	RMS error, n.mi.	Maximum error, n.mi.
2490	no clipping	50.96	78.99	915.89
2079	-4.0 ...0.0	39.43	58.35	519.56
1624	-3.5 ... -1.0	37.62	53.50	361.86
1079	-3.0 ... -1.5	29.21	39.89	314.16

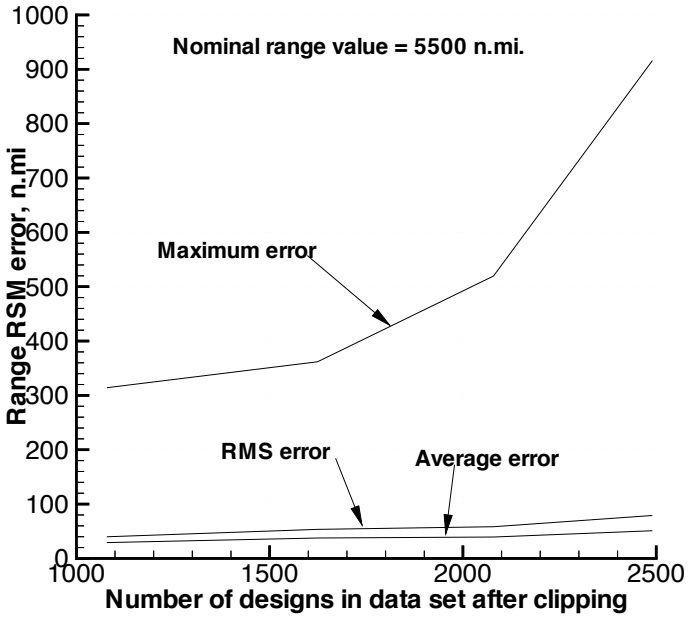

Figure 4.1: Effect of clipping on the range constraint response surface model fitting errors.

Data clipping takes out those design points for which the response function values fall outside of the user specified region. The closer the clipping limits are to each other, the fewer design points will fall into that region. Assuming that the source of designs with the values of the response function far from the average (range constraint in this case) is the noise in the "exact" analysis method used for evaluation, clipping can provide necessary smoothing of the RS data and will improve the overall response surface model accuracy. On the other hand, if the reason for such designs (designs with the value of the response function far from the average) is a poor sampling of the design space, clipping is simply a cheap means of improving an *apparent* error of the model and may very well lead to losses of information and impaired performance of the model. Thus, it is desirable to avoid data clipping when possible. The minimum number of designs left after clipping, and consequently the clipping range of the response function value, were limited by the amount of data points required for reliable fitting of the modeling polynomial. The desired ratio of number of designs to the number of terms in the polynomial was defined earlier to be around 3–4, which means

that for the full polynomial in 25 variables (351 terms) at least 1050 design points are necessary. Since the number of polynomial terms usually may be reduced by the one-step backwards regression, the minimum size of the data set may be lower than the above number.

The allowable clipping limits were determined for each response surface model so that at least 800–1000 design points were left after the clipping procedure in each data set. Table 4.4 lists the clipping ranges for each aerodynamic constraint, except for constraints 47, 50, and 66. These were excluded from consideration due to the reasons discussed below. The designs having the value of the response function (one of the aerodynamic constraints) outside of the specified range were discarded, and the rest of the designs were used for the least squares polynomial fit. This procedure was done for each of the response surface models, so the discarded designs were not necessarily the same in each case.

Next, one-step backwards regression was performed for each constraint by *RSG* to determine the optimum structure of the polynomial that provides the lowest errors. Each time a term with the highest value of the coefficient of variation is removed from the model, *RSG* checks the errors of the response surface model using either the same points (fitting errors) or the second set of data (prediction errors). The latter errors are usually greater than the former ones. In the case of the expensive aerodynamic constraint response surface models the ratio of the errors was about 2, which is quite high and may be an indication of poor response surface approximation.

Figures 4.2 and 4.3 show the effect of removing unreliable terms from the modeling polynomial for the range constraint response surface model. On the first plot errors are based on the same design points that were used for generating the model (fitting errors). As the number of terms goes down, the errors grow steadily, indicating that quality of the least squares fit deteriorates as the available flexibility of the model is reduced. The second plot shows that even though the fitting errors may be greater for the reduced polynomial, when computed on a different set of design points the response surface model performs better without unreliable terms than with the full size polynomial. The errors decrease considerably as unreliable terms are excluded from the model polynomial (Figure 4.3). A similar effect was observed for the rest

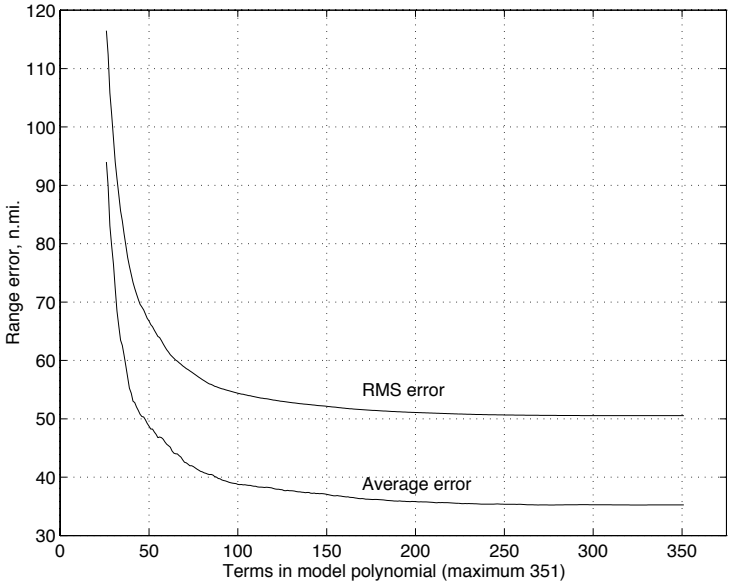

Figure 4.2: Range constraint response surface model fitting errors (computed at the same design points) versus number of terms in the model polynomial.

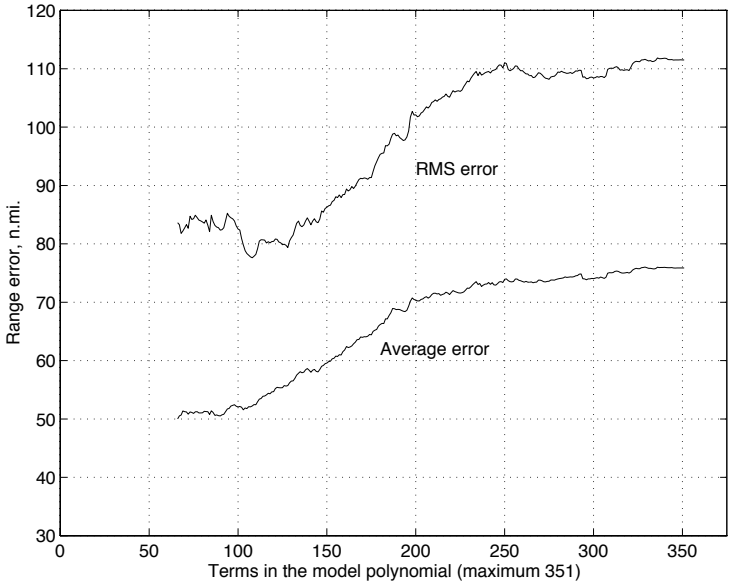

Figure 4.3: Range constraint response surface model prediction errors (computed at different design points) versus number of terms in the model polynomial.

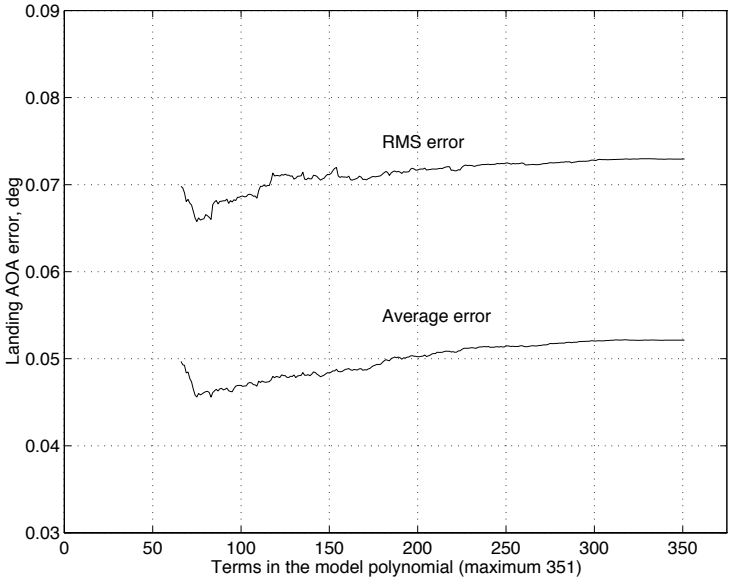

Figure 4.4: Landing AOA constraint response surface model prediction errors (computed at different design points) versus number of terms in the model polynomial.

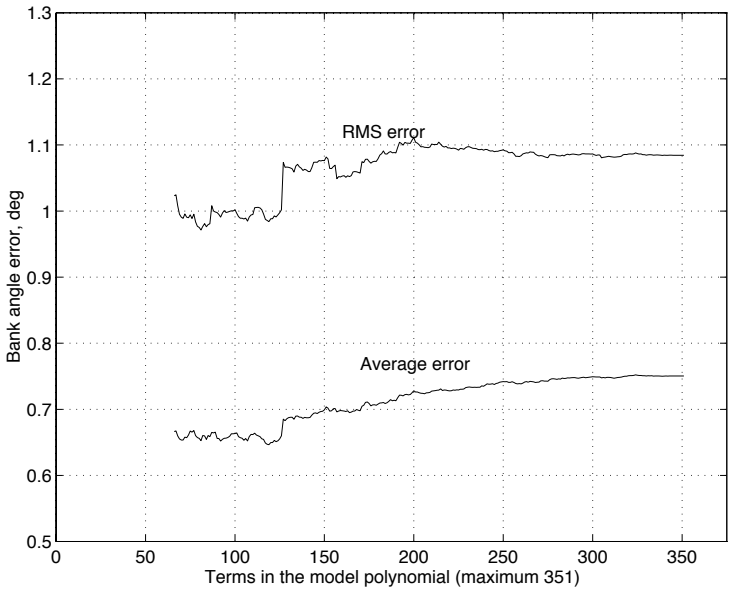

Figure 4.5: Bank angle constraint response surface model prediction errors (computed at different design points) versus number of terms in the model polynomial.

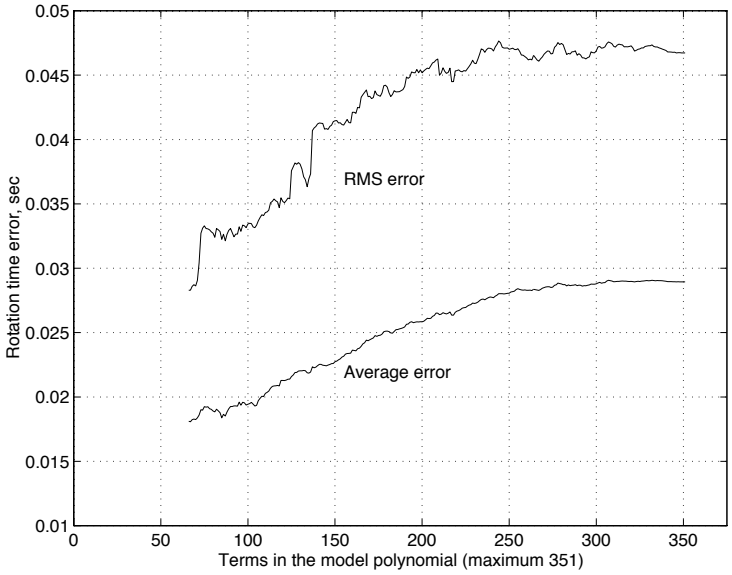

Figure 4.6: Rotation time constraint response surface model prediction errors (computed at different design points) versus number of terms in the model polynomial.

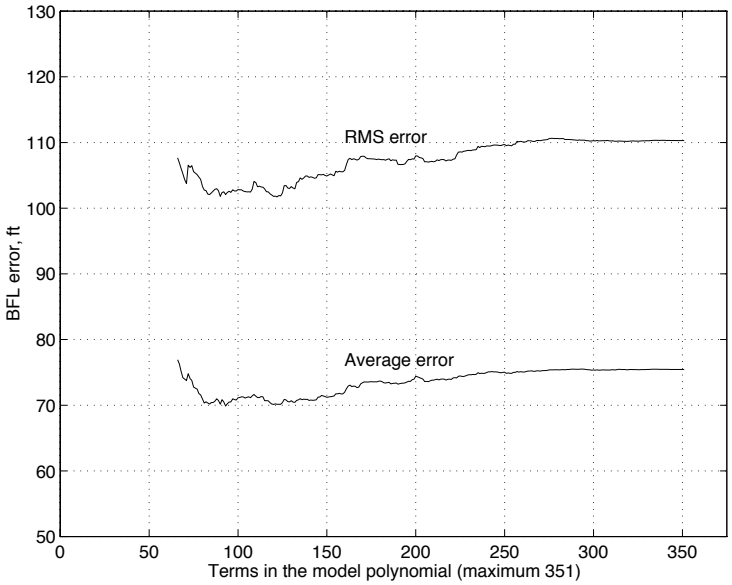

Figure 4.7: BFL constraint response surface model prediction errors (computed at different design points) versus number of terms in the model polynomial.

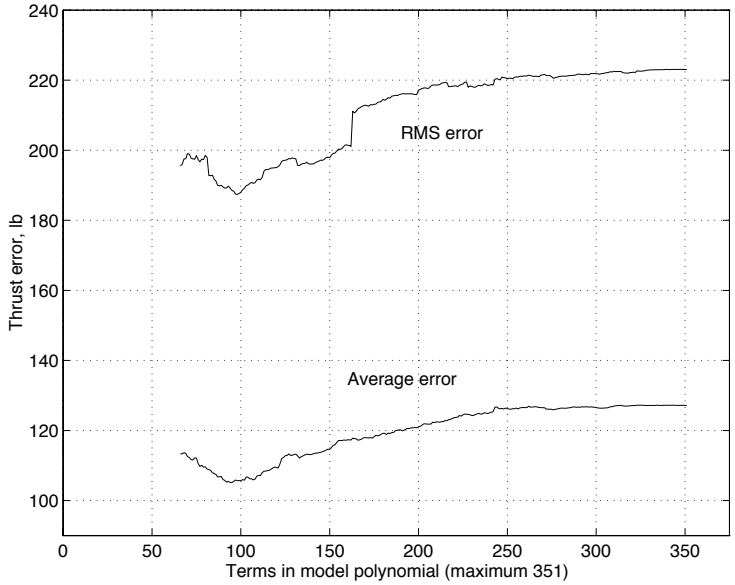

Figure 4.8: Cruise thrust constraint response surface model prediction errors (computed at different design points) versus number of terms in the model polynomial.

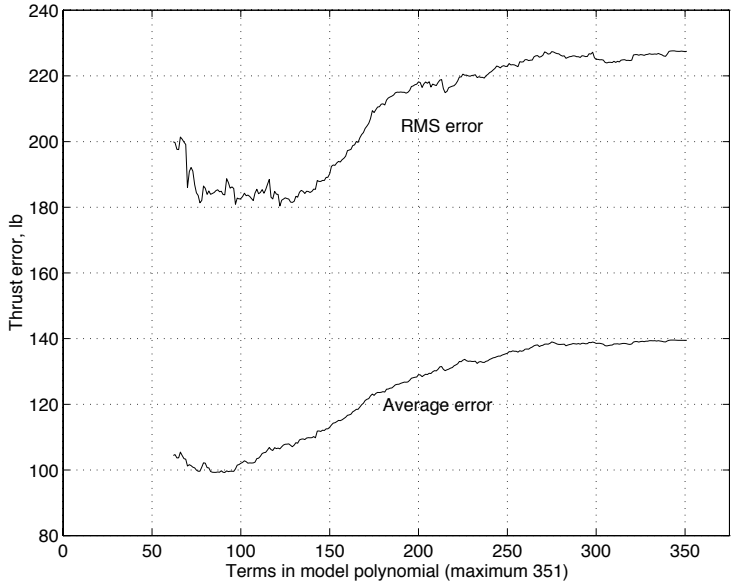

Figure 4.9: Climb thrust constraint response surface model prediction errors (computed at different design points) versus number of terms in the model polynomial.

Table 4.4: Clipping ranges for response surface models for aerodynamic constraints.

#	Description	Clipping range* (non-dimensional)	Clipping range converted to units	Limiting value of the constraint
1	Range	-3.0...-1.5	4675...5087.5 n.mi.	5500 n.mi.
21	Landing AOA	0.1...0.35	12.1...12.4 deg.	12 deg.
48	Bank angle	32.0...42.0	0.116...0.152 deg.	5 deg.
49	Takeoff rotation	0.05...0.21	3.95...4.75 sec.	5 sec.
52	BFL	-0.05...0.20	8750...11053 ft	10500 ft
67	Thrust (climb)	-4.1...-2.9	4 x (23010...27690) lb	4 x 39000 lb
68	Thrust (cruise)	-4.5...-3.4	4 x (21450...25740) lb	4 x 39000 lb

*Non-dimensional clipping limits are values of the lower and upper bounds on each response function value (aerodynamic constraint). Dimensional clipping limits show allowable values of the physical parameters (range, angle-of-attack, etc.) resulting from the clipping limits on each constraint.

of the response surface models, as seen in Figures 4.4 through 4.9. The final form of the response surface model polynomial is then defined as the one having minimum prediction errors. In the case of the range constraint response surface model a 110 term polynomial was chosen (Figure 4.3).

Table 4.5: Final errors of created response surface models for aerodynamic constraints.

#	Description	Polynomial (# of terms)	Average error	RMS error	Reference value
1	Range	110	50.9 n.mi.	82.5 n.mi.	5500 n.mi.
21	Landing AOA	75	0.047 deg	0.066 deg	12 deg
48	Bank angle	120	0.65 deg	0.98 deg	5 deg
49	Takeoff rotation	66	0.0185 sec	0.0285 sec	5 sec
52	BFL	125	73.5 ft	102.4 ft	10500 ft
67	Thrust (climb)	100	105 lb	187 lb	4 x 39000 lb
68	Thrust (cruise)	96	99 lb	183 lb	4 x 39000 lb

Response surface models were generated for a total of seven aerodynamic constraints, excluding constraints 47, 50 and 66. Table 4.5 contains the final results of generating response surface models for expensive aerodynamic constraints. Constraint 47 (rudder deflection) is not included in the table, since it had a constant value for all design points in the set and a response surface model was not created for

this constraint. Constraints 50 (tail deflection) and 66 (engine out) are also not in the table. The reason is that all attempts to fit a polynomial to data points for these constraints failed to produce acceptable results, meaning that the errors were several orders of magnitude greater than the predicted values of the constraints. This had to do with the way the constraints are formulated in the *HSCT* code and will be briefly discussed in the next section.

A few more comments should be made here concerning the accuracy and performance of the response surface models created. First, even though the relative errors of the models look reasonably good (50.9/5500=0.9%), the effect of these inaccuracies on the optimization may be rather significant. With the estimated requirement of 90 lb of fuel to compensate for 1 n.mi. of range deficiency, a 50–80 n.mi. error can result in a 4,500–7,200 lb difference in TOGW, which can easily bring the optimizer to a false optimum far from the true optimum configuration. Second, one has to remember that the optimizer can easily exploit the regions of design space where response surface models have favorable errors for the objective function value. By pursuing these false directions the optimizer can find areas of large discrepancies between the response surface model and the true values of the aerodynamic parameters, effectively making the response surface model invalid.

Figure 4.10 illustrates the performance of the range constraint response surface model. The plot was obtained by taking the baseline design and varying one of the design variables (wing root chord on the top plot and wing semispan on the bottom plot of Figure 4.10) in both directions, holding all other design variables fixed, while evaluating the actual and the response surface model values of the constraint. While the behavior of the response surface model looks acceptable in the direction of the wing root chord axis, the shape of the actual constraint function is quite poorly approximated in the direction of the wing semispan axis, indicating that probably not enough (or no) data was available in the direction of reducing the wing semispan. This situation illustrates that performance of an response surface model may by good in some directions but poor in others where sampling of the design space was insufficient and no data was available for a reliable least squares fit. Such regions of the design space space may be easily exploited by the optimizer. Thus the selection of points in the design space is a critical consideration.

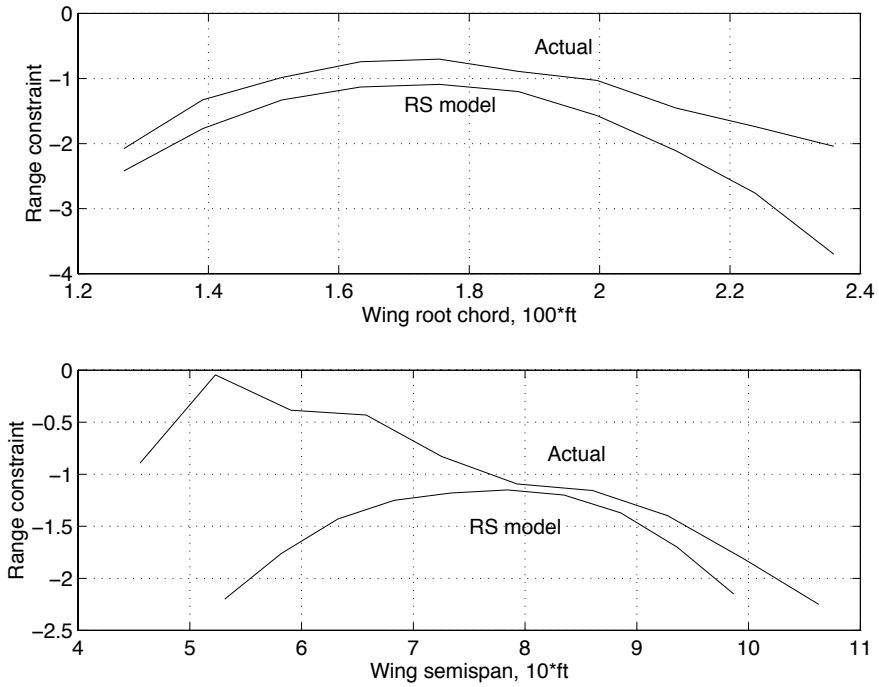

Figure 4.10: The range constraint RS model performance (cuts through the design space along the wing root chord and wing semispan axes).

4.1.4 Issue of Constraint Formulation

It was pointed out in the previous section that constraints 50 (tail deflection) and 66 (engine out) exhibited very irregular behavior unsuitable for fitting with a quadratic polynomial. A closer look at the data in Table 4.2 will reveal that the extremum values of these constraints are very far from the average value, suggesting that very rapid changes in the function value are observed in the region.

Indeed, plotting these constraint functions against some of the design variables (Figures 4.11 and 4.12) confirms the suggestion of irregularity of the functions. Both constraints have clearly defined peaks on the plots, and can not be fit with a quadratic polynomial.

The explanation of the nonquadratic behavior of the constraints comes from examining their formulation in the *HSCT* code. Going back to Table 4.2 one may see that for constraints 50 and 66, as well as for some others, the value of the actual

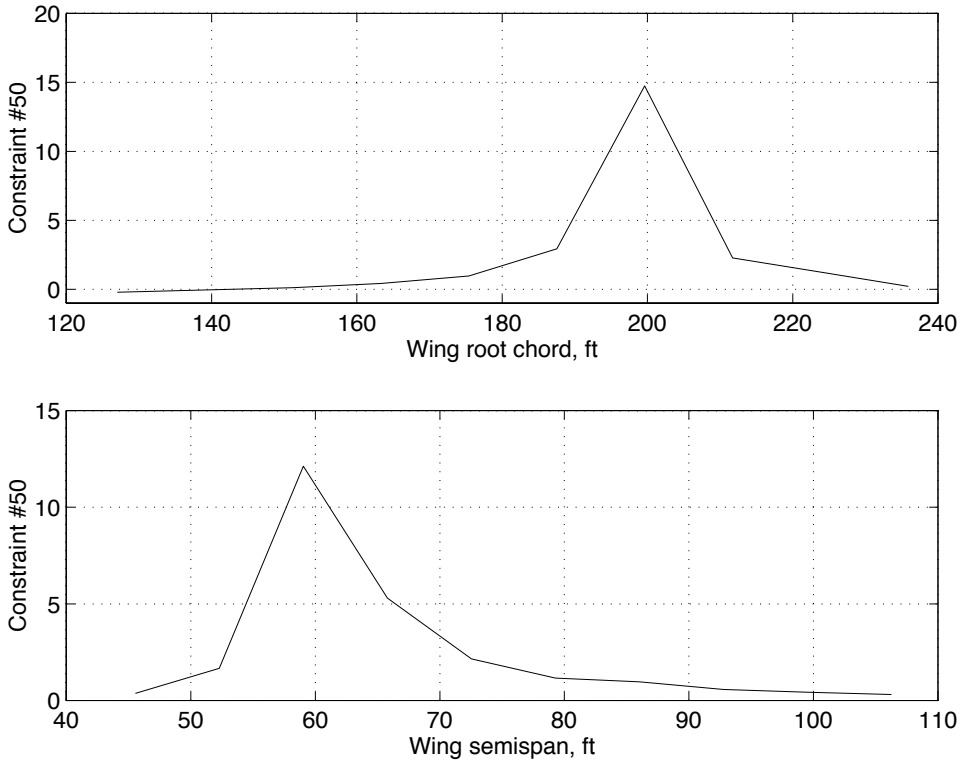

Figure 4.11: Constraint 50 (tail deflection) vs. wing root chord and wing semispan.

physical parameter being restricted is placed in the denominator of the function formula (i.e., $g = UL/|PV| - 1$ for constraint 50, where UL is an upper limit, $|PV|$ is the absolute value of the parameter being limited). This produces a highly nonlinear constraint function even though the parameter itself may have been a linear function of the design variables. While the behavior of a constraint function with the physical parameter in the numerator will be similar to that of the parameter itself, when the physical quantity is placed in the denominator, function behavior changes considerably depending on the range of values of the quantity and it may even have singularities if the quantity is allowed to assume zero values. Figures 4.13 and 4.14 clearly show the described situation. Tail deflection angle required for approach trim, which is the parameter regulated by constraint 50, is plotted in these figures against the wing root chord and wing semispan, along with the actual (numerically computed) and theoretical (computed using the constraint function and a smooth polynomial fit

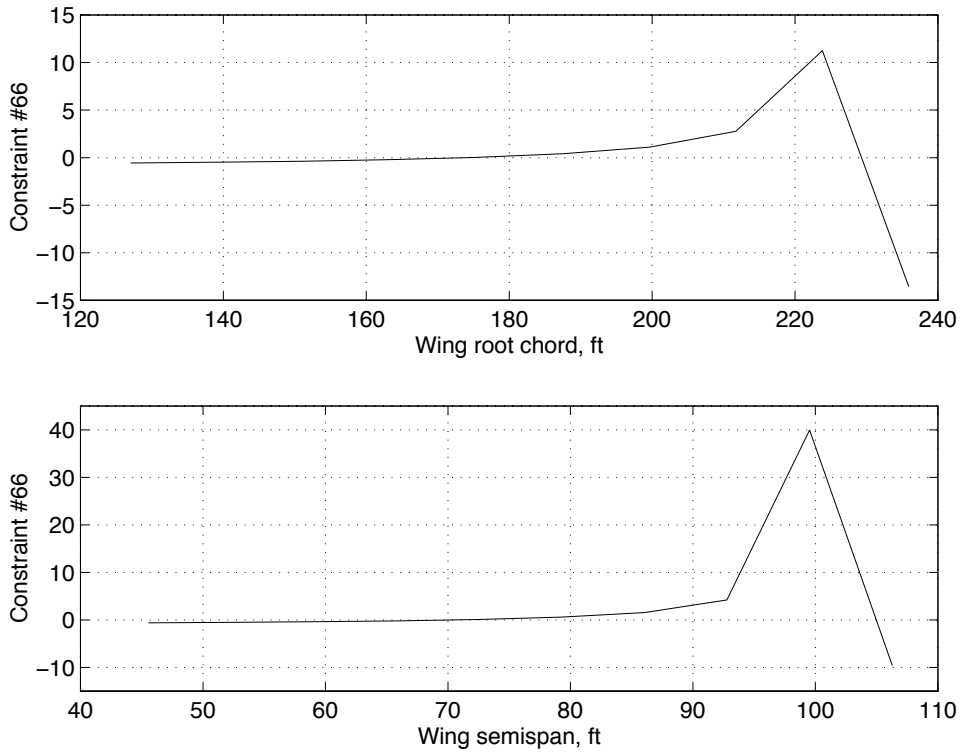

Figure 4.12: Constraint 66 (engine out) vs. wing root chord and wing semispan.

to the tail deflection data) curves for the constraint 50. The tail deflection curve is relatively smooth and does not exhibit any peaks or sharp kinks, but it does go through zero exactly at the places where constraint 50 has peaks, indicating that these peaks are actually points at infinity, as is seen for the theoretical curves. Constraints 50 and 66 were excluded from further consideration in the construction of the RS models. The original formulation of these constraints was poor and resulted in a poor RS approximation.

The lesson learned from working with these data is that such constraint formulations should be avoided. An optimizer may have difficulties working with these constraints, and they should be reformulated in the *HSCT* code. Of course, this data can not be used for polynomial response surface modeling. Actual physical parameters

may be a better choice for response surface model fitting, but in any case checking the behavior of the underlying function is recommended before building response surface models.

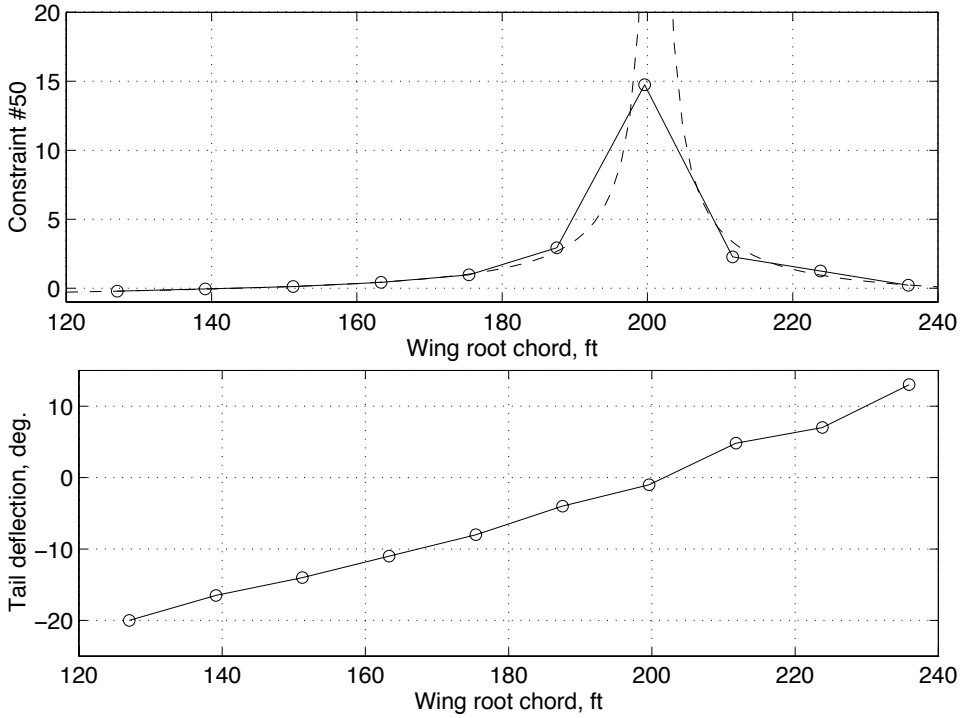

Figure 4.13: Tail deflection for approach trim vs. wing root chord and constraint 50 actual and theoretical curves.

4.2 Range Constraint Response Surface Model in MDO of HSCT.

Even though the quality of the response surface models was not as good as expected, it was decided to try optimization using response surface models in place of some of the aerodynamic calculations. Since one of the most critical constraints for HSCT design is the range constraint, the decision was made to use the response surface model for the range constraint in the optimization trials. Analysis methods needed

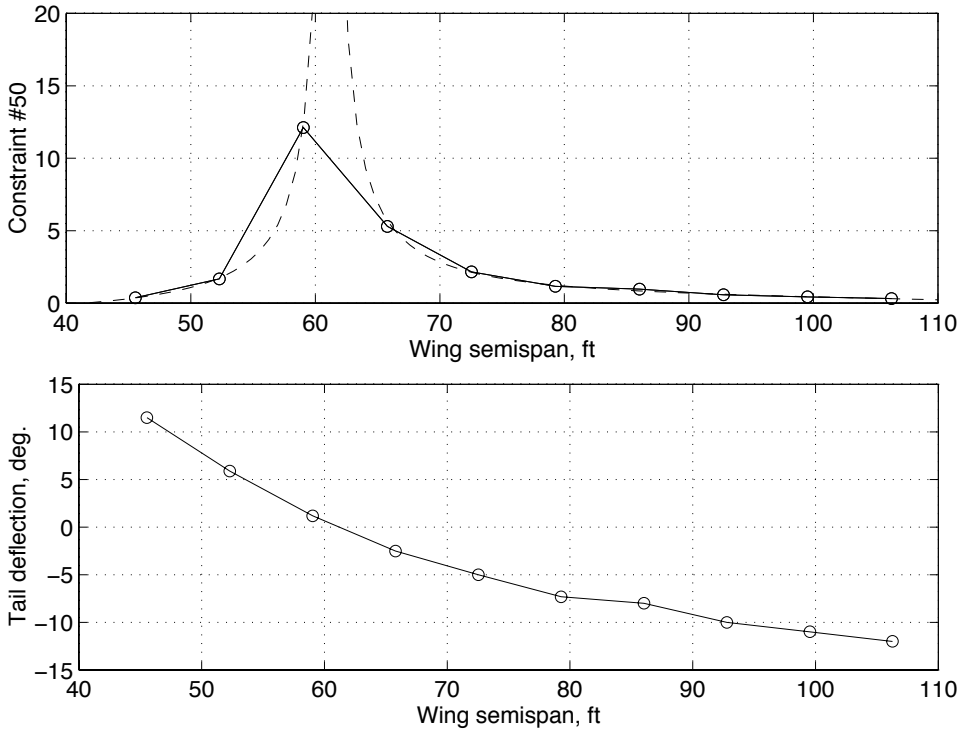

Figure 4.14: Tail deflection for approach trim vs. wing semispan and constraint 50 actual and theoretical curves.

for determining the range of the aircraft, in particular the "exact" and "approximate" wave drag calculation, introduce a lot of noise into the optimization, so success in using this response surface model could be quite beneficial for the optimization.

4.2.1 HSCT Coding Issues

The *HSCT* code was modified to call the RS model subroutine instead of the actual range aerodynamic analysis to evaluate the range constraint value, so that every time the optimizer calls the constraint subroutine, the response surface model function is called. The block diagram in Figure 4.15 illustrates the way the range constraint response surface model was installed in the code. A special flag variable was introduced into the code responsible for choosing the method of range evaluation, so that easy switching from the actual range analysis to the response surface model was possible.

The optimization was started from the baseline design used for generating the design space (central design 1). Design variables 10, 25, 26 and 29, which were not used in generating design points for response surface models, were kept fixed during the optimization, effectively turning the problem into 25 design variable optimization.

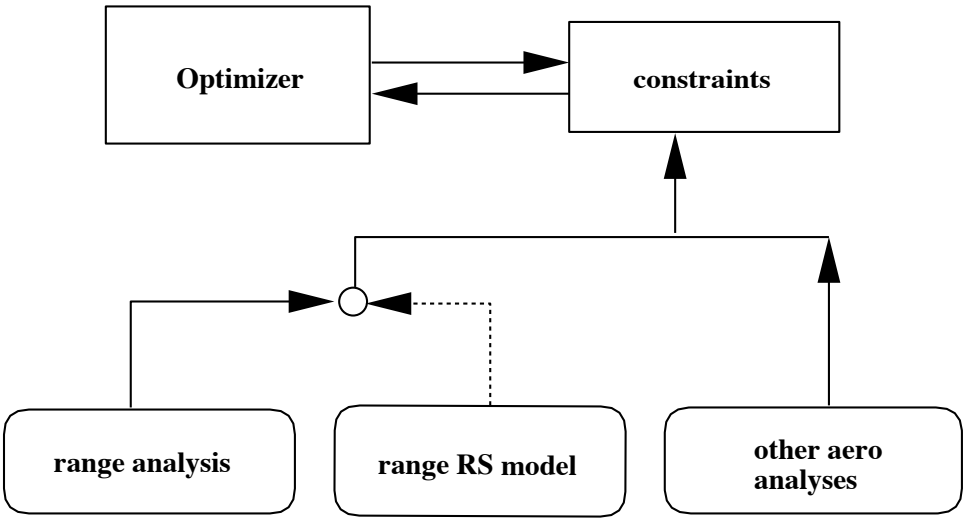

Figure 4.15: Block diagram of range response surface model installation in the *HSCT* code.

To prevent the optimizer from exploiting regions of the design space where the response surface model would be invalid, 52 extra constraints were introduced into the *HSCT* code. These were the same constraints that served for defining the reasonable design space used for generating the response surface models (Section 3.3). Table 4.6 lists all of the 52 extra constraints.

4.2.2 Optimization Trials Using the Range Constraint Response Surface Model

Optimization was started each time from the baseline design (central design 1). Twenty cycles were completed in the first optimization run using the 110 term polynomial for the range constraint response surface model. The optimization was then stopped. The history plots of the actual range, the response surface model range (deduced from the response surface model constraint value) and the take-off gross

Table 4.6: Extra constraints used for optimization with response surface models.

# of constraint	Description
1-2	20,000 lbs $< W_{b_F} <$ 120,000 lbs
3-24	Minimum fuselage radius
25	Inboard $\Lambda_{le} >$ Outboard Λ_{le}
26	$\Lambda_{le} > 0$
27-28	5,000 ft$^2 < S_w <$ 15,000 ft^2
29-30	$1.0 < AR < 3.2$
31	Inboard $\Lambda_{te} < 40°$
32-49	$c_{y_{i+1}}/c_{y_i} < 1.0$
50	Approximate range > 5,000 n. mi.
51-52	0.8*Thrust required < Thrust available ("approximate" analysis)

weight are shown in Figure 4.16. The plots show that almost immediately after starting optimization the optimizer went into a region of design space where errors of range prediction by response surface model were very large. The difference between the actual and the response surface model predicted range increased to about 2,500 n.mi., and was still increasing at cycle 20 when the optimization process was stopped.

Planforms of the configurations after cycle 10 and 20 are shown in Figure 4.17 together with the baseline design. The plots show that optimization went in a somewhat nonsense direction of decreasing the wing area by reducing the root chord and in general pursued strange wing shapes. Apparently, the response surface model artificially maintained the required range, which allowed the optimizer to use such configurations in order to satisfy other constraints and reduce TOGW.

After several attempts to run an optimization with similar results, it was decided to use a different polynomial for the response surface model. As described earlier, the 110 term polynomial was used up to this point, since it produced low prediction errors (Figure 4.3). Next, a 200 term polynomial was chosen from the series of polynomials produced by the one-step backwards regression process. This model gives higher prediction errors when computed on the available set of design points, but possibly contains more information about the range constraint which may have been lost in

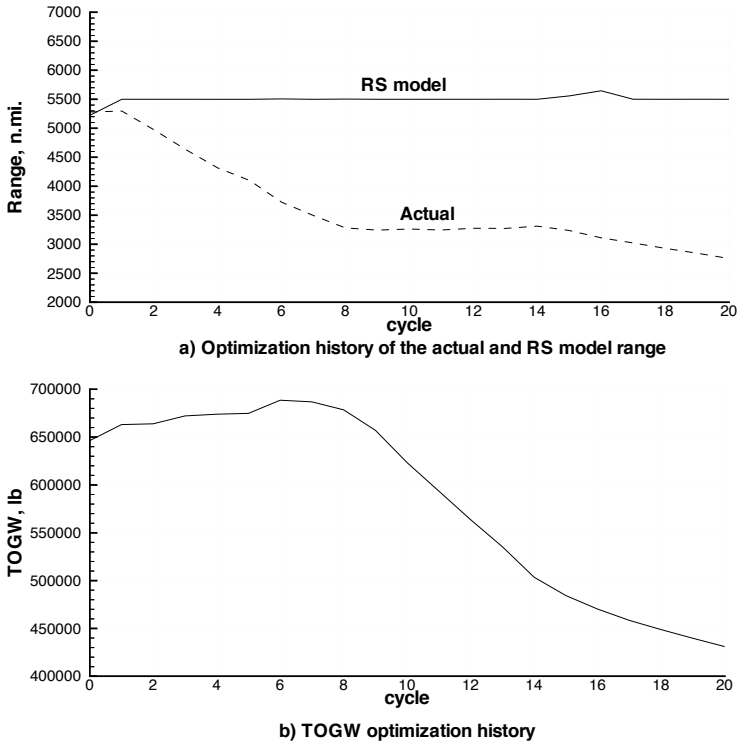

Figure 4.16: History plots of range and TOGW for optimization run with the range constraint response surface model (RS model range is calculated from constraint value).

110 term model. Move limits for the optimizer were reduced from about 8–10% in the previous runs to about 4–5%.

Figure 4.18 shows the history plots of this optimization run, and planforms are shown in Figure 4.19. As one can see, the optimizer went in a different direction this time, but again reducing wing area and overall size of the aircraft and creating nonsensical configurations. Interestingly, after cycle 12 the range predicted by the response surface model began increasing above the 5500 n.mi. constraint, which seemed strange as the optimizer could further reduce TOGW by simply reducing the fuel weight. A closer look at the design variables showed that the fuel weight was being reduced at this time by the full 4% each cycle and couldn't be reduced farther without violating the move limits.

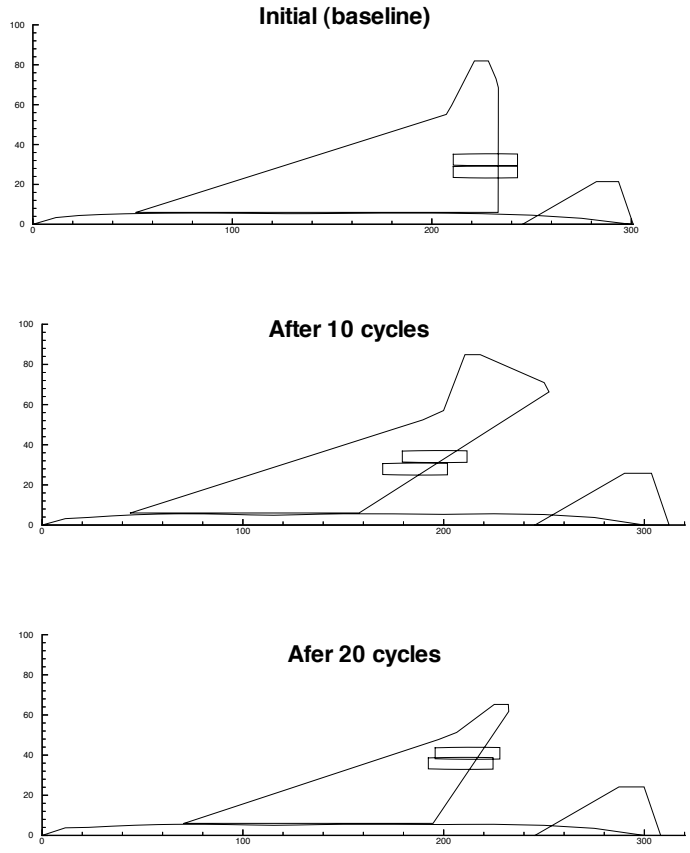

Figure 4.17: Planforms of optimization run with the range constraint response surface model.

It was clear at this point that the created response surface models did not provide adequate accuracy for use in optimization. Since one of the main reasons for poor response surface models' quality was suspected to be an unsatisfactory design space in which the models were created, further attempts to improve the optimization process were discontinued at this time in favor of generating a new reasonable design space closer to the feasible space of the current HSCT problem.

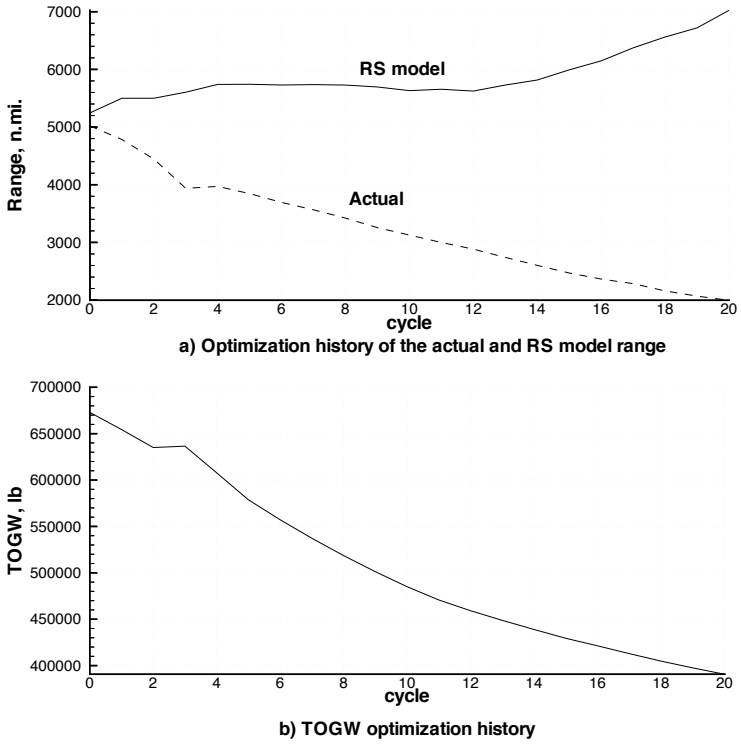

Figure 4.18: History plots of range and TOGW for optimization run with 200 term range constraint response surface model (RS model range is calculated from constraint value).

4.3 Response Surface Models for Drag Components

4.3.1 Generation of Response Surface Models and Accuracy Analysis

One of the possible reasons for poor performance of the response surface model for the range constraint could be a non-quadratic behavior of the range itself as a function of the design variables (e.g., see Figure 4.10). Range directly depends on the value of the cruise drag coefficient of the aircraft, which in turn is comprised of several components depending on the design variables themselves. Five major parameters contributing to the value of the cruise drag coefficient may be identified: $C_{D_{fric}}$ — friction drag

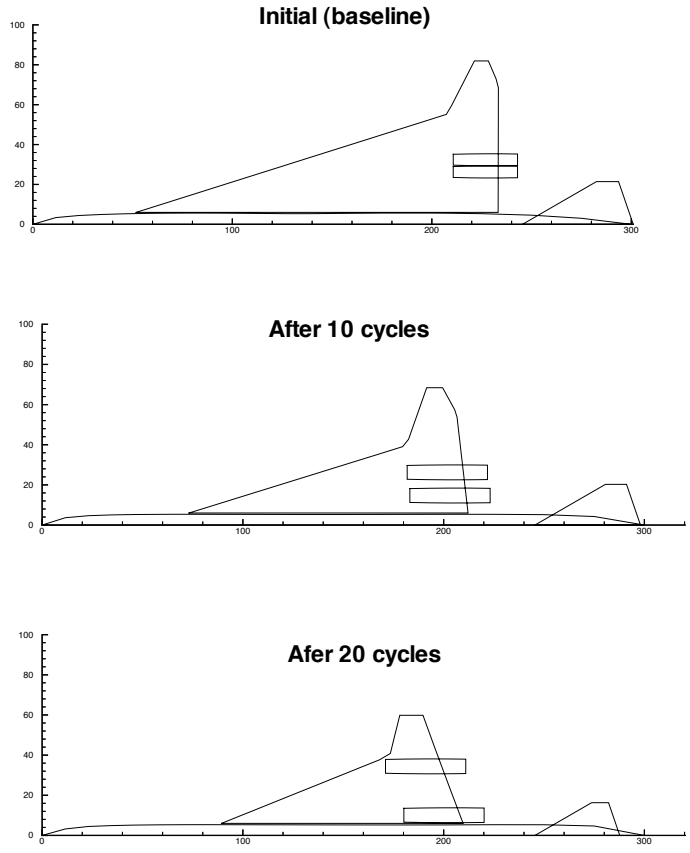

Figure 4.19: Planforms of optimization run with 200 term range constraint response surface model.

coefficient, $C_{D_{wave}}$ — wave drag coefficient, C_{L_α} — lift curve slope, C_T/C_L^2 — leading edge suction term, LES_{att} — amount of attainable leading edge suction. The most expensive calculation, and also the one introducing the most noise, is the wave drag analysis. Induced drag terms (lift curve slope and leading edge suction terms) are determined by the high speed aerodynamic analysis routines and also are costly when "exact" analysis is required. Friction drag is the least expensive calculation.

The decision was made to create response surface models to all drag components using the same set of 2490 design points used for the range constraint response surface model and compare the performance of these models in predicting the HSCT range

with the performance of the range constraint response surface model. Since each individual component is a simpler function of design variables than a combination of all of them, some benefits may be expected from this approach in the sense that a better quadratic fit can be obtained for each separate function. This may reduce the final errors of range prediction.

The `ANALYZE` routine in the *HSCT* code was set up to print out the values of the drag components and all designs in the set were fed into the code again to get the values of all the coefficients. The *RSG* code was then used in the same manner as before to generate response surface models for the drag components. Data clipping and one-step backwards regression were performed as described earlier using one half of the set of designs. Table 4.7 lists the resulting prediction errors of the response surface models as computed on the second half of the set.

Table 4.7: Final errors of created response surface models for drag components

Parameter	Average error	RMS error	Typical value
$C_{D_{fric}}$	0.64×10^{-5}	1.01×10^{-5}	400×10^{-5}
$C_{D_{wave}}$	0.55×10^{-4}	0.84×10^{-4}	18×10^{-4}
C_{L_α}	0.0045	0.0075	1.6
C_T/C_L^2	0.0017	0.0050	0.12
LES_{att}	0.0128	0.0214	0.7...0.8

To make the accuracy comparison of range prediction between the range constraint response surface model and the drag components' response surface models, range evaluations were performed first using the actual aerodynamic routines of the *HSCT* code, then using the range constraint response surface model and the drag components' response surface models. Differences between the latter two and the actual range were recorded and the distribution of the errors was then plotted.

Figure 4.20 shows histograms of the error distribution for both methods using all 2490 designs. The standard deviations for the range prediction error are 340 n.mi. for the range constraint response surface model and 109 n.mi. for the drag components' response surface models, meaning that the error is about 3 times smaller when using the drag components' RS models based range prediction.

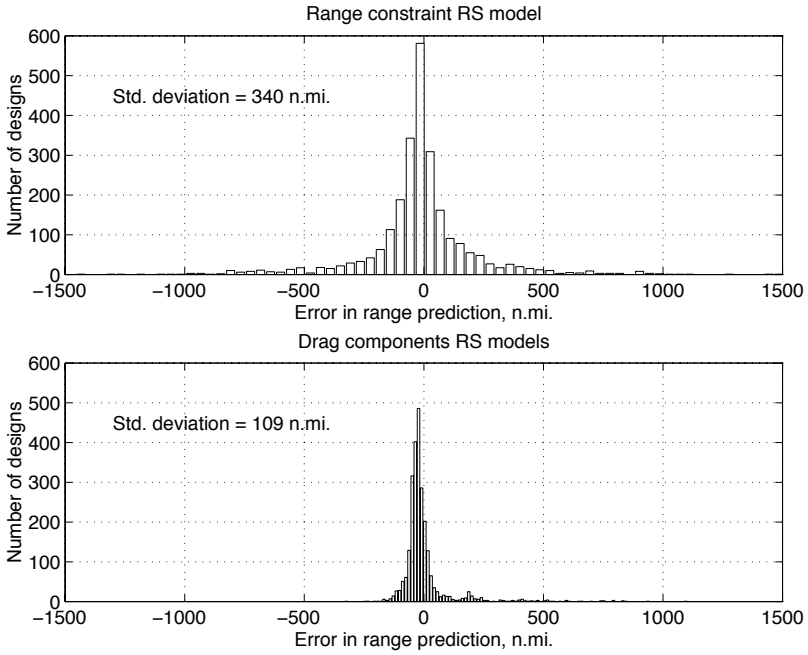

Figure 4.20: Distribution of errors for predicted range using the constraint response surface model and drag components' response surface models. Errors computed at all 2490 design points.

Figure 4.21 shows similar histograms for the case when data clipping is made before error processing. This means that only those designs are included in the error calculation that were used for creating the range constraint response surface model. The standard deviations for this case reduced to 78 n.mi. and 43 n.mi. with about 45% improvement in the expected prediction error value for the drag components' response surface models prediction method. The shift of the histograms for drag components' response surface models prediction errors may be explained by the fact that data clipping was based on different parameters for each response surface model, so that the designs used for the range constraint response surface model are not necessarily the same as those used for each of the drag components' response surface models.

The error comparison showed that in general, smaller prediction errors may be expected from using several approximations to simpler functions than one response

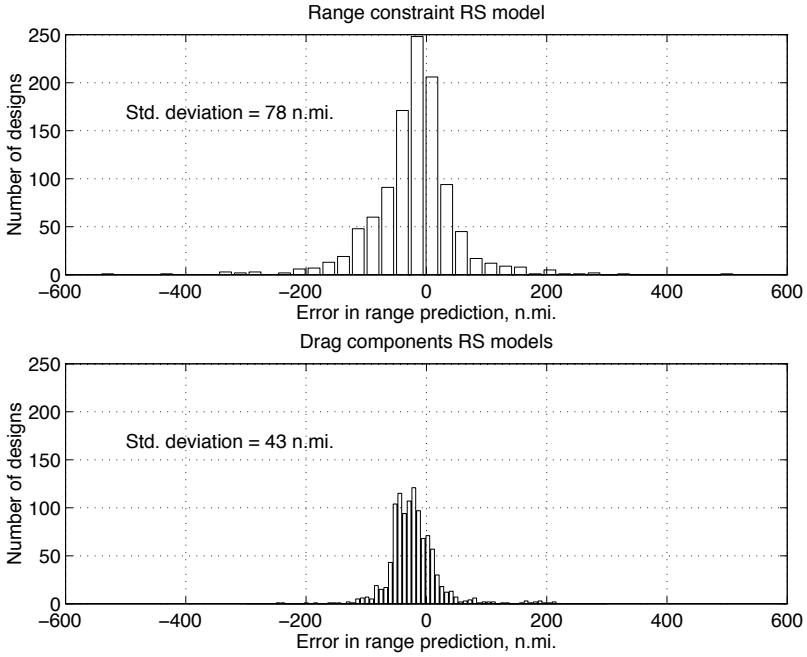

Figure 4.21: Distribution of errors for predicted range using the constraint response surface model and drag components' response surface models. Set of design points was clipped using the same clipping limits as for range constraint response surface model creation.

surface model for a complex function of aerodynamic parameters, such as the HSCT range. This difference decreases when data clipping is used to improve the apparent prediction errors. The same trend can probably be expected for a better sampled design space of smaller volume, when the actual function of design variables is closer to a quadratic and can be better approximated by a quadratic polynomial.

4.3.2 Drag Components' Response Surface Models in HSCT Code

Response surface models for drag components were installed in the *HSCT* code for trial optimization runs to see if any improvement in response surface model performance could be achieved compared to using the range constraint response surface

model. The code was set up to use the response surface models for all five parameters affecting cruise drag coefficient during optimization.

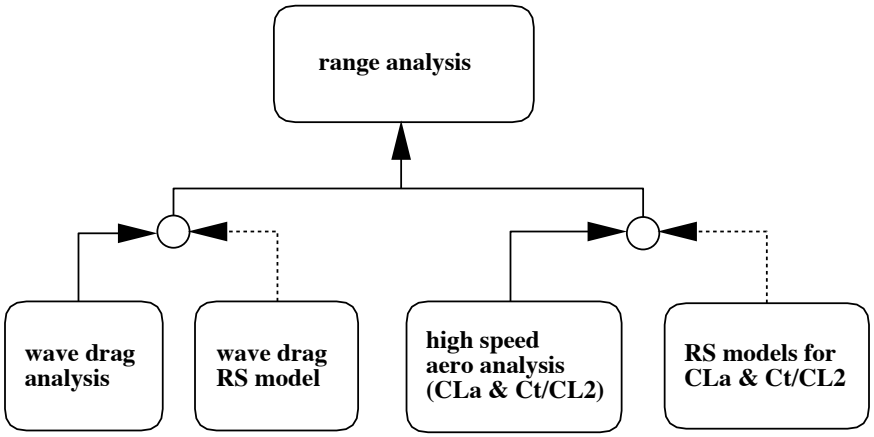

Figure 4.22: Block diagram of drag components' response surface models in the *HSCT* code (Friction drag ($C_{D_{fric}}$) and attainable LE suction term (LES_{att}) response surface models were used in the same fashion).

Figure 4.22 shows how the response surface models were used in the code. As shown on the block diagram, either actual drag analysis routines or response surface models could be used for range evaluation, depending on the value of the special flag variable responsible for this (see Appendix A for more detailed description of coding issues and location of the flag variables in the command file). The range analysis block on the diagram is the same routine pictured on the Figure 4.15. As one can see from these two diagrams, the difference between the two methods of applying response surface models is that instead of replacing the entire "range analysis" block, only drag analyses routines are replaced by response surface models and the range calculation is done using the same algorithms inside the range block that are used for normal range calculation. The wave drag, lift curve slope and leading edge suction related response surface models are called by the range routine only once per range calculation. The friction drag response surface model is called several times during the range integration since the actual friction drag is changing with the change in altitude (the algorithm of the range routine was preserved intact).

4.3.3 Optimization Trial Using Drag Response Surface Models

Optimization was started from the baseline design (central design 1) and stopped after 6 cycles. Figure 4.23 shows the optimization history plots of range and TOGW for this run.

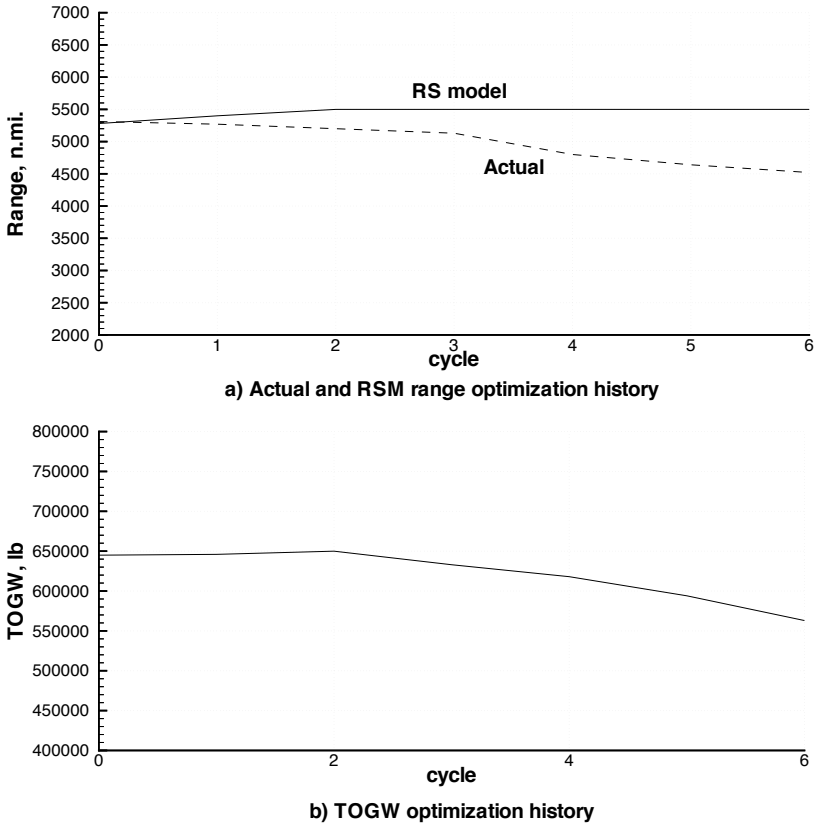

Figure 4.23: Optimization history plots of range and TOGW for optimization run with drag components' response surface models.

As in previous optimization runs with the range constraint response surface model, the optimizer quickly went in a direction of high errors of predicted range from response surface models. The difference between the actual and the response surface model predicted range reached about 1000 n.mi. after 6 optimization cycles, which

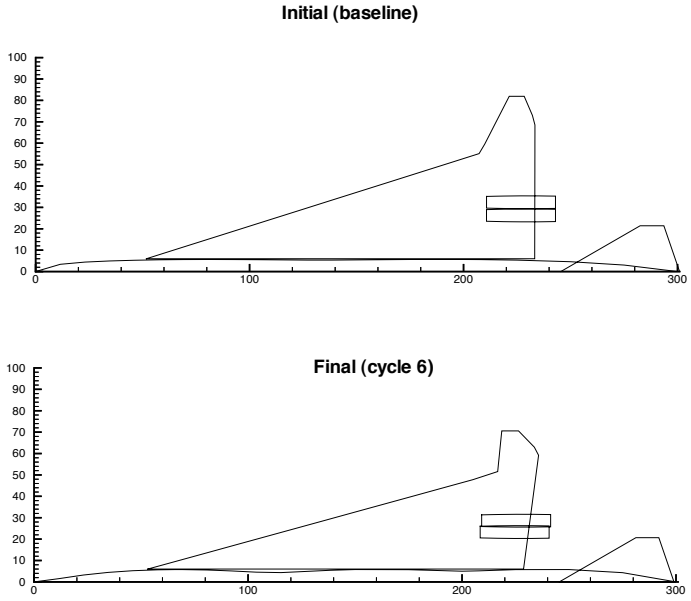

Figure 4.24: Initial and final (cycle 6) planforms for optimization run with drag components' response surface models.

is a smaller value than in previous runs but is still unacceptable. Initial and final planforms of this optimization run are shown in Figure 4.24. Obviously, the optimizer was pursuing "unnatural" configurations, although the size of the aircraft did not decrease as much as in the previous runs.

The quality of the created response surface models was low in the sense that false optimum regions exist in the design space where the response surface model predicted range can be kept at the required revel while the actual range has very low values and the configuration of the aircraft is in general nonsensical. At this point no further attempts were made to improve the performance of the response surface models, as one of the reasons for their low prediction capabilities was improper design space sampling. As already mentioned, practically the whole region of design space where the response surface models were built and are expected to be valid lies in the infeasible domain. Thus, it was decided to abandon these response surface models and generate a new reasonable design space closer to possible optimum designs, and

preferably in the feasible domain. Then new response surface models that would be valid in the feasible domain, would be created.

4.4 Lessons Learned

Several observations and conclusions should be pointed out here before proceeding:

1. Response surface models to aerodynamic constraints of the HSCT can be constructed with reasonable values of fitting and prediction errors, but in some cases building approximations to the actual physical parameters (range, landing AOA, etc.) instead of the constraint functions may be more beneficial. Care should be taken to avoid fitting highly non-quadratic functions, especially those having singularities in the considered range of design variables, since this makes fitting a polynomial to the function impossible. In general, the constraint formulation should be done so that the constraint is a linear function of the physical parameter. In any case, inspection of the behavior of the function in the region of interest is necessary before proceeding with response surface model generation.

2. Proper sampling of the design space is extremely important for successful generation of response surface models. The design points chosen for response analyses and response surface model generation should be located in the region of expected optimum design for reliable use of response surface models in optimization. If the optimum design is located far outside of the valid response surface model region, optimization with response surface models will produce unreasonable errors.

3. Apparent prediction errors of the response surface models checked on the preselected set of deign points may not be a fair estimate of the response surface model performance in optimization — much greater errors can be expected in optimization as the optimizer will always be exploiting regions of weakness of the models. Special measures may be necessary to prevent errors from growing

— either by updating information about the true response and revising the response surface model, or by means of preventing the optimizer from going into invalid response surface model regions.

Chapter 5

Range and Drag Components' Response Surface Models in HSCT Optimization (29 Design Variable Problem)

5.1 Changes in the Design Space Used

Working with response surface models in 25 dimensional space, described in the previous chapter, revealed the problems with the models built on the old set of 2490 designs. It was decided to generate a new reasonable design space using the current version of the *HSCT* code, which includes several new constraints. A new baseline design was chosen as described in Section 3.1 by running an optimization of the HSCT with tightened constraints. This produced a somewhat oversized feasible design, central design 2 (Figure 3.3 and Table 3.1), which served as the base point (nominal design) for generating a reasonable design space for new response surface models. The increased weight and size of the configuration are the result of making constraints more severe. Although far from the actual optimum configuration with normal constraint levels, this design is located farther inside the feasible domain, with

the only active constraint being 49 (take-off rotation time $\leq$ 5sec.) and all other constraints satisfied with some margins. This allows some freedom of movement around the baseline design without significant violation of the constraints. An optimum design (global or local) on the other hand would be located in a corner (or a "pocket") of the feasible design space and any movement from that location will be limited to a specific direction to avoid grossly violating the constraints. Since selection of the design points for response surface models is done by changing design variables in random directions with only 1-3 DVs changing at a time, most of the designs end up in the unfeasible domain and then have to be moved back to the central design according to Equation 3.3. Having the central design farther inside the constraint boundaries helps to increase the number of the feasible or near feasible designs in the generated set. Because of the algorithm used for creating the set of reasonable designs, where all grossly infeasible designs are moved towards the baseline design (see Section 3.3), it is very important to have as many as possible feasible or near feasible designs in the generated initial set to avoid close placement of the designs moved back toward the baseline design.

The same steps for reducing the reasonable design space and *D*-optimal selection were performed as in the previous problem. This resulted in two sets of design points: set A of 1446 designs for response surface model generation and set B of 1426 designs for model error estimation, as described in Section 3.4. Designs in both sets were evaluated using the specially set up `ANALYZE` case (Section 3.5) in the *HSCT* code to get values of the range and drag components for each design.

5.2 Generating Response Surface Models

Response surface models for the range of the HSCT, $C_{D_{wave}}$, C_{L_α}, and C_T/C_L^2 were generated. Using the *RSG* code, one-step backwards regression (Section 3.6.3) was performed to get the error data for each response surface model while varying the number of coefficients in the model polynomials. One term with the highest value of the coefficient of variation was removed from the response surface model polynomial on each step and errors were evaluated for this model polynomial. The error data for

the range response surface model are plotted in Figures 5.1 and 5.2. On the first plot the errors computed at the same points that were used for response surface model generation (data set A) are shown (fitting errors). On the second plot the prediction errors (computed on data set B) are plotted.

The overall level of errors is much less now than it was for the 25 DV problem. Another thing to notice here is that the difference in fitting errors and prediction errors is much smaller now than it was for the 25 DV problem. This means that the design set A provides sufficient information for response surface model fitting so that the prediction performance of the model is much better. Another consideration is that the prediction errors again decrease down to a certain number of polynomial terms, where most of the unreliable terms have been removed. The majority of the discarded terms are second order interactions that did not have a large effect on the range or were difficult to define using the available information in the data set A. Among the linear terms discarded were some of the fuselage design variables, leading edge radius parameter, and nacelle 1 position. Further polynomial reduction leads to losses of information and increases the prediction errors. The optimum number of terms, judging by Figure 5.2, is about 130–150. Thus, a 150 term polynomial was chosen for the range response surface model.

Similar plots for the response surface models of the drag components are shown in Figures 5.3 through 5.5. The response surface models were generated using data set A and computed at data points of set B in each case. For each response surface model the optimum number of terms in the polynomial was determined by the minimum RMS value of the prediction error. The polynomials have 125 terms for the wave drag coefficient ($C_{D_{wave}}$) response surface model, 50 terms for the lift curve slope (C_{L_α}), and 40 terms for the leading edge suction coefficient (C_T/C_L^2) response surface models. Both the lift curve slope and the leading edge suction coefficient response surface models contain primarily wing planform related design variables and their second order interactions. The wave drag response surface model, besides the wing planform variables, also contains other parameters which affect the value of the wave

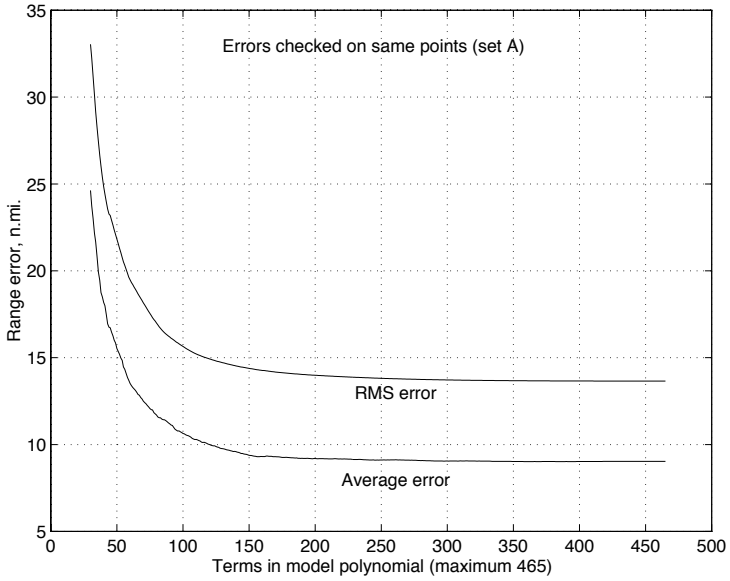

Figure 5.1: Range response surface model fitting errors (computed at the same design points) versus number of terms in the model polynomial.

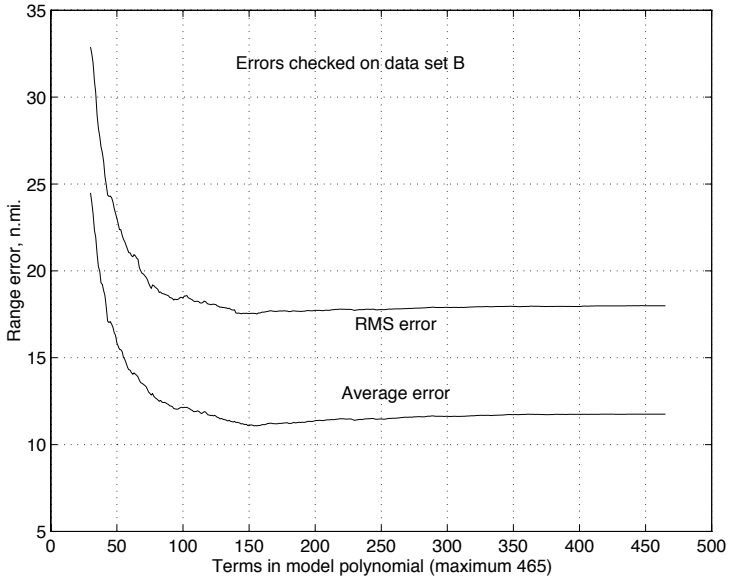

Figure 5.2: Range response surface model prediction errors (computed at the design points of set B) versus number of terms in the model polynomial.

drag coefficient, namely most of the fuselage design variables, the horizontal and vertical tail size design variables, and the engine thrust, along with their second order interactions. Table 5.1 lists the errors for all generated drag components' response surface models.

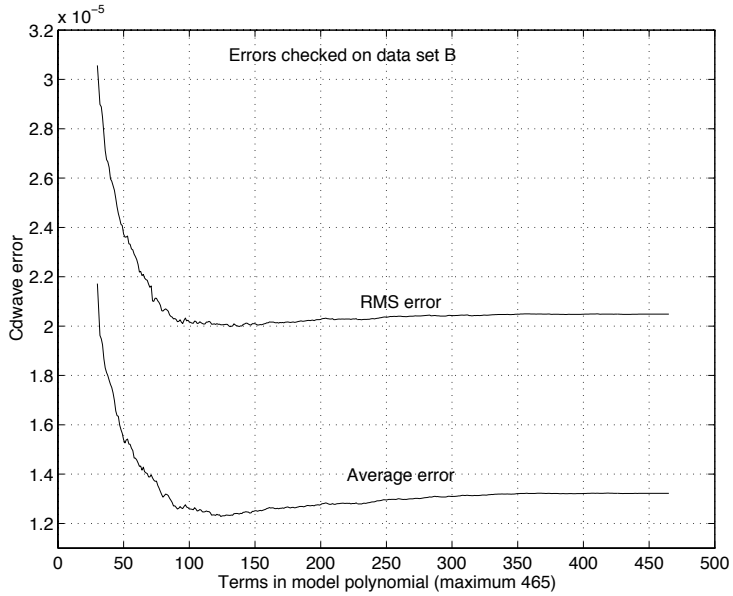

Figure 5.3: Wave drag coefficient ($C_{D_{wave}}$) response surface model prediction errors (computed at the design points of set B) versus number of terms in the model polynomial.

Table 5.1: Final errors of created response surface models for range and drag components.

Parameter	Average error	RMS error	Typical value
Range	11.07 n.mi.	17.51 n.mi	5500 n.mi.
$C_{D_{wave}}$	1.23×10^{-5}	2.00×10^{-5}	18×10^{-4}
C_{L_α}	0.00095	0.0020	1.6
C_T/C_L^2	0.00033	0.00093	0.12

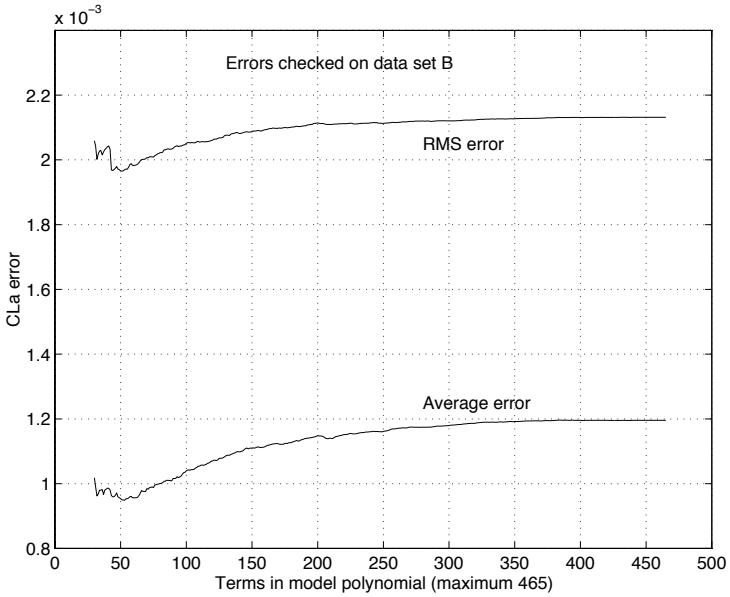

Figure 5.4: Lift curve slope (C_{L_α}) response surface model prediction errors (computed at the design points of set B) versus number of terms in the model polynomial.

5.2.1 Error Comparison

Comparison of accuracy of range prediction by both methods — using the range response surface model and using the drag response surface models — was made in the same manner as described in Section 4.3.1. The range calculation was done on the 1426 designs of data set B. The values of actual range calculated by *HSCT* routines and predicted by response surface models were printed out to a file and then histograms of error distribution were made. Figure 5.6 shows the resulting histograms.

As one can see from the plots, the situation is similar now to what it was with the 25 DV problem and the old design space. The prediction error for the range response surface model is again slightly higher than that for the drag response surface models. However, the overall level of error is reduced drastically compared to the old design space, with standard deviations of the prediction errors of only 11–17 n.mi. as opposed to 43–78 n.mi. in the previous case. The results show that the drag response surface models may be expected to perform slightly better in optimization than the range response surface model.

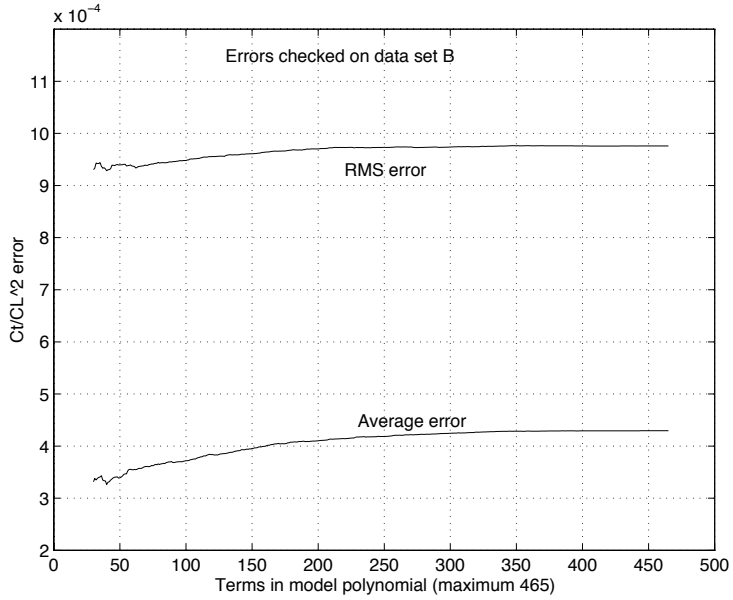

Figure 5.5: Leading edge suction coefficient (C_T/C_L^2) response surface model prediction errors (computed at the design points of set B) versus number of terms in the model polynomial.

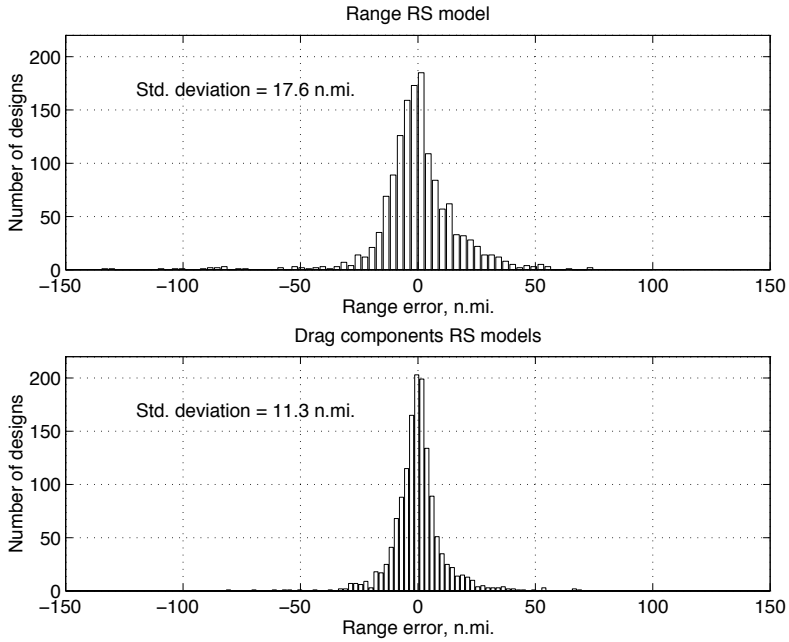

Figure 5.6: Distribution of range prediction errors using range response surface model and drag response surface models.

5.3 Range Response Surface Model in HSCT Optimization

5.3.1 Unrestricted Design Space Optimization

First, it was decided to run the HSCT optimization with the range response surface model providing information to the optimizer about the range of the aircraft. The *HSCT* code was set up again to use the range response surface model in place of the normal aerodynamic analyses to determine the range value, as shown in Figure 4.15. The 52 extra constraints listed in Table 4.6 were used each time when optimizing with response surface models. The optimization was started from the baseline design (central design 2) and stopped after 15 cycles. Figure 5.7 shows history plots of this optimization run.

As one can see from the plot, after cycle 6 the optimizer went too far from the valid region of the RS model and errors began to increase very rapidly. Planforms at

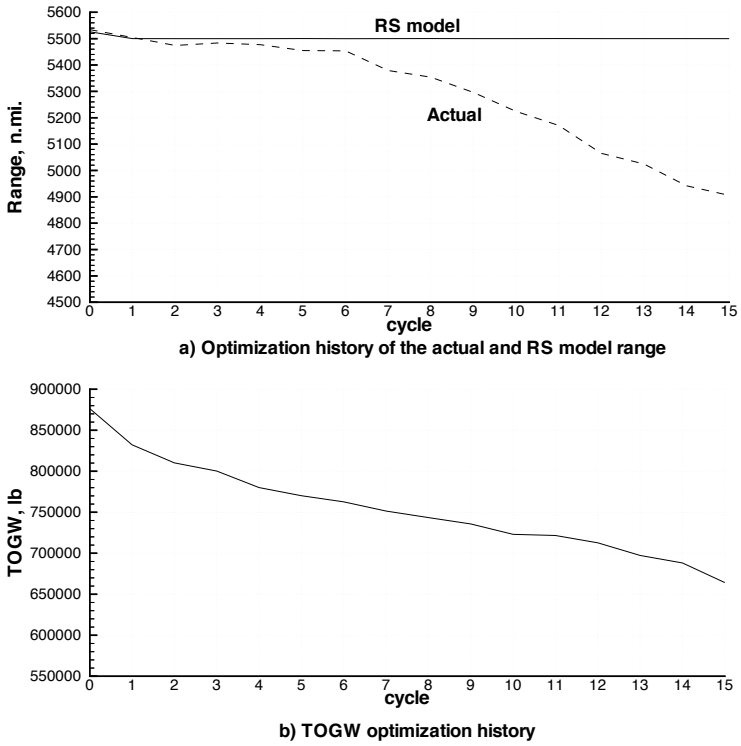

Figure 5.7: Optimization history plots of actual and RS model range and TOGW for optimization run with range response surface model.

the start of the optimization, after 6 cycles and at the end are compared in Figure 5.8. While the planform after cycle 6 may be referred to as a normal one, the final configuration is clearly a nonsensical one, indicating that the optimizer was exploiting the weakness of the response surface model in this region where the predicted range was much higher than the actual value.

Examining the values of the design variables of the final design of this optimization run and comparing distances (2-norms) indicated that the design was much farther from the central design than any design in the data set A used for response surface model generation. Thus the 52 extra constraints did not prevent the optimizer from going outside of the valid response surface model design space. The design

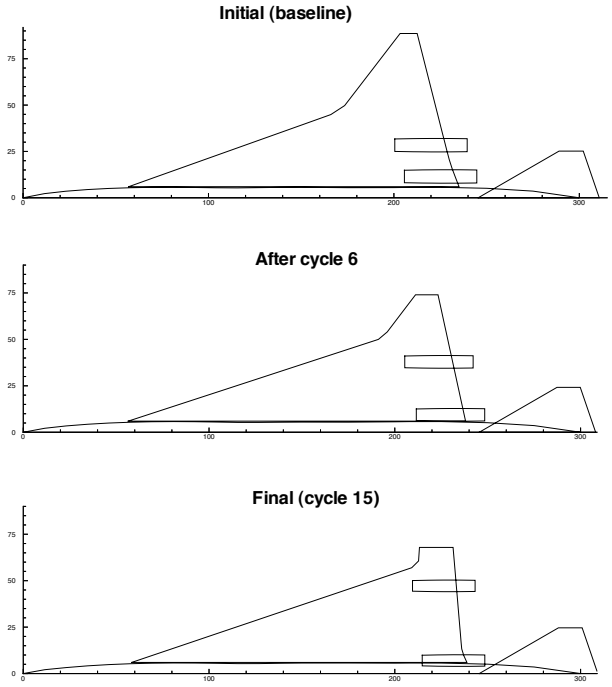

Figure 5.8: Planforms (initial, cycle 6, and final) of the optimization run with range response surface model.

space restricted by these constraints still included poor HSCT configurations with low aerodynamic perfomance for which the response surface model predictions were not valid.

5.3.2 Optimization Inside a "Box"

Since the constraints intended for keeping the optimizer inside the valid response surface model region proved to be inefficient, other measures were needed to do the job. The decision was made to use explicit bounds on the values of each design variable, so that the optimizer is only allowed to work inside a multidimensional "box" around the baseline design. This is a standard approach for using approximations in optimization, but it could not be used in the 25 DV problem due to the infeasible domain where the response surface models were built. The limits of the box were defined to be the same as the maximum and minimum values of the design variables

for all designs in the data set A, which was used for generating all RS models. To perform the task, 58 additional constraints were employed in the *HSCT* code, limiting lower and upper values of each design variable. Table 5.2 contains the values of the lower and upper limits on design variables.

Recall that any of the designs in data set A have at maximum 3 design variables perturbed from the baseline value at one time, so that the region of the design space described by these designs has a sphere-like shape rather than a cuboidal shape. This means that the optimizer operating inside the "box" is still allowed to assume designs much farther from the baseline than any design in the data set A, simply by going to one of the corners of the "box". But even these "box" limits seemed to be sufficient to keep the errors of response surface model to reasonable values of 50–90 n.mi. as opposed to 500–700 n.mi. for the unresticted design space optimization.

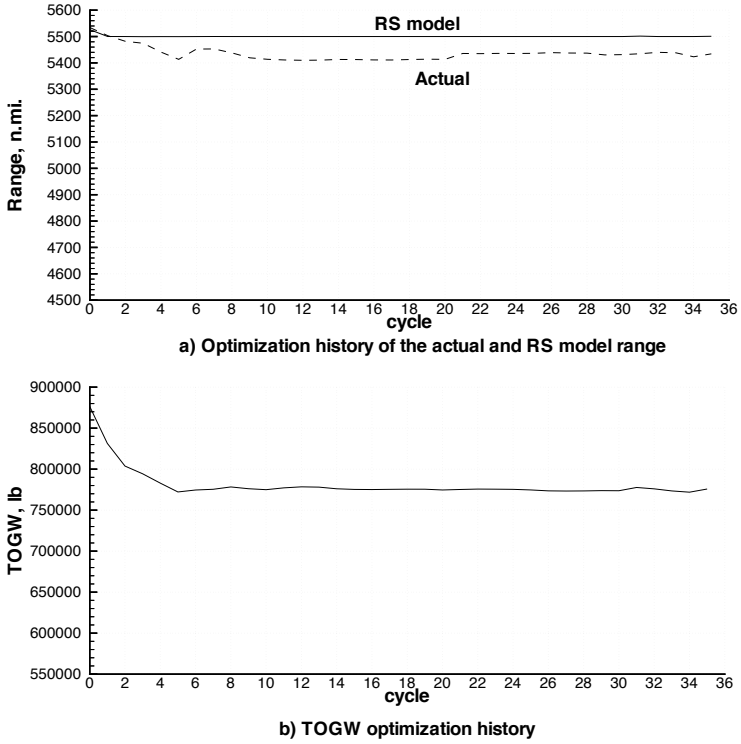

Figure 5.9: Optimization history plots of actual and RS model range and TOGW for optimization run with the range response surface model inside the "box."

Table 5.2: Box around central design 2.

#	Baseline	Min value	Max value	Multiplier	Description
1	1.781470	1.6339	2.1378	100	Wing root chord (ft)
2	1.141291	0.9130	1.3695	100	LE Break, x (ft)
3	4.070442	3.2564	4.8845	10	LE Break, y (ft)
4	1.734057	1.3872	1.8831	100	TE Break, x (ft)
5	1.222726	0.9782	1.4673	10	TE Break, y (ft)
6	1.463565	1.1709	1.7563	100	LE of wing tip, x (ft)
7	0.920425	0.7363	1.1045	10	Tip chord (ft)
8	8.260918	6.6087	9.9131	10	Wing semi-span (ft)
9	5.114403	4.0915	6.1373	0.10	Chordwise location of max. t/c
10	2.525195	2.0202	3.0302	1	Airfoil LE radius parameter, r_t
11	2.818364	2.2547	3.3820	0.01	Airfoil t/c at root
12	1.900977	1.5208	2.2812	0.01	Airfoil t/c at LE break
13	1.704753	1.5010	2.0457	0.01	Airfoil t/c at tip
14	0.026108	0.0209	0.0313	100	Fuselage restraint 1, x (ft)
15	0.046578	0.0373	0.0559	10	Fuselage restraint 1, r (ft)
16	0.132450	0.1246	0.1589	100	Fuselage restraint 2, x (ft)
17	0.249456	0.1996	0.2993	10	Fuselage restraint 2, r (ft)
18	1.116824	0.8935	1.3402	100	Fuselage restraint 3, x (ft)
19	0.532127	0.4257	0.6386	10	Fuselage restraint 3, r (ft)
20	1.869078	1.4953	2.2429	100	Fuselage restraint 4, x (ft)
21	0.534270	0.4274	0.6411	10	Fuselage restraint 4, r (ft)
22	1.149741	0.9198	1.3797	10	Nacelle 1, x_9 (ft)
23	2.837171	2.2697	3.4046	10	Nacelle 2, x_{10} (ft)
24	4.647425	3.7179	5.5769	100000	Mission fuel (lbs)
25	5.840310	4.6722	6.4152	10000	Starting cruise altitude (ft)
26	0.379744	0.3038	0.4557	100	Cruise climb rate (ft/min)
27	9.211897	7.3695	11.0543	100	Vertical tail area (ft^2)
28	9.866076	7.8929	11.8393	100	Horizontal tail area (ft^2)
29	5.727139	4.5817	6.8726	10000	Thrust per engine (lbs)

Table 5.3: Comparison of initial and final designs, optimization with range response surface model inside the "box."

Parameter	Initial	Final
Gross Weight (*lbs*)	876,487.5	775,791.7
Corrected Gross Weight (*lbs*)	873,418.5	781,794.7
Fuel Weight (*lbs*)	464,743	397,121
Fuel Wt / Gross Wt	53.0%	51.1%
Wing Area (ft^2)	14,157	13,392
Aspect Ratio	2.22	1.76
Vertical Tail Area (ft^2)	921.1	852.0
Horizontal Tail Area (ft^2)	1,973.2	1,914.0
Nacelle 1 position, y (*ft*)	11.5	9.2
Nacelle 2 position, y (*ft*)	28.3	33.9
Range actual (*n.mi.*)	5,534.1	5,434.3
Range RSM (*n.mi.*)	5,526.0	5,501.0
Landing angle of attack	10.3°	11.1°

Figure 5.9 shows the results from this optimization, where the convergence history of the actual and the response surface model predicted range and the TOGW are presented. Convergence was achieved here by means of restricting the optimization to the specified volume in design space. Figure 5.10 compares the final HSCT configuration to the baseline. The final range error is 66.7 n.mi. or 1.21% of the absolute range value. Assuming the amout of fuel to compensate a range deficiency to be 90 lb/n.mi., this range error would result in a 6002 lb increase in TOGW and bring the TOGW value from 775,791.7 lb up to 781,794.7 lb. The values of some major parameters of the final design are listed in Table 5.3. In general, the final configuration, even with the corrected value of TOGW for the range deficiency, is a very efficient design. Optimizations without response surface models for the same mission requirements produced designs with TOGW values of about 800,000 lb (see Section 5.3.3). Thus, about an 18,000 lb saving in TOGW value was achieved by using a response surface model for the range constraint in optimization. However, this weight saving should be viewed with caution for two reasons. First, adding fuel

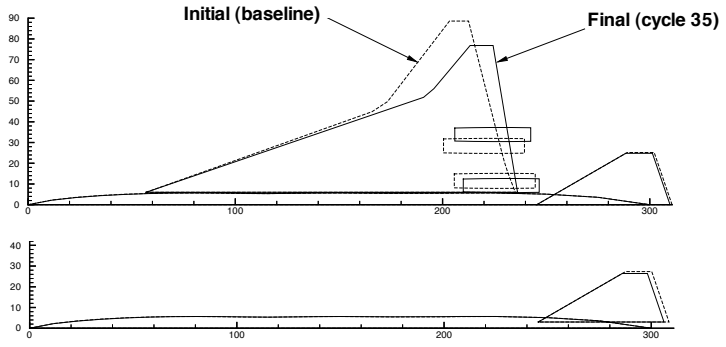

Figure 5.10: Initial and final configurations for optimization run with range response surface model inside the "box."

to compensate for a range error may require reconfiguring the aircraft for the higher loads and higher required lift coefficient, thus even further increasing the TOGW. Second, since the range calculation is done using a response surface model and no "exact" drag analyses are performed during optimization, the required thrust value is based on the "approximate" drag analysis, which is performed to get the value of the simplified range constraint (see Table 4.6). The "approximate" drag analysis in most cases underpredicts drag values, thus artificially decreasing values of the required thrust in flight. Indeed, when checked using "exact" analyses, the required thrust for the final design was 1.1% higher than available engine thrust. Although this is not a big discrepancy, satisfying the true thrust constraint would require bigger engines, which in turn would also increase loads on the aircraft. This would require some reconfiguring of the aircraft and increasing the TOGW.

Another interesting piece of information is shown on Figures 5.11 through 5.14, where traces of all design variables for the two optimizations are plotted along with the "normal" optimization's traces. Notice that for the unrestricted design space optimization, after a few initial cycles, the values of several design variables were outside of the valid design space region, resulting in high prediction errors. In the second case, when the "box" was used around the baseline design, 9 design variables were driven to the boundaries and hit the limits of the allowed space, after which

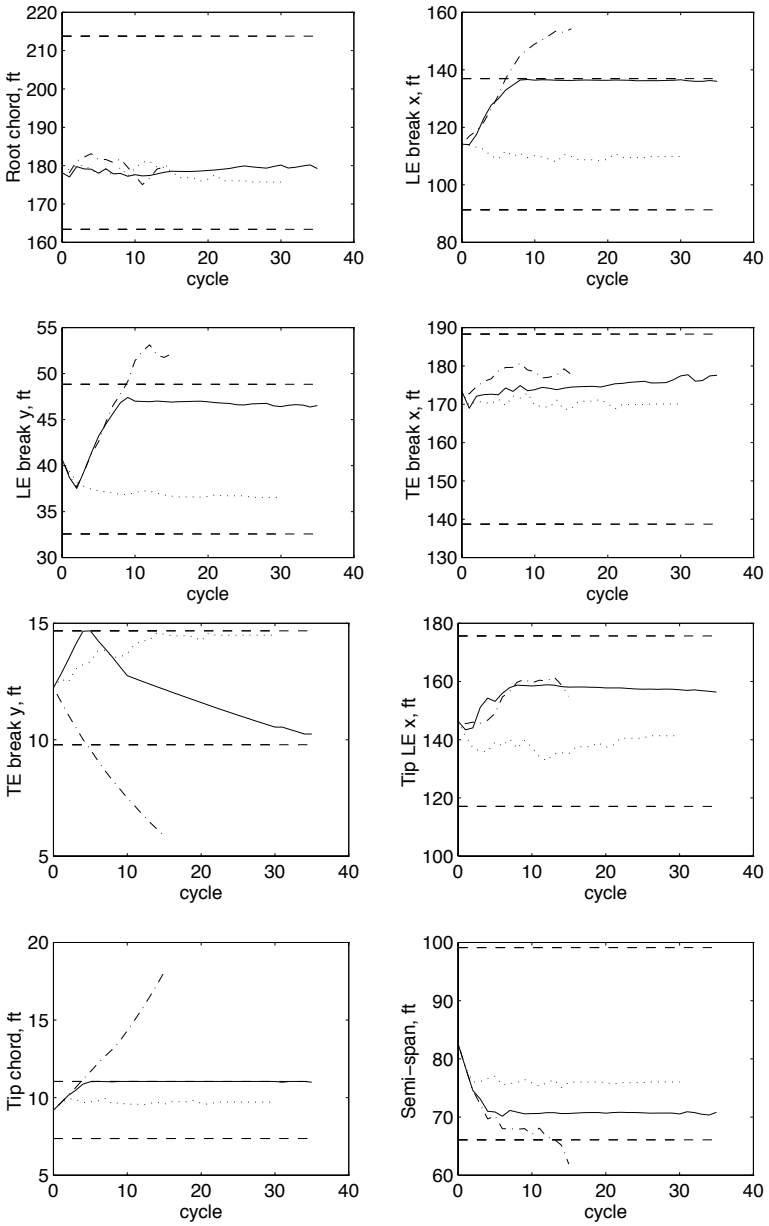

Figure 5.11: Design variable traces for two optimization runs with the range response surface model. Solid lines correspond to optimization inside the "box". Dash-dotted lines show unrestricted design space optimization. Dotted lines show optimization without using the response surface model, i.e., using the standard setup of the *HSCT* code. Dashed lines show the lower and upper limits of the "box".

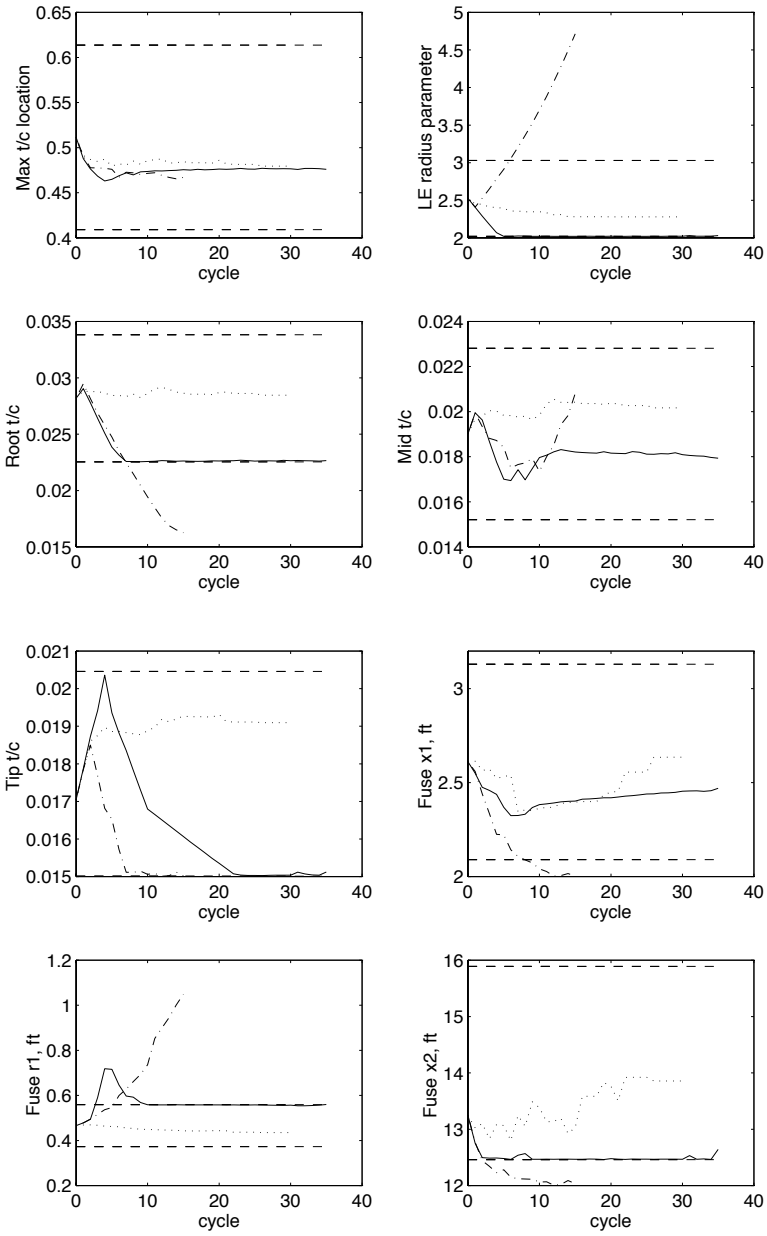

Figure 5.12: Design variable traces (contd.)

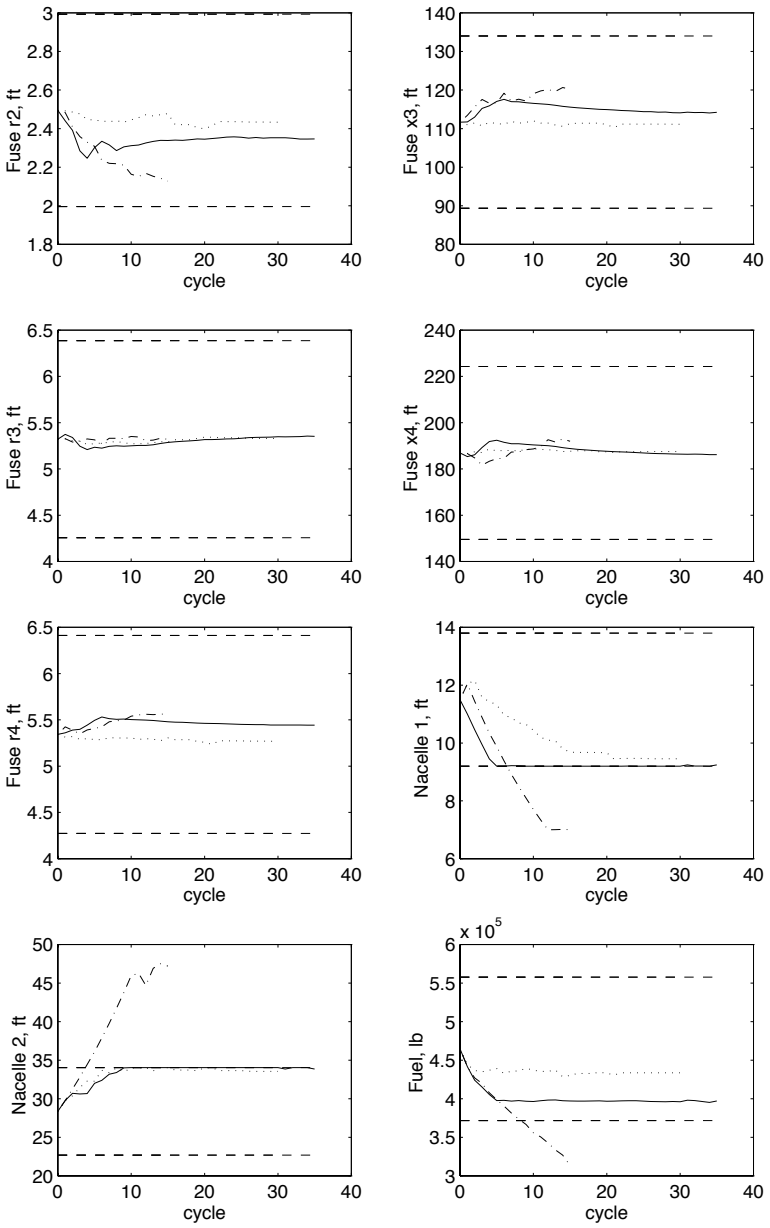

Figure 5.13: Design variable traces (contd.)

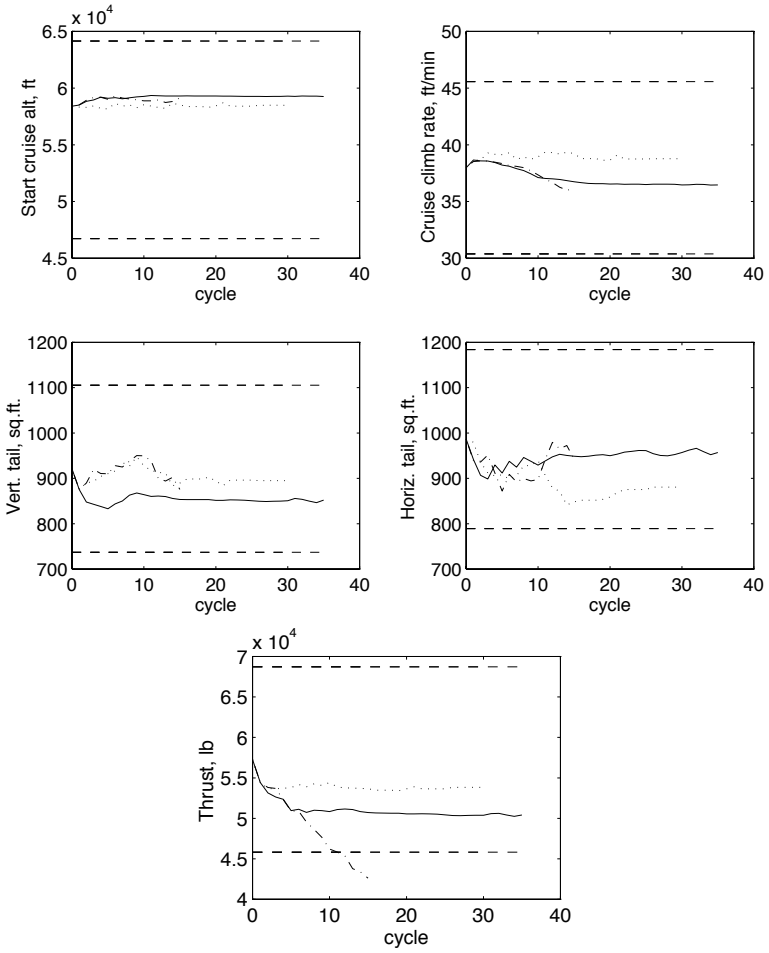

Figure 5.14: Design variable traces (contd.)

the optimizer was sliding along the boundaries in the search of a better design. This prevented extreme values of prediction errors of the range response surface model.

5.3.3 "Standard" HSCT Optimization

As a means for evaluating the effectiveness of using response surface models in optimization, an optimization run without response surface models was conducted. All standard aerodynamic analyses and all standard constraints were employed in this optimization. Started from the baseline design (central design 2) the optimization was stopped after 40 cycles when convergence of TOGW was achieved.

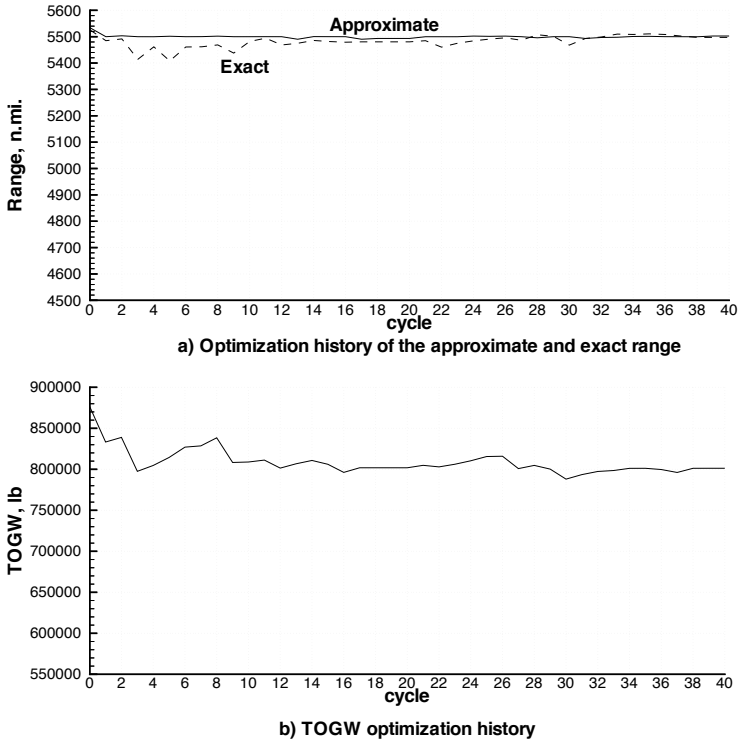

Figure 5.15: Design history plots of range and TOGW for standard HSCT optimization.

Figure 5.15 shows the history plots of the "approximate" and "exact" range and TOGW during this optimization run. Inital and final planforms are compared in Figure 5.16. The final TOGW value of 801,287 lb indicates that the final design

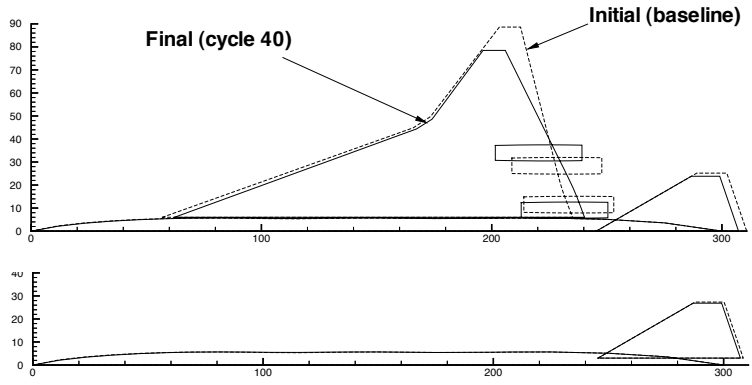

Figure 5.16: Planforms for standard HSCT optimization.

is a local optimum, since in previous optimization runs [5] weights on the order of 773,000 lb were achieved using the same constraint values. The optimizer can follow a different path when given different move limits and then get trapped in a locally optimum design. Table 5.4 compares the final designs of this optimization run and the one with the range response surface model inside the "box".

5.4 Drag Components' Response Surface Models in HSCT Optimization

5.4.1 First Optimization Run (Run 1a). Analysis of the Final Design Location

Since initial error analysis (Section 4.3.1) showed that lower errors were possible with drag components' RS models as opposed to one response surface model for the entire range of the aircraft, a big effort was placed on developing and applying the drag components' response surface models in an HSCT optimization. The first optimization run with the drag response surface models was done using the setup described in Section 4.3.2 and the same 52 extra constraints (Table 4.6). No "box" was used in this optimization. All three response surface models for the wave drag coefficient ($C_{D_{wave}}$), the lift curve slope (C_{L_α}), and the leading edge thrust coefficient (C_T/C_L^2) were used in the optimization. The friction drag coefficient ($C_{D_{fric}}$) and

Table 5.4: Comparison of final designs, optimization with range response surface model inside the "box" and standard optimization.

Parameter	Standard	Range RS model
Gross Weight (*lbs*)	801,287.3	775,791.7
Corrected Gross Weight (*lbs*)	801,053.3	781,794.7
Fuel Weight (*lbs*)	421,212	397,121
Fuel Wt / Gross Wt	52.5%	51.1%
Wing Area (ft^2)	13,356	13,392
Aspect Ratio	1.84	1.76
Vertical Tail Area (ft^2)	885.1	852.0
Horizontal Tail Area (ft^2)	1,764.6	1,914.0
Nacelle 1 position, y (*ft*)	9.1	9.2
Nacelle 2 position, y (*ft*)	34.0	33.9
Range actual (*n.mi.*)	5,502.6	5,434.3
Range RSM (*n.mi.*)	n/a	5,501.0
Landing angle of attack	11.7°	11.1°

the attainable leading edge suction coefficient (LES_{att}) were calculated using normal aerodynamic subroutines of the *HSCT* code.

Figure 5.17 shows the history plots of this optimization run. Apparently, a similar pattern was exibited by the optimizer here as in the previous optimizations with the same setup. Soon after the start, the optimizer went into an invalid region for response surface models and after cycle 10, range errors reached the value of almost 500 n.mi. Figure 5.18 compares the initial (baseline) and the final (cycle 10) planforms for this optimization run. The optimizer decreased the wing area and the overall aircraft size. The engines were spread out, and the leading edge sweep increased considerably compared to the baseline design.

To better understand the location of the final design relative to the baseline design and all other designs in the data set A, planforms of all 1446 designs were plotted on one figure with the baseline and final planforms superimposed on top. Figure 5.19 shows the collection of the planforms. Examining the figures gives an impression that the "cycle 10" design wing shape is quite close to wing shapes of the data set A

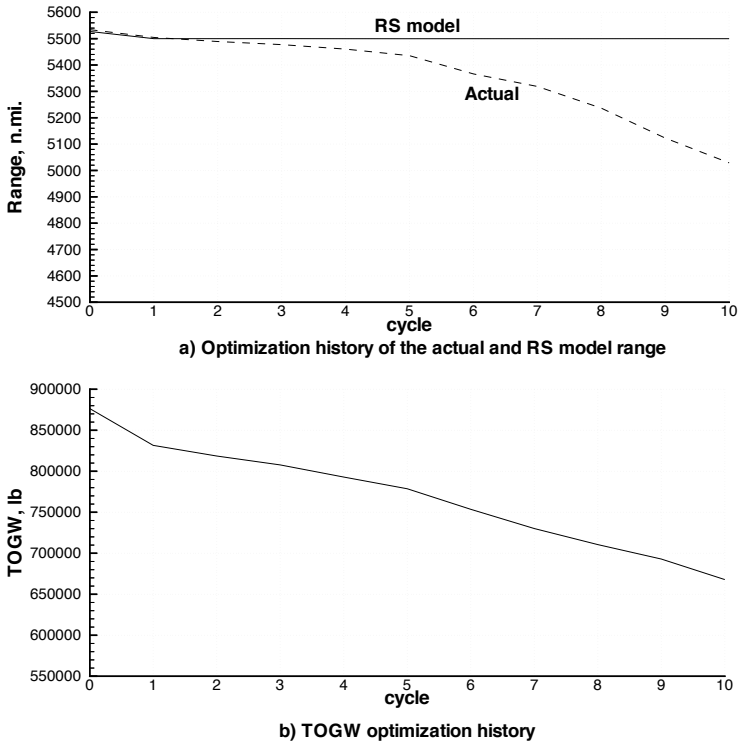

Figure 5.17: Optimization history plots of actual and RS model range and TOGW for optimization run with drag response surface models (run 1a).

designs and should be located inside the valid response surface model design space and well approximated by the models. But a closer look at the plot will indicate that the "cycle 10" wing shape is obtained by varying all 8 design variables defining wing shape from their baseline values. At the same time, all designs in the data set A were obtained by varying no more than 3 design variables at a time. Thus, even considering only the wing shape design variables, the "cycle 10" design is much farther from the baseline than any design in the response surface model data set, measuring the distance as the 2-norm of the vector between the two designs. Considering all other design variables places the "cycle 10" configuration well outside of the region of design space covered by the response surface models. Hence, although from the aerodynamic point of view the final design may seem to be a reasonable one, from the response surface model point of view it lies well outside of the covered design

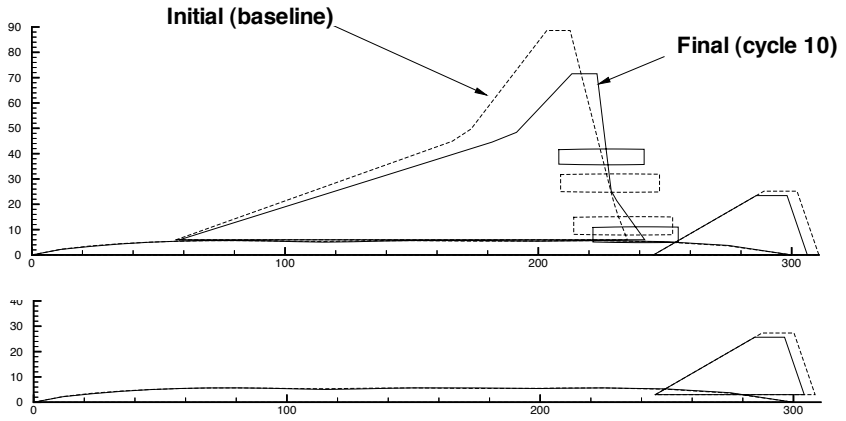

Figure 5.18: Initial and final (cycle 10) planforms of optimization run with drag response surface models (run 1a).

space. Calculation of the distances (2-norms of the vectors) using normalized design variables (divided by their baseline values) proved that the "cycle 10" design is 6 times farther from the baseline than any design in the data set A. Some of the design variables for this design have values exceeding minimum/maximum values of data set A.

5.4.2 Using the "Box" for Drag Response Surface Models (Run 1b)

Since it was clear that the extra constraints aimed at keeping the optimizer in the valid response surface model design space could not perform their task, again the "box" approach was used for optimization with drag response surface models, the same way as with the range response surface model. The same values of the limits for the design variables were used here, resulting in 58 side constraints. Optimization was started from the baseline design and continued for 35 cycles. At this point most of the design variables converged to constant values and only a few of them were

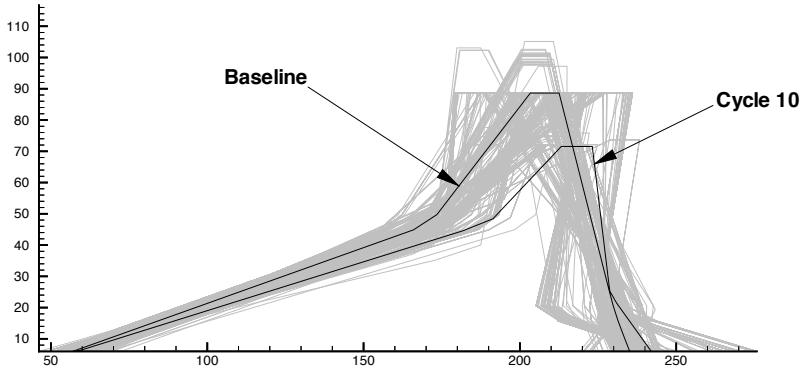

Figure 5.19: Comparison of the wing planforms in data set A with the baseline and final (cycle 10) wing planforms.

still changing their values slightly without much effect on the TOGW and overall configuration performance.

Figure 5.20 shows the history plots for this optimization run, and verifies that convergence was achieved in this run, as both TOGW and range error values stabilized after 28-30 cycles. The final error for range prediction is 81.7 n.mi giving about 7353 lb of extra fuel needed to compenstae for the range deficiency. The TOGW value for the final design is 814,401.6 lb, which after adding the correction becomes 821,754.6 lb. Table 5.5 lists some important parameters of the final design.

The final design appears to be inferior compared to the design obtained using the range response surface model in optimization. The size of the aircraft here did not change as much as in the previous range RS model optimization run, and the final configuration is not as far from the baseline design. The final design obviously is not a global optimum but rather a local optimum. The optimizer went in a different direction this time than for the optimization without the "box", which means that there is still noise present in the process, since only part of the aerodynamics is replaced with response surface models.

Figures 5.22 through 5.25 show the traces of all design variables for the two optimization runs with the drag response surface models. Notice, in the first run, with the

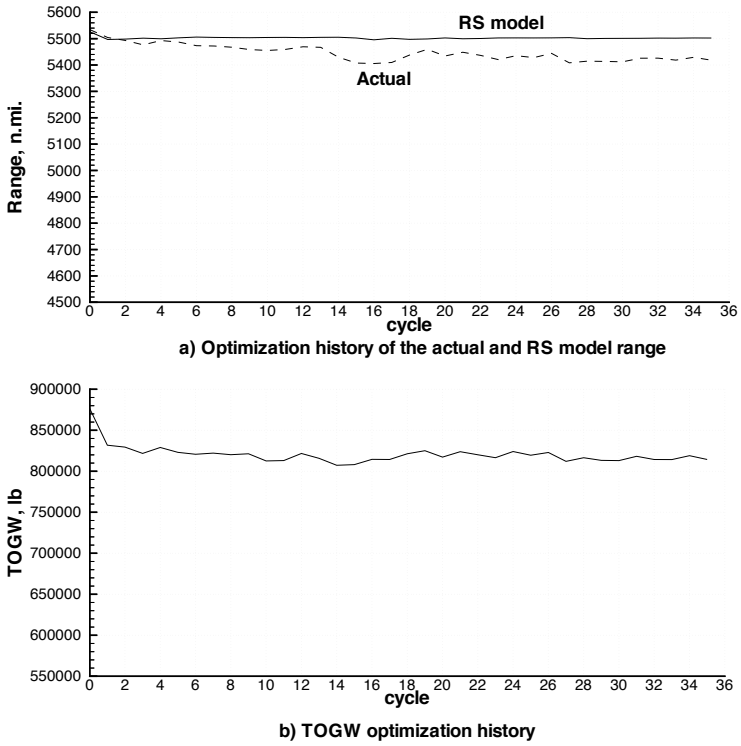

Figure 5.20: Optimization history plots of actual and response surface model range and TOGW for optimization run with drag response surface models inside a "box" (run 1b).

unrestricted design space, several design variables ended up far outside of the minimum/maximum boundaries of the data set. Surprisingly, in the second optimization run with the "box", the optimizer went in a completely different direction, as one can see from the figures, and not a very favorable one. It came to a local optimum with only 5 design variables at their limiting values, in contrast to the optimization with the range response surface model when 9 design variables hit the limits of the "box".

5.4.3 Updating RSM Data to Improve Accuracy

To better understand the sources of the prediction errors of the drag response surface models in optimization run 1, a "cut" through the design space was made by

Table 5.5: Comparison of initial and final designs, optimization with drag RSMs inside the "box"

Parameter	Initial	Final
Gross Weight (*lbs*)	876,487.5	814,401.6
Corrected Gross Weight (*lbs*)	873,418.5	821,754.6
Fuel Weight (*lbs*)	464,743	434,714
Fuel Wt / Gross Wt	53.0%	52.9%
Wing Area (ft^2)	14,157	12,954
Aspect Ratio	2.22	2.09
Vertical Tail Area (ft^2)	921.1	875.4
Horizontal Tail Area (ft^2)	1,973.2	1,719.5
Nacelle 1 position, y (*ft*)	11.5	9.2
Nacelle 2 position, y (*ft*)	28.3	34.0
Range actual (*n.mi.*)	5,534.1	5,418.3
Range RSM (*n.mi.*)	5,526.0	5,500.0
Landing angle of attack	10.3°	10.9°

connecting the baseline design and the final ("cycle 10") design of the run 1a. Plots of the actual values and response surface model predicted values of range, wave drag $C_{D_{wave}}$, lift curve slope C_{L_α}, and leading edge suction term C_T/C_L^2 were then made as the design variables were changing along that line between the two designs. Figure 5.26 shows the so-called α-plots described above. Smooth quadratic lines on the plots correspond to the RS model values, while the wiggling lines represent the actual aerodynamic data. It's clear from the plots that most of the prediction error comes in this case from the wave drag response surface model, which deviates considerably from the actual aerodynamic analysis results. The other two response surface models appear to be reasonably accurate in this region of the design space. As discussed before, the reason for the response surface model inaccuracy is the absence of information for the models in this particular region.

Since the source of the prediction errors was the lack of data in the direction of the search, the logical solution to the problem could be to analyze new data points in the vicinity of the final design and supply this new information to the response

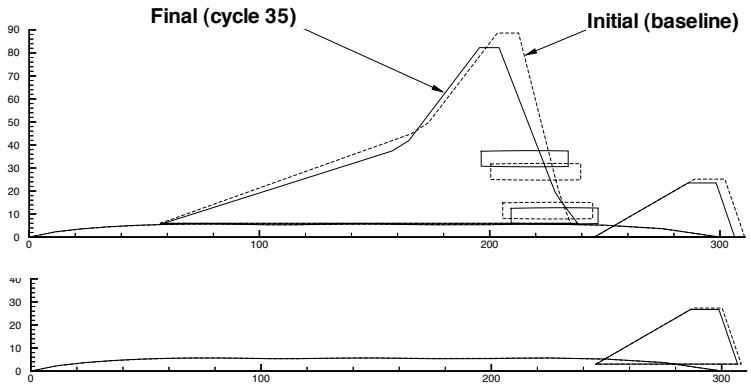

Figure 5.21: Initial and final (cycle 35) configurations of optimization run with drag response surface models inside a "box" (run 1b).

surface models. Provided with this information, new response surface models should be capable of better prediction performance in the previously exploited region of design space resulting in smaller errors. One simple way to choose the data points for additional analyses is to take designs from the trace of the optimizer. This would garantee that the sampling of the design space is done in the space previously exploited by the optimizer.

Ten designs found by the optimizer in the optimization run 1 were analyzed to get the values of the drag related coefficients and added to the 1446 data points of the data set A. With this new 1456 design set, new response surface models were generated using the same polynomials as for the initial models. The same α-plots were made now using new updated response surface models, which were called *Series 1* response surface models. Initial response surface models then would be called *Series 0*. Figure 5.27 shows the resulting α-plots between the baseline and "cycle 10" designs. As one may see, a drastic improvement was observed in the prediction performance of the models in this direction in the design space. Prediction error at the final design was reduced from almost 500 n.mi. to less than 20 n.mi., and the errors for the wave drag coefficient were reduced from 8.1 counts to only 0.6 counts for the final design. These

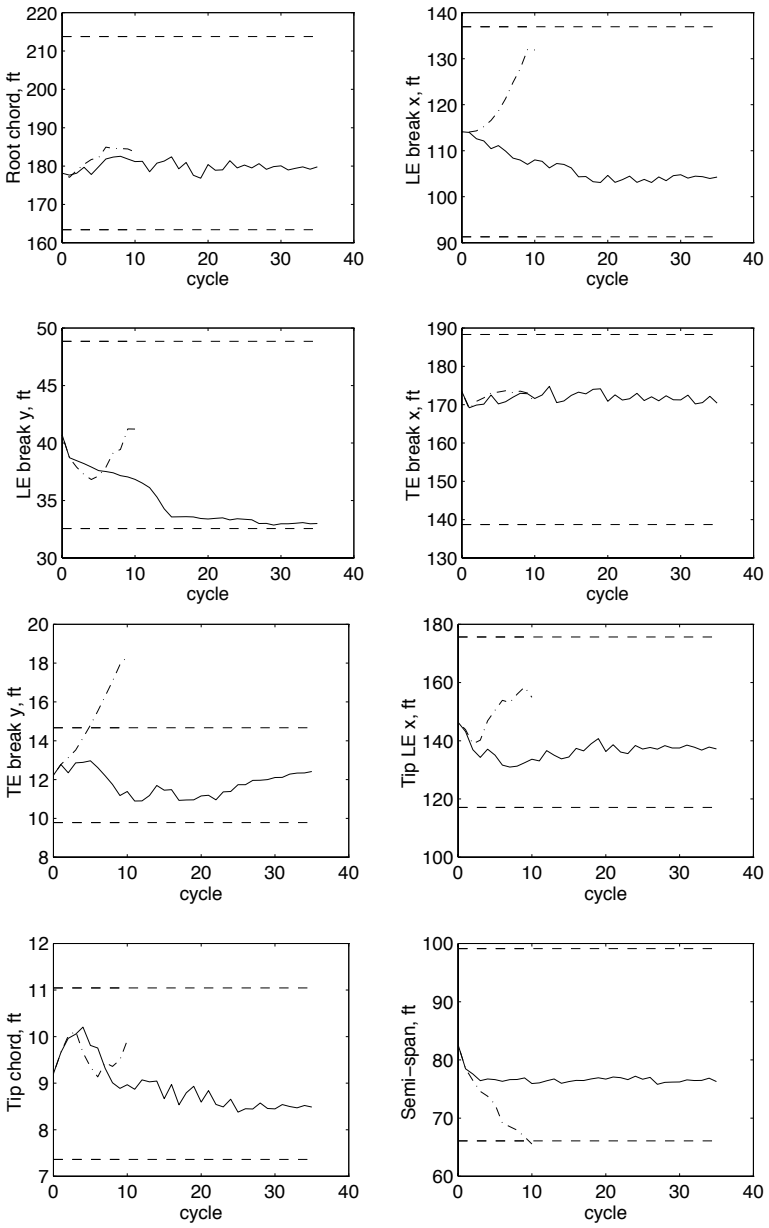

Figure 5.22: Design variable traces for two optimization runs with drag response surface models. Solid lines correspond to optimization inside the "box". Dash-dotted lines show unrestricted design space optimization. Dashed lines show the lower and upper limits.

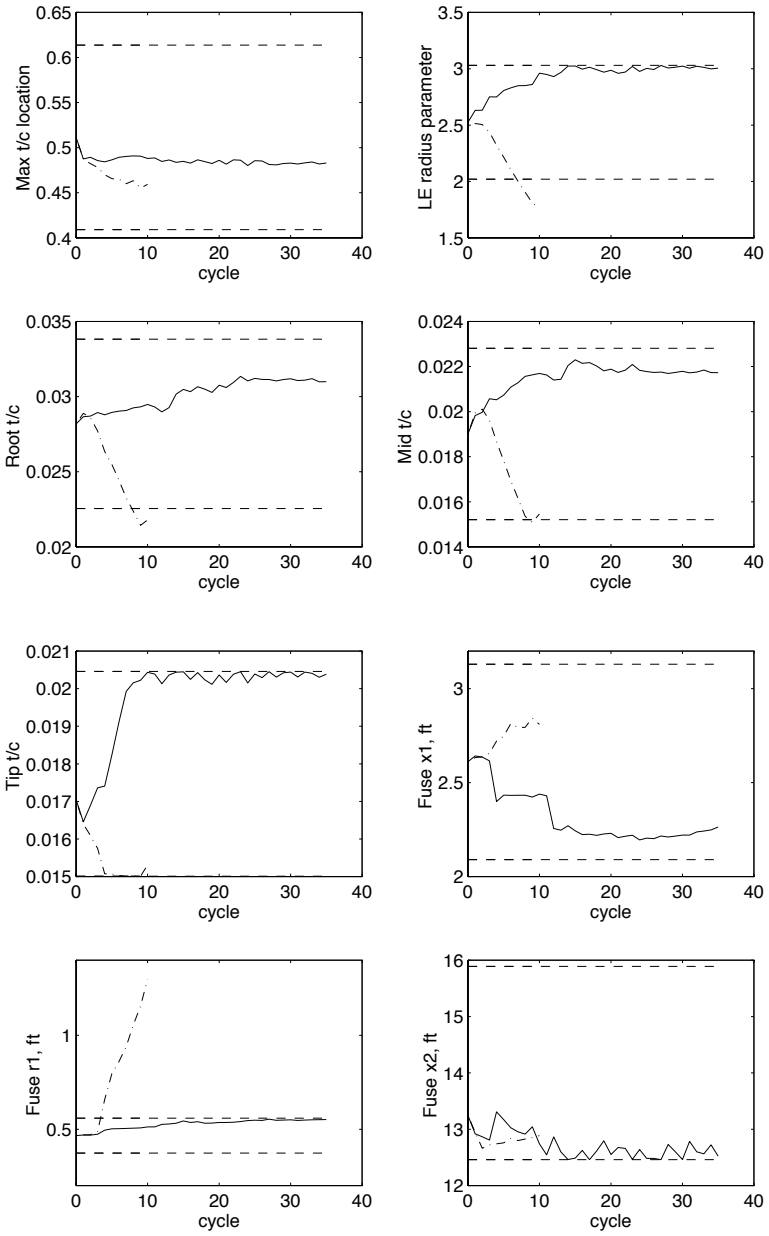

Figure 5.23: Design variable traces (contd.)

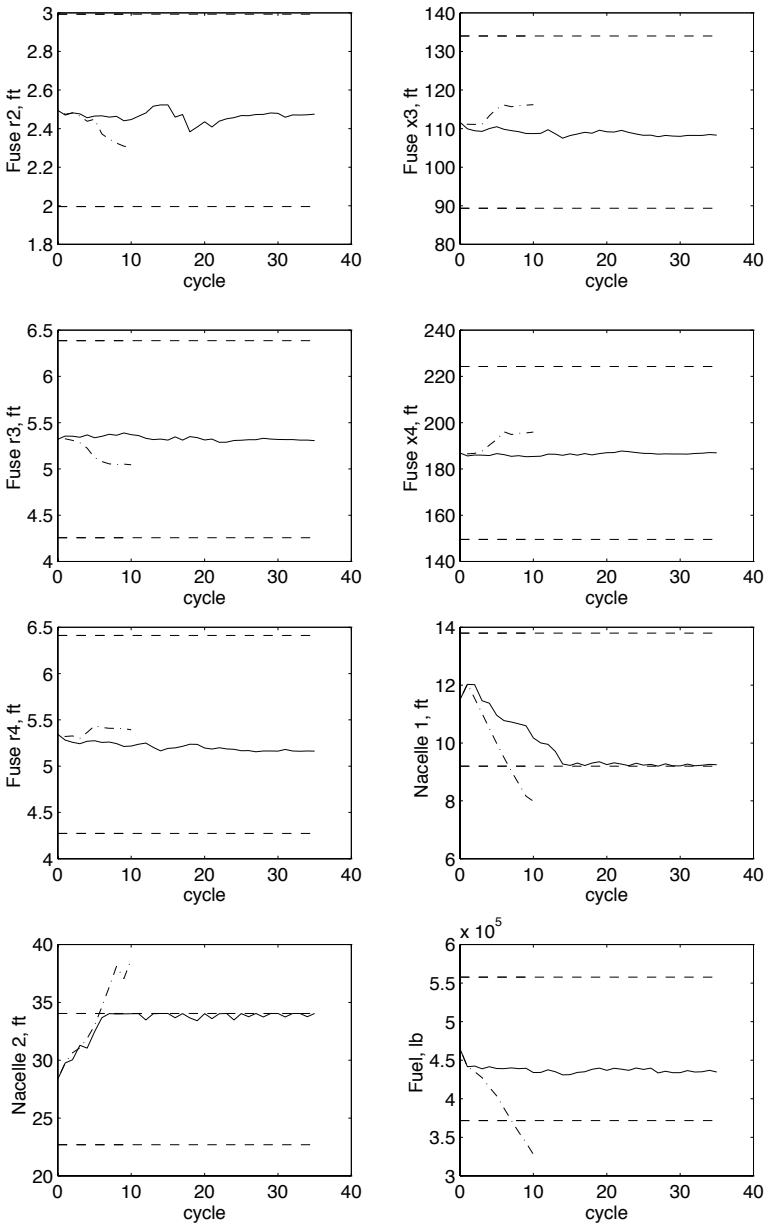

Figure 5.24: Design variable traces (contd.)

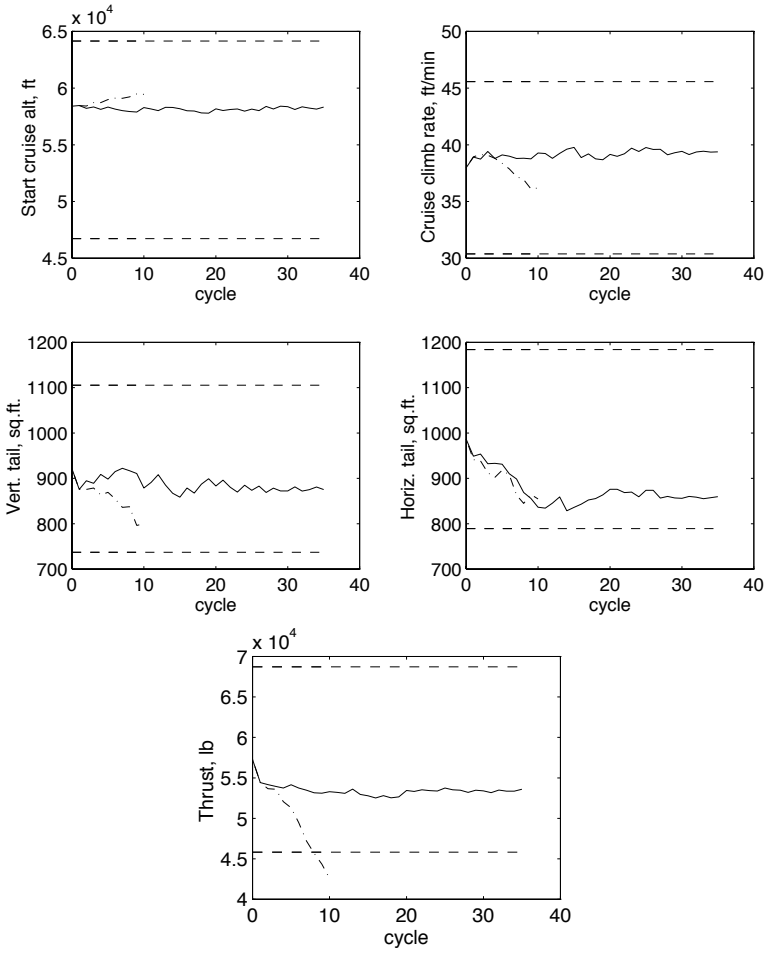

Figure 5.25: Design variable traces (contd.)

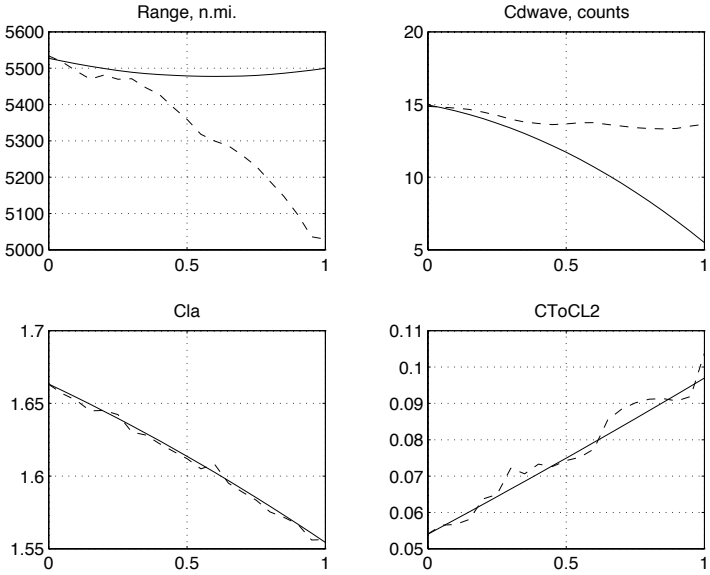

Figure 5.26: α-plots between the baseline and "cycle 10" designs of optimization run 1. Solid lines are RS model values, dashed lines correspond to actual aerodynamic data.

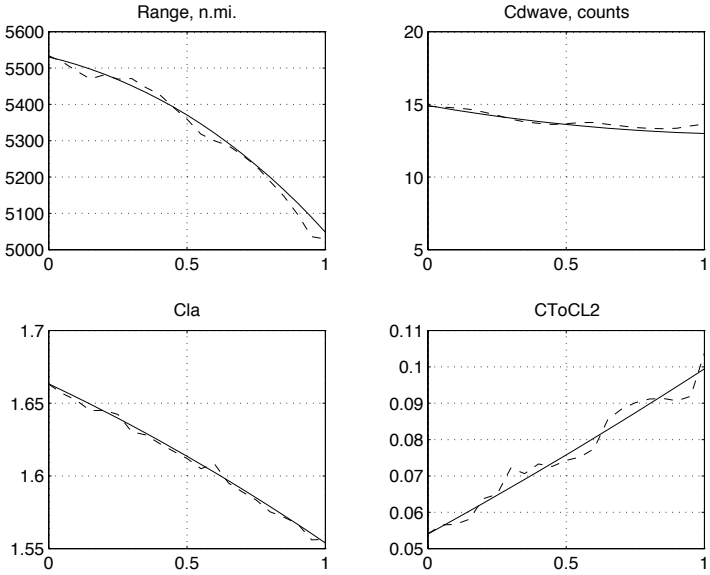

Figure 5.27: α-plots between the baseline and "cycle 10" designs of optimization run 1 with modified response surface models (Series 1, 10 new designs). Solid lines are RS model values, dashed lines correspond to actual aerodynamic data.

changes in the RS models' data will prevent the optimizer from exploiting the same area, but can not garantee, of course, that other such spaces will not be found.

The updated drag response surface models were installed into the *HSCT* code and another optimization run (run 2) was made to see if any improvement was achieved in the prediction capabilities of the models and also to get new design samples for the RS models' data set. Started from the baseline design again, the optimization was stopped after 10 cycles so that 10 new designs from the optimization trace could be analyzed and added to data set A. The maximum range prediction error reached only about 60 n.mi. during these 10 optimization cycles. History plots for this run are shown in Figure 5.28 and planforms are plotted in Figure 5.29.

Once again the α-plots between the baseline design and the final design were made for this optimization run and they are shown in Figure 5.30. As in the previous run, the major contributor to the prediction error was the wave drag response surface model, although this time the discrepancy was only about 0.7 counts at the final design. The 10 designs from optimization run 2 were analyzed and added to the RSM data set. New response surface models were generated based on the updated set and new α-plots plotted to check the effect of new design samples. Figure 5.31 shows the α-plots with *Series 2* response surface models. Again, a considerable improvement was observed with range error reduction from 40 n.mi to about 15 n.mi at the final design.

Another optimization run was carried out with these modified drag response surface models (*Series 2* response surface models, 20 new designs). The optimization was started again at the baseline design and was first stopped after cycle 10. Prediction errors of the drag response surface models did not exceed 40 n.mi. during these initial 10 cycles and it was decided to continue the optimization run farther to see if the optimizer would converge to an optimum without restricting the design space. Note that both this and the previous optimization runs did not use "box" constraints on the design variables. As shown on the history plots in Figure 5.32, after approximately cycle 10, the optimizer left the zone of the design space where response surface models performed well and went into a region of high prediction errors. The errors were constantly growing as the optimizer went farther from the

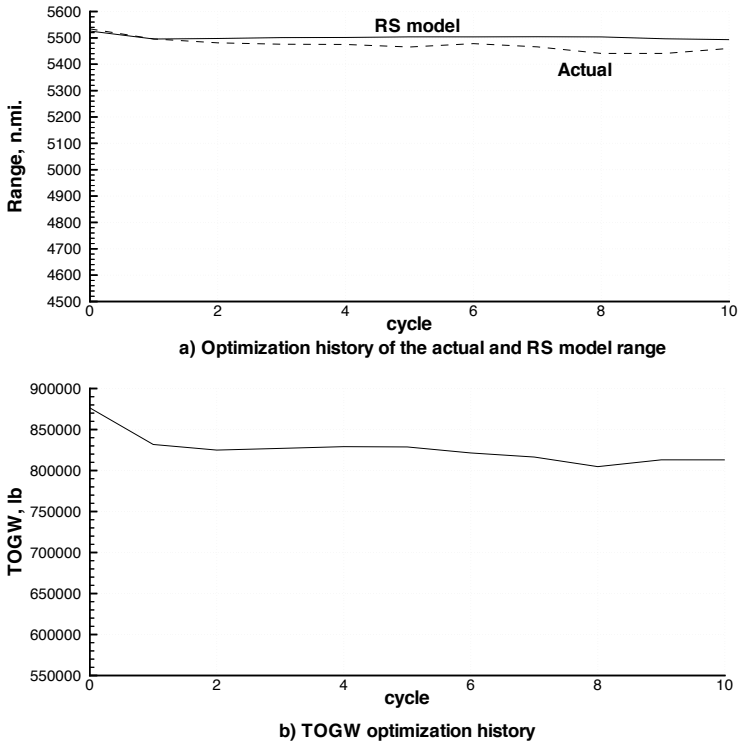

Figure 5.28: History plots of optimization run 2 with modified response surface models (Series 1).

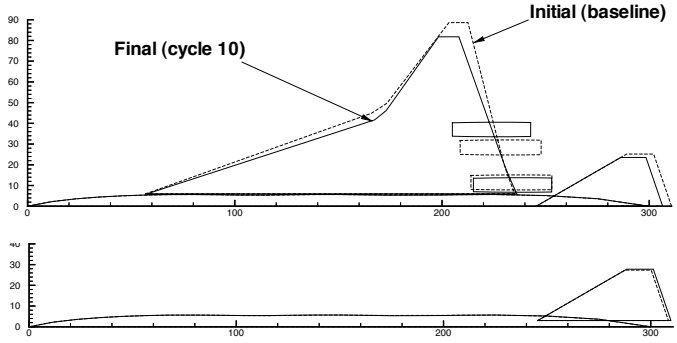

Figure 5.29: Initial and final planforms of optimization run 2 with modified drag response surface models (Series 1).

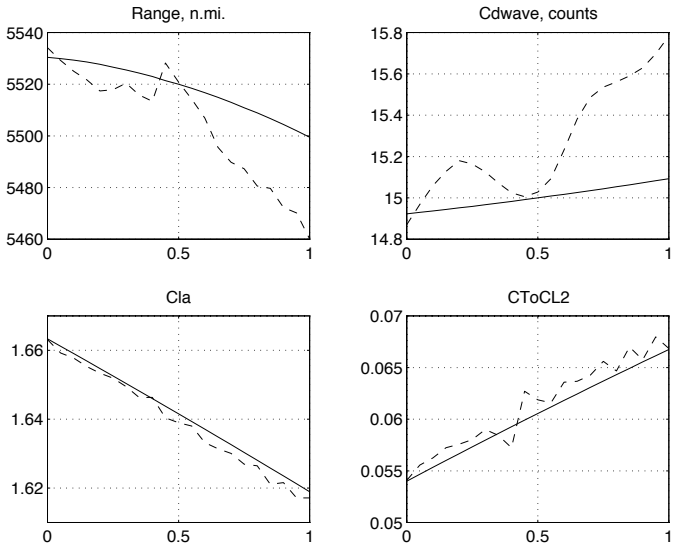

Figure 5.30: α-plots between the baseline and "cycle 10" designs of optimization run 2 with Series 1 response surface models (10 new designs). Solid lines are RS models' values, dashed lines correspond to actual aerodynamic data.

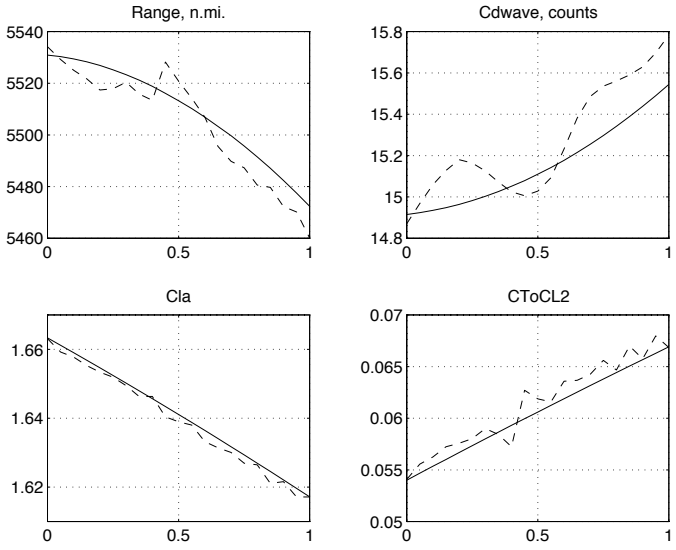

Figure 5.31: α-plots between the baseline and "cycle 10" designs of optimization run 2 with Series 2 response surface models (20 new designs). Solid lines are RS models' values, dashed lines correspond to actual aerodynamic data.

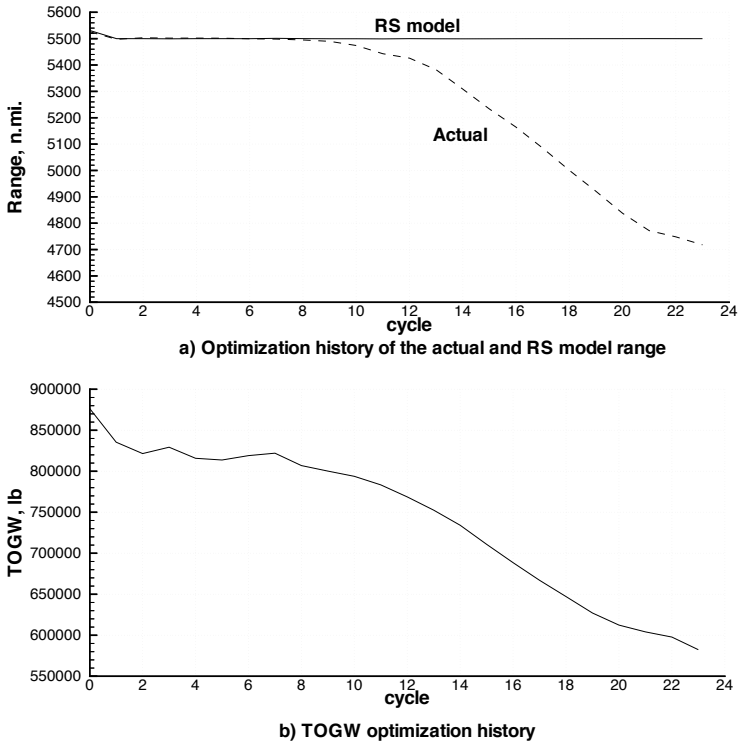

Figure 5.32: History plots of optimization run 3 with modified response surface models (Series 2, 20 new designs).

valid response surface model zone. The optimization was stopped after 23 cycles. Planforms of configurations found by optimizer are shown in Figure 5.33.

5.4.4 Updated Response Surface Models Inside a "Box"

Experience with using drag response surface models in optimization up to this point showed that updating information and regenerating response surface models, although helping immeasurably in the previously exploited regions of design space, did not prevent the optimizer from exploiting inaccurate RS approximations or simply going beyond the boundaries of the valid design space. Thus, imposing the side constraints ("box") was necessary for keeping prediction errors at an acceptable level. Combining the two approaches — updated response surface models and the "box" around the baseline design — a new optimization run produced very promising results from the

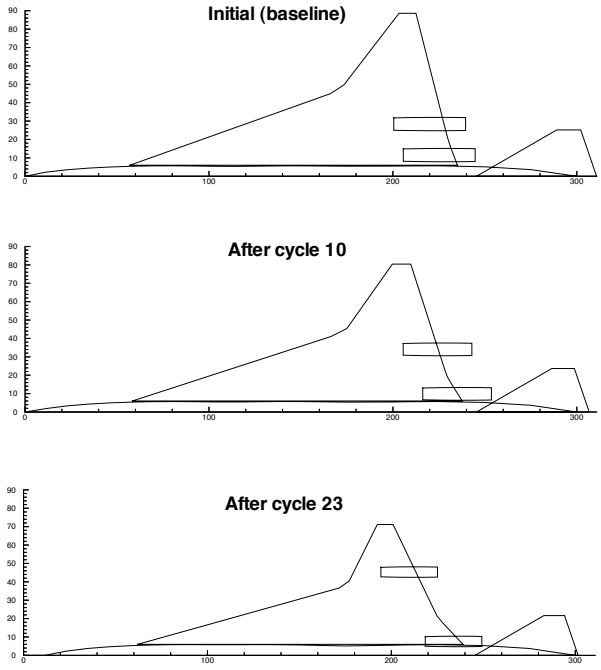

Figure 5.33: Planforms of optimization run 3 with modified drag response surface models (Series 2, 20 new designs).

point of view of the prediction errors of the response surface models. The level of error was reduced to only 6–10 n.mi. at the end of the optimization run, and convergence was easily achieved after 20–25 optimization cycles.

Shown in Figure 5.34 are the histoy plots of range and TOGW for this optimization run. Initial and final planforms are presented in Figure 5.35. Once again the final design is far from the global optimum configuration, as the TOGW value of 818,766.6 lb for the final design is much higher than the value of 773,000 lb obtained for the same optimization problem without response surface models [5]. So the optimizer is still susceptible to getting trapped in local optima due to the presense of numerical noise from the low-speed aerodynamic analyses and the non-convexity of the design space. Table 5.6 compares some parameters of the final and baseline designs.

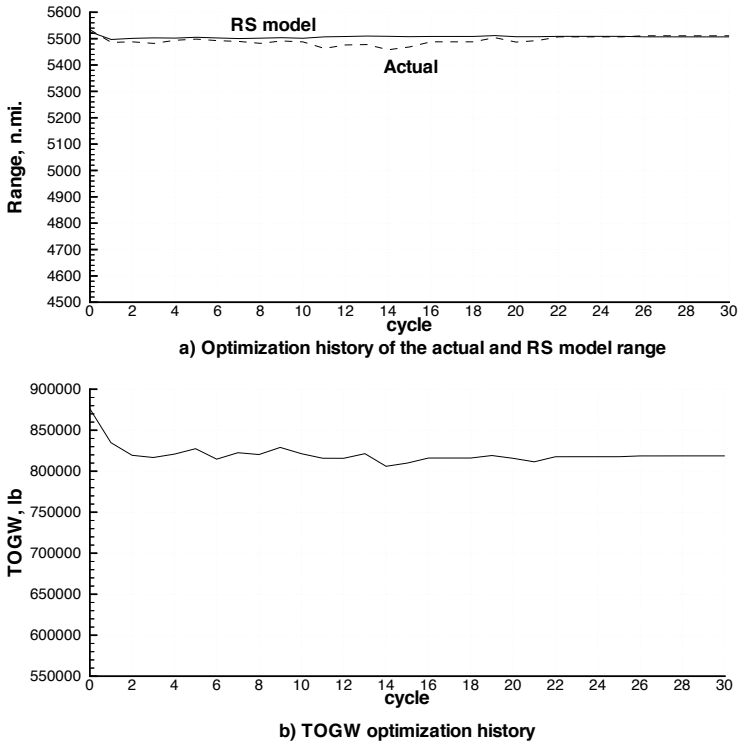

Figure 5.34: History plots of optimization with modified response surface models (Series 2, 20 new designs) inside a "box."

5.5 Comparison of Optimization Results

To clearly see the results of applying RS models in optimization, the convergence histories of the take-off gross weight for three optimization runs — with the range RS model inside a "box", with the updated drag RS models inside a "box", and a "standard" optimization (Case 29c from [5]) — were compared. Figure 5.36 shows the combined convergence history of these three optimization runs.

The plot shows that the optimization converged much faster in both runs with RS models — 30 cycles as opposed to 74 cycles for the "standard" optimization. Also the amplitude of TOGW oscillations during optimization is considerably lower for both of the RS model optimization runs. This is an effect of filtering numerical noise due to the high speed aerodynamics by the RS models.

As mentioned earlier, both final designs of the RS model optimization runs are

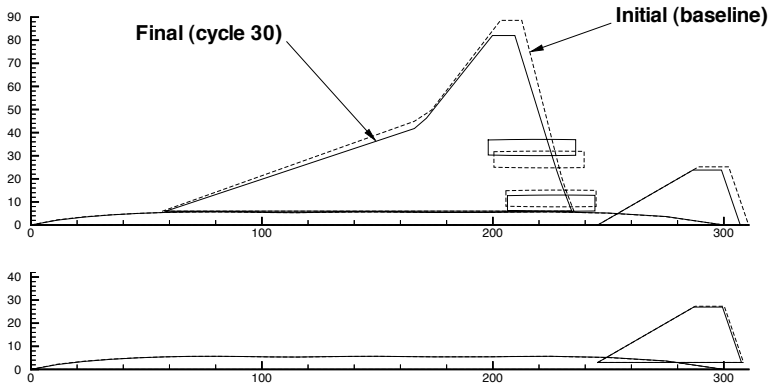

Figure 5.35: Planforms of optimization with modified drag response surface models (Series 2, 20 new designs) inside a "box."

heavier than the one for the "standard" optimization. The difference in TOGW between the range RS model final design and "standard" final design is relatively small and the design would have been lighter if TOGW was not adjusted for the range deficiency due to the prediction error. The final design for the drag RS model optimization case is clearly a local optimimum as it is much heavier than the "standard" optimum design. Table 5.7 lists all major parameters of the three designs being compared. Values of all the design variables and constraints for these three designs are listed in Appendix B.

5.6 Optimization Runs with RS Models from "Standard" Optimum

As mentioned before, the final designs of the optimization runs with both the range and drag RS models were heavier than the optimum from the "standard" optimization. Thus, two new optimization runs were carried out starting from the "standard" optimum design — with the range RS model and with the drag RS models — to

Table 5.6: Comparison of initial and final designs, optimization with updated drag response surface models inside the "box."

Parameter	Initial	Final
Gross Weight (*lbs*)	876,487.5	818,766.6
Corrected Gross Weight (*lbs*)	873,418.5	817,794.6
Fuel Weight (*lbs*)	464,743	433,595
Fuel Wt / Gross Wt	53.0%	53.0%
Wing Area (ft^2)	14,157	13,081
Aspect Ratio	2.22	2.06
Vertical Tail Area (ft^2)	921.1	895.0
Horizontal Tail Area (ft^2)	1,973.2	1,761.4
Nacelle 1 position, y (*ft*)	11.5	9.5
Nacelle 2 position, y (*ft*)	28.3	33.5
Range actual (*n.mi.*)	5,534.1	5,510.8
Range RSM (*n.mi.*)	5,526.0	5,500.5
Landing angle of attack	10.3°	11.0°

see if a better design could be found by the optimizer for the RS model approaches. Both new optimization runs converged rather quickly and resulted in slightly heavier designs than the "standard" optimum configuration. Figures 5.37 to 5.40 show the convergence history plots and planforms for these two optimization runs. Note that in both optimization runs "box" constraints were used.

The reason for the heavier final designs for both new optimization runs is that the initial design ("standard" optimum) was outside of the "box", and the optimizer had to move the initial design inside the "box" each time after the start of the optimization. This was sufficient to get out of the small "pocket" of the design space where the "standard" optimum was located. Figures 5.41 through 5.44 show the traces of the design variables for these two optimization runs. Notice that 6 design

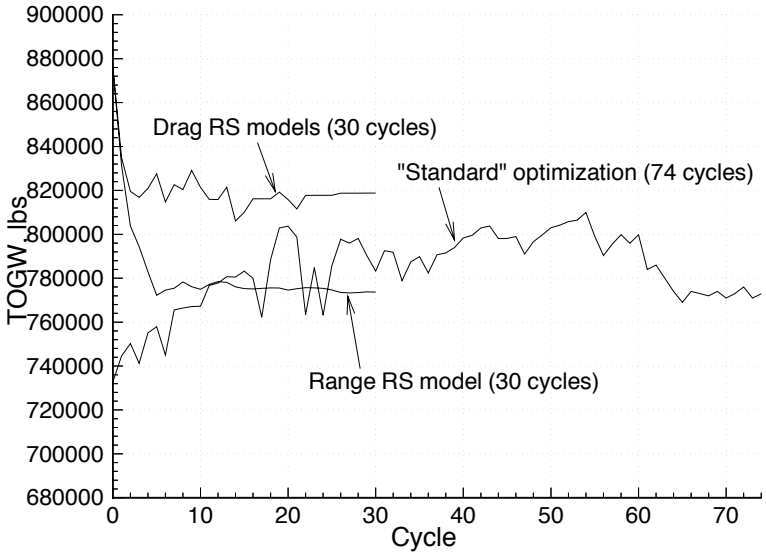

Figure 5.36: Convergence histories of TOGW for three optimization runs.

variables have values outside of the "box" limits for the initial design (trailing edge y-coordinate, fuselage radius 1, both nacelle positions, vertical and horizontal tail areas). All of these design variables were brought to the limiting values of the "box" constraints. Also note that after 1-2 initial cycles the prediction error of the RS models reduces, as the optimizer enters the design space inside the "box". Table 5.8 lists all major parameters of the final designs of these optimization runs along with the "standard" optimum design.

Table 5.7: Comparison of the three optimum designs for RS model optimization runs and a "standard" optimization (Case 29c from [5]).

Parameter	Range RS model optimization	Drag RS models optimization	"Standard" optimization
Gross Weight (*lbs*)	775,791.7	818,766.6	772,981
Corrected Gross Weight (*lbs*)	781,794.7	817,794.6	772,752
Fuel Weight (*lbs*)	397,121	433,595	403,345
Fuel Wt / Gross Wt	53.0%	53.0%	52.2%
Wing Area (ft^2)	13,992	13,081	13,191
Aspect Ratio	1.76	2.06	1.99
Wing thickness at root, %	2.26	2.84	2.37
Vertical Tail Area (ft^2)	852.0	895.0	454.1
Horizontal Tail Area (ft^2)	1,914.0	1,761.4	1,494.4
Nacelle 1 position, y (*ft*)	9.2	9.5	7.1
Nacelle 2 position, y (*ft*)	33.9	33.5	14.4
Range actual (*n.mi.*)	5,434.3	5,510.8	5,503.0
Range RSM (*n.mi.*)	5,501.0	5,500.5	n/a
Landing angle of attack	11.1°	11.0°	10.6°

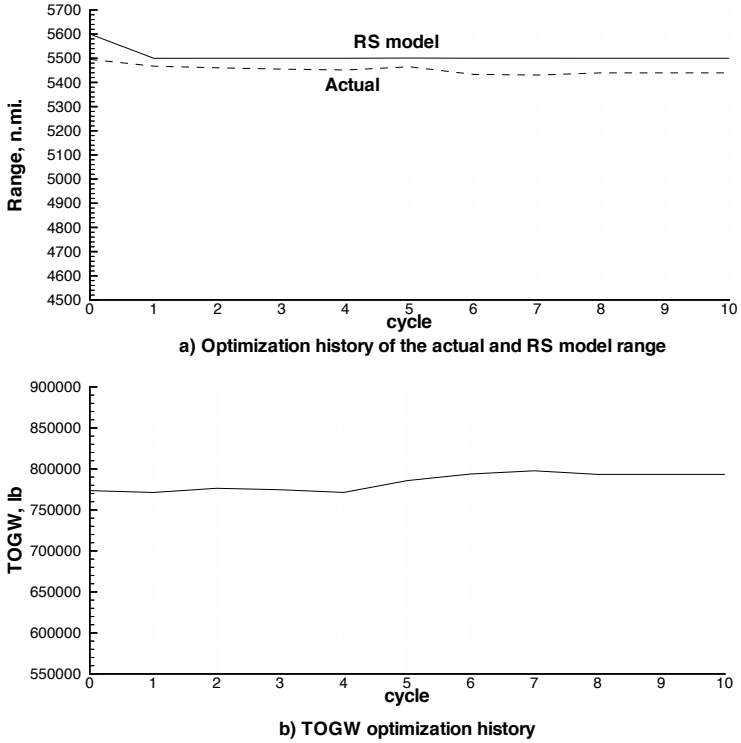

Figure 5.37: History plots of optimization with the range RS model started from "standard" optimum.

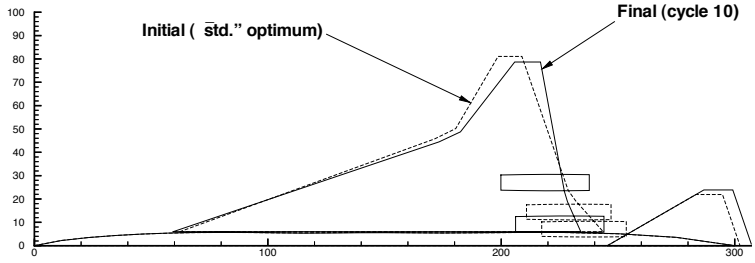

Figure 5.38: Planforms of optimization with the range RS model started from "standard" optimum.

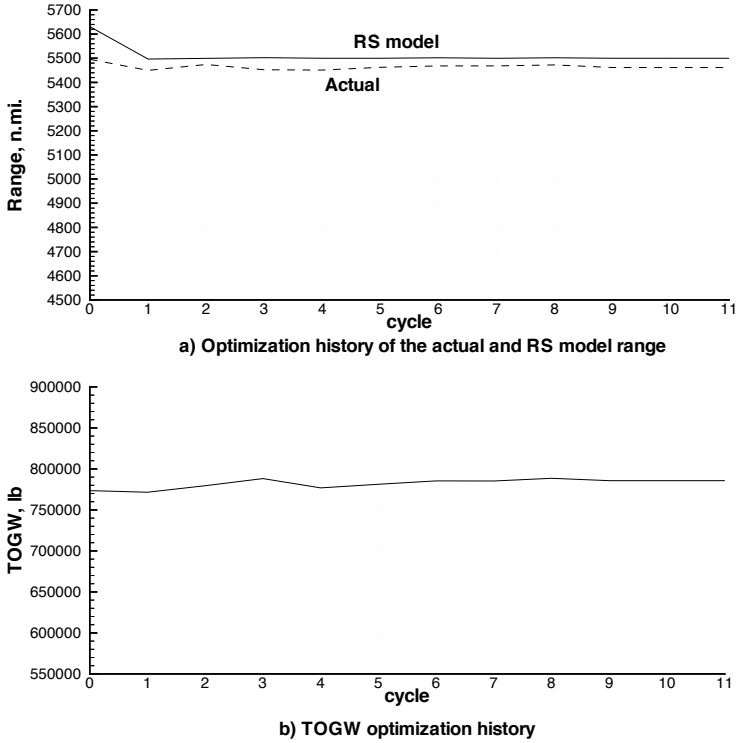

Figure 5.39: History plots of optimization with the drag RS models started from "standard" optimum.

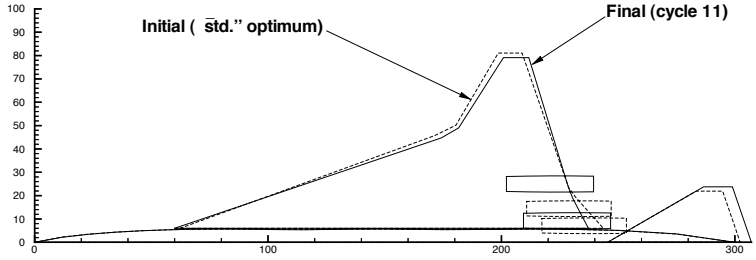

Figure 5.40: Planforms of optimization with the drag RS models started from "standard" optimum.

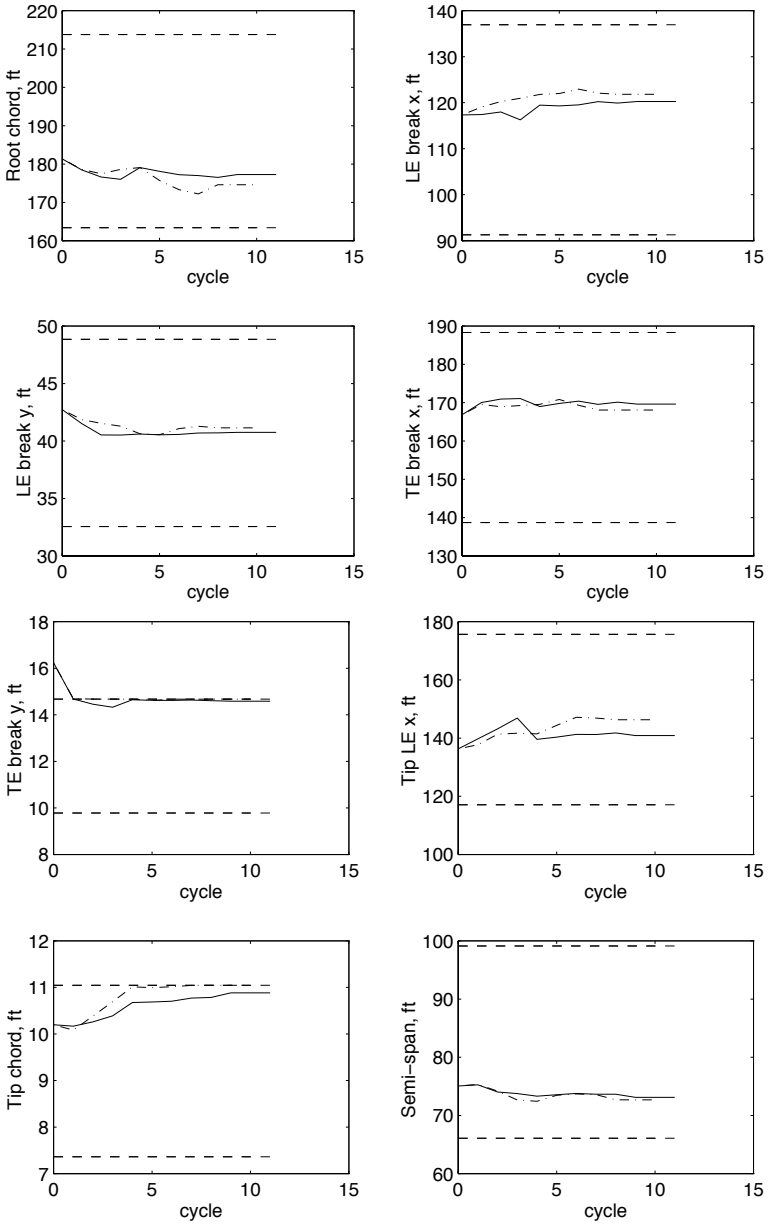

Figure 5.41: Design variable traces for two optimization runs with the RS models from "standard" optimum. Solid lines correspond to optimization with the range RS model. Dash-dotted lines show optimization with the drag RS models. Dashed lines show the lower and upper limits of the "box".

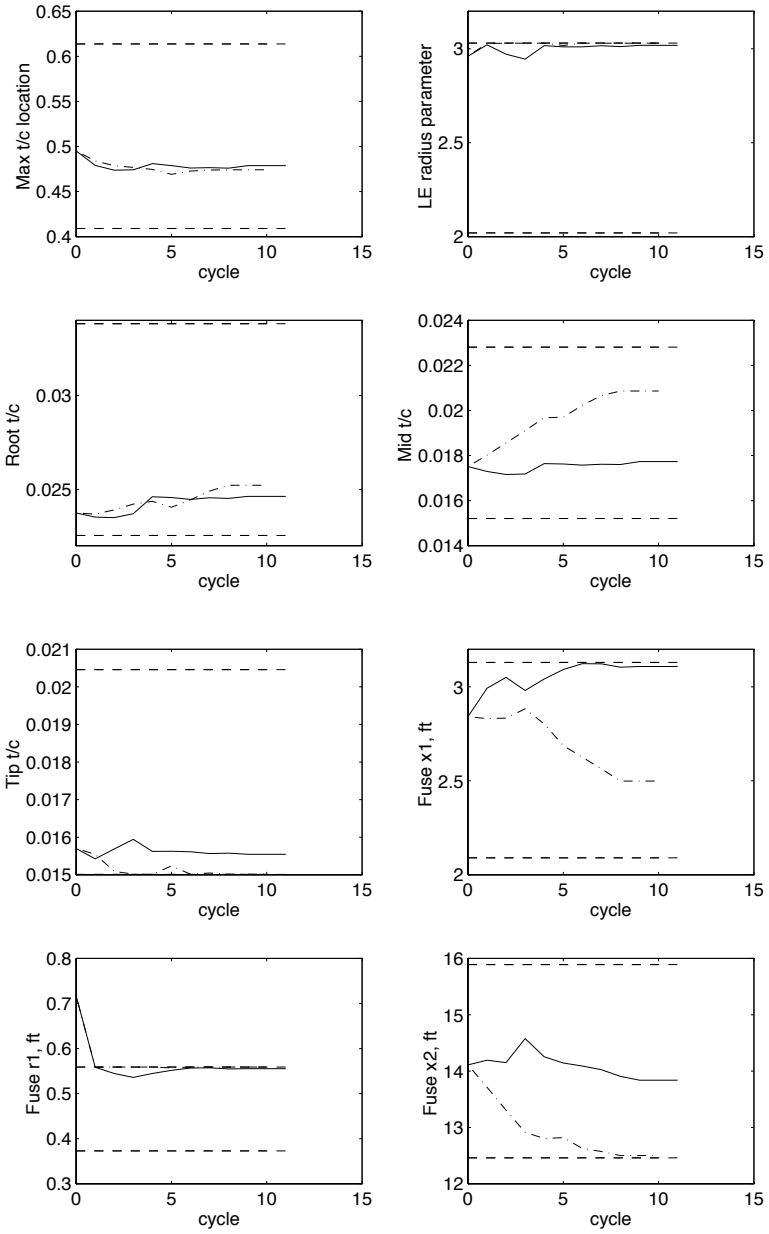

Figure 5.42: Design variable traces (contd.)

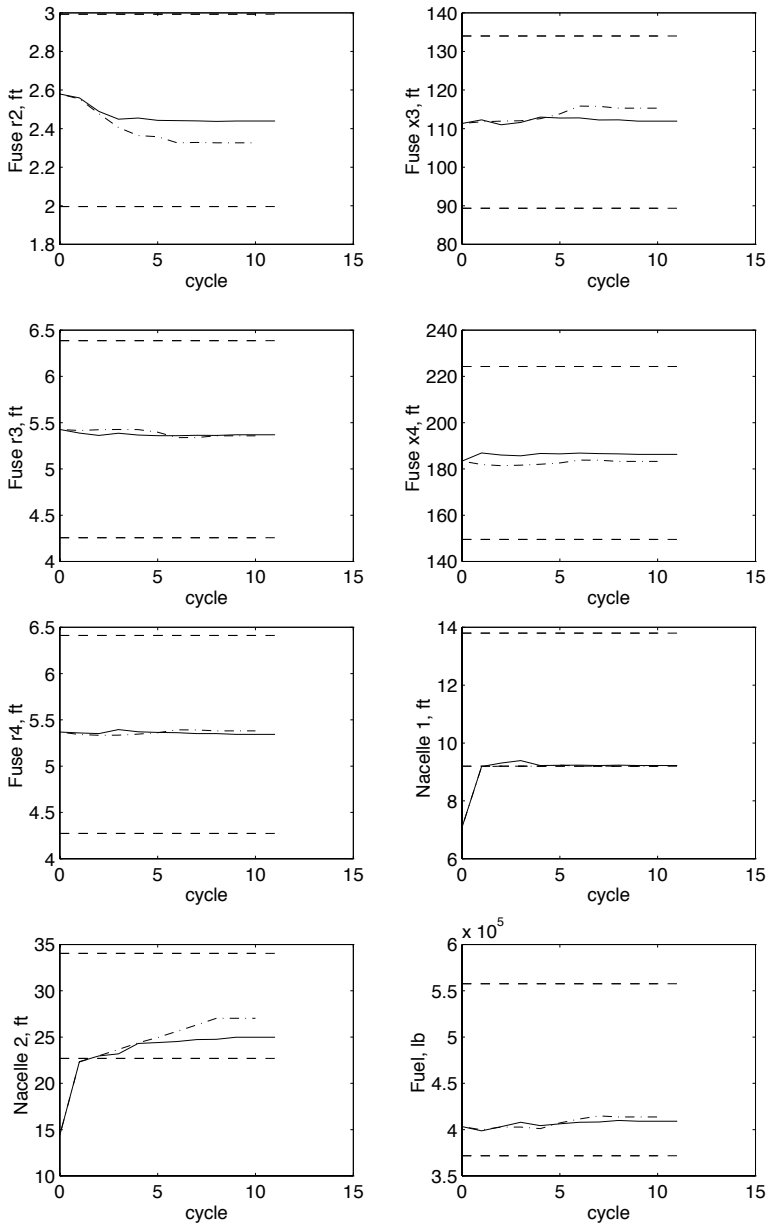

Figure 5.43: Design variable traces (contd.)

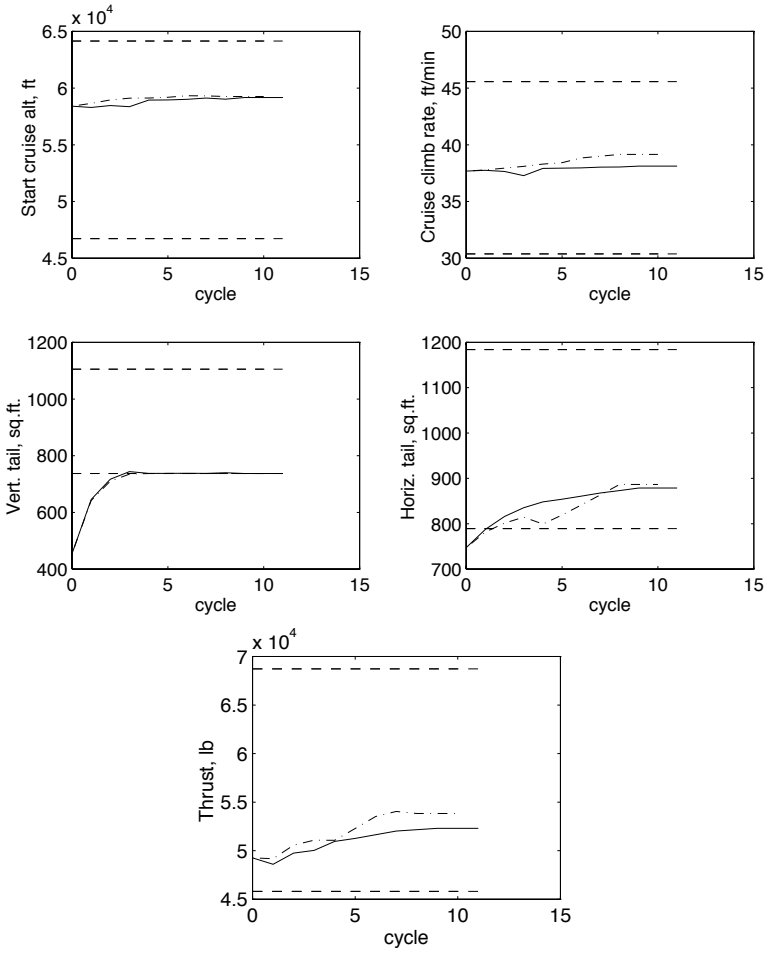

Figure 5.44: Design variable traces (contd.)

Table 5.8: Comparison of the final designs for RS model optimization runs started from "standard" optimization optimum (Case 29c from [5]).

Parameter	Range RS model optimization	Drag RS models optimization	"Standard" optimization
Gross Weight (*lbs*)	793,328.2	785,679.1	772,981
Corrected Gross Weight (*lbs*)	798,764.2	789,126.1	772,752
Fuel Weight (*lbs*)	413,732	409,002	403,345
Fuel Wt / Gross Wt	52.1%	52.0%	52.2%
Wing Area (ft^2)	12,666	12,783	13,191
Aspect Ratio	1.95	1.96	1.99
Wing thickness at root, %	2.52	2.84	2.37
Vertical Tail Area (ft^2)	736.9	737.3	454.1
Horizontal Tail Area (ft^2)	1,733.4	1,757.7	1,494.4
Nacelle 1 position, y (*ft*)	9.2	9.2	7.1
Nacelle 2 position, y (*ft*)	27.0	25.0	14.4
Range actual (*n.mi.*)	5,439.6	5,461.7	5,503.0
Range RSM (*n.mi.*)	5,498.5	5,500.0	n/a
Landing angle of attack	11.5°	11.2°	10.6°

Chapter 6

Conclusions

Response surface methodology has been used to build variable-complexity response surface models for aerodynamic parameters of the HSCT and their use in an HSCT optimization has been investigated. The approach was applied to the HSCT optimization problem with both a reduced (25) and the full (29) number of design variables. Response surface models for both the range of the HSCT and drag related coefficients were built during the work and used in optimization to reduce the detrimental effect of numerical noise during optimization. The results of the work show that aerodynamic response surface approximations in high dimensional space can be generated and successfully used in an HSCT optimization, provided that special measures are taken to control the prediction errors of the response surface models. Using response surface models reduced the amount of numerical noise produced by the expensive aerodynamic analyses during optimization, which in turn improved the convergence of the optimization (25-30 cycles were enough to complete an optimization with response surface models, as opposed to 40-50 cycles without the response surface models). Studies also indicated that noise is still present in the optimization, possibly due to different constraints becoming active/inactive during optimization, since in many cases the optimizer did not follow the same direction when started from the same initial design but with different move limits. Further investigation is required to determine the source of the noisy convergence.

A considerable saving in CPU time can be achieved by using response surface

models in optimization, when compared to using the high fidelity methods. Each detailed aerodynamic analysis requires a CPU time on the order of several minutes (4.5–5.0 CPU min depending on the processor used), while response surface model evaluation takes fractions of a second (0.12–0.16 CPU sec). These large time savings were not fully realized in this work, because our "standard" optimization uses only a small number of detailed analyses at the beginning of each cycle. The majority of the analyses are performed using "approximate" methods based on algebraic expressions which require CPU times comparable to the RS model evaluation time (0.12–0.16 CPU sec). If only "exact" analyses were used in the optimization, response surface models would have reduced the time by several orders of magnitude. Even so, the number of optimization cycles was almost halved.

In the first part of the work, a reduced number of design variables (25) were used to construct response surface approximations for *expensive* aerodynamic constraints of the HSCT. A data set of 2490 designs from the previous work by Balabanov, *et al.* [21] was used in this study. Values of the constaints were calculated using the high fidelity analyses of the *HSCT* code. Due to changes in the *HSCT* code all these designs were found to be infeasible for the current HSCT problem. The data obtained was then processed by the *RSG* code to fit polynomial approximations to the constraint functions. Data clipping was used at this stage to reduce the fitting errors. Unreliable terms in the polynomials were then identified using the statistical techniques of regression analysis and ANOVA. Polynomial terms with high values of the coefficient of variation were excluded from the models to improve the prediction. Two of the constraints were found to be difficult to fit with a polynomial due to their incorrect formulation as functions with poles. Response surface models for these two constraints were not made.

A range constraint response surface model built on the 2490 design set was used in the trial optimization runs. Results indicated that the optimizer quickly goes out of the valid response surface model region so the model prediction errors can be very large. The optimum design location far outside of the valid response surface model design space was suspected as one of the reasons for poor response surface model performance in optimization.

Response surface models for coefficients related to the cruise drag were also built in the first part of the work. The same 2490 designs were again used. Values of the wave drag, friction drag, lift curve slope and leading edge suction coefficients were obtained. Response surface models were built for all these parameters using the same technique as for the aerodynamic constraints. Prediction error analyses indicated that using individual response surface models for the drag components instead of one model for the range constraint is more beneficial, so the drag response surface models were installed in the *HSCT* code for optimization. Results of optimization trials again illustrated the poor RS models' prediction capabilities, as the optimizer was quickly finding the areas with extremly high prediction errors. Work with the infeasible 2490 design data set was discontinued in favor of generating new feasible designs for range and drag response surface models.

All 29 design variables of the *HSCT* code were used in the second part of the work, when response surface approximations for range and drag components were built and used in the optimization. First, a baseline design was obtained using the standard HSCT optimization approach with constraints tightened by 1-2% to get a design inside the feasible domain. Next, 30,915 candidate designs were generated around the baseline design using a fractional factorial experimental design. Out of these candidate designs two sets of approximately 1500 designs each were selected randomly. Then, the D-optimality criterion was used to replace the 400 worst designs in each set to improve the point distribution. The two sets of designs were analysed to obtain values of range and drag related coefficients — wave drag, lift curve slope, and leading edge suction coefficient. These aerodynamic parameters are computationally expensive to calculate using high fidelity analyses and are some of the primary sources of numerical noise in optimization. Quadratic polynomials were fit to the data for the range and drag coefficients in the first data set (set A) using the *RSG* code. Regression analysis and ANOVA were used again to identify and exclude unreliable terms from the models.

An error analysis showed a drastic improvement in the prediction capabilities of the response surface models compared to the previous design space (25 DV problem). The standard deviations of the prediction errors were reduced to only 17.5 n.mi.

for the range response surface model and 11.3 n.mi. for the drag response surface models when computed on the designs of set B. Both range and drag response surface models were tested in the HSCT optimization. When allowed to work everywhere in the design space the optimizer was quickly going away from the valid region of the response surface models, exploiting areas where response surface models could not predict range accurately. On the other hand, when side constraints were imposed on each design variable so that the optimizer was working inside a "box" around the baseline design, the prediction errors of the response surface models were kept at a reasonable level and convergence was achieved in each optimization run. Optimization with the range response surface model produced an efficient design with the TOGW nearly the same as from our previous standard optimizations (around 780,000 lb), but not lighter. Optimization with the drag response surface models mostly resulted in heavier locally optimum designs. This is a matter of the starting design and other optimization runs with different initial points may produce better final designs. For both range and drag response surface models, using a "box" approach prevented large prediction errors.

To try to understand why the "standard" approach produced lighter designs, the range and drag RS model optimization runs were started from the values of the design variables for the final "standard" design. It turned out that this design had design variable values outside of the "box" limits. Thus, the optimizer immediately moved the design to have the design variable values within the limits of the allowable design space. This helps to explain why the RSM-based designs had a higher TOGW than the "standard" optimum design.

Another approach for reducing prediction errors of response surface models in the region of interest was studied. That was by updating the information set with new design results obtained from previous optimization runs, where the optimizer selected designs were added to the data set and the response surface models regenerated using this new data set. Experience with this method showed that drastic improvement in the response surface model performance may be achieved in those areas where extrapolation of the models produced extremely high errors. Combining the two approaches — "box" and updating — resulted in very good agreement between the

actual and predicted values of range, with only 6–10 n.mi. errors.

Variable-complexity response surface approximations for aerodynamic parameters have been shown to be a viable and effective way of dealing with problems of numerical noise in multidisciplinary optimization of the HSCT. The number of optimization cycles required to find an optimum was reduced to 25–30 as opposed to 40–50 in optimizations without response surface models. Although the amount of numerical noise was reduced and optimization convergence improved, noise was still present in the optimization. The approach also permits effective use of parallel computation in MDO procedures, when the computational cost of numerous function evaluations using high fidelity aerodynamic tools can be shifted prior to the optimization, where it is easily *parallelizable*. This approach was used by Balabanov, *et al.* [21] when creating structural response surface models. Parallel computing was not used in this work because aerodynamic tools employing linear theory methods were used, which were not computationally expensive. It will be required when the same approach is applied to more expensive analysis methods, such as Euler/Navier-Stokes flow solvers.

Questions about the practical reliability of response surface models and their accuracy and prediction capabilities during optimization are still open. Special considerations are needed for ensuring acceptable levels of prediction errors. More research needs to be done on the problem of design space sampling and developing new experimental designs, as D-optimality proved to be impractical in high dimensional problems. Future work may also include combining aerodynamic and structural response surface approximations in HSCT optimization.

Bibliography

[1] Haftka, R. T. and Sobieszczanski-Sobieski, J., "Multidisciplinary Aerospace Design Optimization: Survey of Recent Developments," AIAA Paper 96-0711, *34th Aerospace Sciences Meeting and Exhibit*,Reno, NV, Jan. 1996.

[2] Hutchison, M. G., Huang, X., Mason, W. H., Haftka, R. T., and Grossman, B., "Variable-Complexity Aerodynamic-Structural Design of a High-Speed Civil Transport Wing," AIAA Paper 92-4695, Sept. 1992.

[3] Hutchison, M. G., Unger, E., Mason, W. H., Grossman, B., and Haftka, R. T., "Variable-Complexity Aerodynamic Optimization of a High Speed Civil Transport Wing," *Journal of Aircraft*, vol. 31, pp. 110–116, Jan.-Feb. 1994.

[4] Hutchison, M. G., Mason, W. H., Grossman, B., and Haftka, R. T., "Aerodynamic Optimization of an HSCT Configuration Using Variable-Complexity Modeling," AIAA Paper 93-0101, Jan. 1993.

[5] MacMillin, P., Golovidov, O., Mason, W., Grossman, B., and Haftka, R., "Trim, Control and Performance Effects in Variable-Complexity High-Speed Civil Transport Design," MAD Center Report 96-07-01, July 1996, http://www.aoe.vt.edu/mad/Publications/reports/96/rep1.html.

[6] MacMillin, P. E., Golovidov, O. B., Mason, W. H., Grossman, B., and Haftka, R. T., "An MDO Investigation of the Impact of Practical Constraints on an HSCT Optimization," AIAA Paper 97-0098, Jan. 1997.

[7] McCullers, L. A., "Aircraft Configuration Optimization Including Optimize Flight Profiles," in *Proceedings of a Symposium on Recent Experiences in Multidisciplinary Analysis and Optimization*, pp. 395–412, April, 1984. J. Sobieski, compiler, NASA CP–2327.

[8] Jayaram, S., Myklebust, A., and Gelhausen, P., "ACSYNT – A Standards-Based System for PArametric Computer Aided Conceptual Design of Aircraft," AIAA Paper 92-1268, 1992.

[9] Dudley, J., Huang, X., Haftka, R. T., Grossman, B., and Mason, W. H., "Variable-Complexity Interlacing of Weight Equation and Structural Optimization for the Design of the High-Speed Civil Transport," AIAA Paper 94-4377, Sept. 1994.

[10] Box, G. E. P. and Wilson, K. B., "On the Experimental Attainment of Optimum Conditions," *Journal of Royal Statistical Society*, vol. B13, pp. 38–45, 1951.

[11] Box, G. E. P., Hunter, W. G., and S., H. J., *Statistics for Experiments: An Introduction to Design, Data Analysis, and Model Building.* New York, N. Y.: John Wiley & Sons, 1978.

[12] Myers, R. H. and Montgomery, D. C., *Response Surface Methodology: Process and Product Optimization Using Designed Experiments*, pp. 650–651. New York, N. Y.: John Wiley & Sons, 1995.

[13] Montgomery, D. C., *Design and Analysis of Experiments*, pp. 180–263,340–364. New York, N. Y.: John Wiley & Sons, 1976.

[14] Tai, J. C., Mavris, D. N., and Schrage, D. P., "Application of a Response Surface Method to the Design of Tipjet Driven Stopped Rotor/Wing Concepts," AIAA 95-3965, Sept 1995. *1st AIAA Aircraft Engineering, Technology, and Operations Congress*, Los Angeles, CA,.

[15] Engelund, W. C., Stanley, D. O., Lepsch, R. A., and McMillian, M. M., "Aerodynamic Configuration Design Using Response Methodology Analysis," AIAA

93-3967, Aug 1993. *AIAA Aircraft Design, Systems, and Operations Meeting*, Monterey, CA,.

[16] Giunta, A. A., Dudley, J. M., Grossman, B., Haftka, R. T., Mason, W. H., and Watson, L. T., "Noisy Aerodynamic Response and Smooth Approximations in HSCT Design," AIAA Paper 94-4376, Sept. 1994.

[17] Giunta, A., Balabanov, V., Haim, D., Grossman, B., Mason, W., Watson, L., and Haftka, R., "Wing Design for a High-Speed Civil Transport Using a Design of Experiments Methodology," AIAA Paper 96-4001, Proceedings of the *6th AIAA/NASA/ISSMO Symposium on Multidisciplinary Analysis and Optimization*, pp. 168–183, Sept. 1996. http://www.aoe.vt.edu/mad/Publications/96/papers96.html.

[18] Giunta, A. A., "Aircraft Multidisciplinary Design Optimization Using Design of Experiments Theory and Response Surface Modeling Methods," MAD Center Report 97-05-01, May 1997.

[19] Kaufman, M., Balabanov, V., Burgee, S., Giunta, A., Grossman, B., Haftka, R., Mason, W., and Watson, L., "Variable-complexity response surface approximations for wing structural weight in HSCT design," *Computational Mechanics*, vol. 18, pp. 112–126, June 1996.

[20] Balabanov, V., Kaufman, M., Giunta, A., Haftka, R. T., Grossman, B., Mason, W. H., and Watson, L. T., "Developing Customized Wing Weight Function by Structural Optimization on Parallel Computers," AIAA Paper 96-1336, Proceedings of the *37th AIAA/ASME/ASCE/AHS/ASC Structures, Structural Dynamics, and Materials Conference and Exhibit*, Salt Lake City, UT, pp. 113–125, Apr. 1996.

[21] Balabanov, V., Kaufman, M., Knill, D. L., Haim, D., Golovidov, O., Giunta, A. A., Haftka, R. T., Grossman, B., Mason, W. H., and Watson, L. T., "Dependence of Optimal Structural Weight on Aerodynamic Shape for a High-Speed Civil Transport," AIAA Paper 96-4046-CP, Proceedings of the *6th*

AIAA/NASA/ISSMO Symposium on Multidisciplinary Analysis and Optimization, Bellevue, WA, pp. 599–612, Sept. 1996.

[22] Crisafulli, P., Kaufman, M., Giunta, A., Mason, W., Grossman, B., Watson, L., and Haftka, R., "Response Surface Approximations for Pitching Moment, Including Pitch-Up, in the MDO Design of an HSCT," AIAA Paper 96-4136, Proceedings of the *6th AIAA/NASA/ISSMO Symposium on Multidisciplinary Analysis and Optimization*, pp. 1308–1322, Sept. 1996. http://www.aoe.vt.edu/aoe/faculty/Mason_f/MRRpubs96.html.

[23] Dudley, J., Huang, X., MacMillin, P. E., Grossman, B., Haftka, R. T., and Mason, W. H., "Multidisciplinary Optimization of the High-Speed Civil Transport," AIAA 95-0124, Sept 1995. *33rd Aerospace Sciences Meeting and Exhibit*. Reno, NV.

[24] Hutchison, M. G., Unger, E. R., Mason, W. H., Grossman, B., and Haftka, R. T., "Variable-Complexity Aerodynamic Optimization of an HSCT Wing Using Structural Wing-Weight Equations," *Journal of Aircraft*, vol. 31, no. 1, pp. 110–116, 1994.

[25] Grandhi, R. V., Thareja, R., and Haftka, R. T., "NEWSUMT-A: A General Purpose Program for Constrained Optimization Using Approximation," *ASME Journal of Mechanisms, Transmissions and Automation in Design*, vol. 107, pp. 94–99, 1985.

[26] Bertin, J. and Smith, M., *Aerodynamics for Engineers*. Prentice Hall, 2 ed., 1989.

[27] Carlson, H., Mack, R., and Barger, R., "Estimation of Attainable Leading Edge Thrust for Wings at Subsonic and Supersonic Speeds," NASA TP-1500, 1979.

[28] Carlson, H. and Miller, D., "Numerical Methods for the Design and Analysis of Wings at Supersonic Speeds," NASA TN D-7713, 1974.

[29] Harris, Jr., R. V., "An Analysis and Correlation of Aircraft Wave Drag," NASA TM X-947, 1964.

[30] Hutchison, M. G., *Multidisciplinary Optimization of High-Speed Civil Transport Configurations Using Variable-Complexity Modeling*. PhD thesis, Virginia Polytechnic Institute and State University, Blacksburg, Virginia, Mar. 1993.

[31] Cohen, D. and Friedman, M. D., "Theoretical Investigation of the Supersonic Lift and Drag of Thin, Sweptback Wings with Increased Sweep near the Root," NACA TN-2959, June 1953.

[32] Roskam, J., *Methods for Estimating Stability and Control Derivatives of Conventional Subsonic Airplanes*. Kansas: Roskam Aviation and Engineering Corporation, 1971.

[33] Hoak, D. E. *et al.*, *USAF Stability and Control DATCOM*. Flight Control Division, Air Force Flight Dynamics Laboratory, WPAFB, Ohio, 45433-0000, 1978. Revised.

[34] Kay, J., Mason, W., Durham, W., Lutze, F., and Benoliel, A., "Control Power Issues in Conceptual Design: Critical Conditions, Estimation Methodology, Spreadsheet Assessment, Trim and Bibliography," VPI-Aero-200, Nov. 1993. http://www.aoe.vt.edu/aoe/faculty/Mason_f/SD1.html.

[35] Kaufman, M. D., "Variable-Complexity Response Surface Approximation for Wing Structural Weight in HSCT Design," Master's thesis, Virginia Polytechnic Institute and State University, Blacksburg, Virginia, Apr. 1996. http://scholar.lib.vt.edu/theses/public/etd-24012559631561/etd-title.html.

[36] Hinkelman, K., *Design and analysis of experiments*. New York, N. Y.: John Wiley & Sons, Inc., 1994.

[37] Box, M. J. and Draper, N. R., "Factorial Designs, the $|\mathbf{X}^T\mathbf{X}|$ Criterion, and Some Related Matters," *Technometrics*, vol. 13, no. 4, 1971.

[38] Giunta, A., Narducci, R., Burgee, S., Grossman, B., Mason, W., Watson, L., and Haftka, R., "Variable-Complexity Response Response Surface Aerodynamic Design of an HSCT Wing," AIAA 95-1886, Proceedings of the *13th AIAA Applied Aerodynamics Conference*, San Diego, CA, pp. 994–1002, June 1995.

[39] Mitchell, T., "An Algorithm for the Construction of *D*-Optimal Experimental Designs," *Technometrics*, vol. 16, no. 2, 1974.

[40] Anderson, E., Bai, Z., Bischof, C., Demmel, J., Dongarra, J., Du Coz, J., Greenbaum, A., Hammarling, S., McKenney, A., and Sorensen, D., *LAPACK User's Guide*. Philadelphia: Society for Industrial and Applied Mathematics, 1992.

[41] Burden, R. L. and Faires, J. D., *Numerical Analysis*. Boston: PWS Publishing company, 1993.

[42] Huber, P., *Robust Statistics*. New-York: Wiley, 1987.

[43] Rosseeuw, P. and Leroy, A., *Robust Regression and Outlier Detection*. New-York: Wiley, 1987.

[44] Khuri, A. I. and Cornell, J. A., *Response Surfaces: Designs and Analyses*. New York, N. Y.: Marcel Dekker, 1987.

[45] Kay, J., Mason, W. H., Durham, W., and Lutze, F., "Control Authority Assessment in Aircraft Conceptual Design," AIAA Paper 93-3968, Aug. 1993.

Appendix A

Modifications to the HSCT Code

A detailed description of the *HSCT* code can be found in Ref. [5], where all numerous input/output and command files are described along with the analysis and optimization subroutines of the code. In this chapter only minor modifications to the software will be described which were used to develop and implement response-surface approximations in the optimization of HSCT. The changes can be divided into three categories depending on the purpose of the modification (more detailed description follows below):

1. **Changes for performing multiple design analyses** include a special case `ANALYZE` (see also section 4.3.1) which was included into the `main()` subroutine of the code. This also required definition of the new command `ANALYZE` inside the code, so that it can be recognized by the subroutine reading in the command file, `Read_Command_File()`. The input file for this case is `analyze.in` and the output file is `analyze.out`. The i/o files and changes to the source files are described below.

2. **Changes for using RS models in optimization** include a new source file `RSM.c` containing all RS model functions, and also special provisions in the code for using the models. Command file `hsct.command` was modified to include special flag parameters controlling the use of RS models. The number of constraints is increased by 52 to include the extra constraints (Table 4.6) used for defining

the reasonable design space. The constraints are activated depending on the value of the flag parameters. Besides these, 58 more constraints are included into the `constraints()` subroutine to define the minimum and maximum values for each design variable when using "box" approach during optimization and may be activated by the special flag variable. The limits of the box should be placed in a file called `box.in`. Changes were made in the `Lift_Drag()` and `Wave_Drag()` subroutines to call RS model functions instead of the actual aero analyses.

3. **Changes for postprocessing** consist of the special case `ALHA6` set up in the `main()` subroutine for doing parametric α-plots of the exact and RSM predicted values of range and drag components. Changes were made also in the `doAlpha()` subroutine, where the data tables are actually generated and in the `Read_Command_File()` to interpret the new command `ALPHA6`.

A.1 Control and I/O Files

hsct.command

Three new flag parameters were included into the `hsct.command` file which control the use of RS models and the way they are used: *"Use Range RSM", "Use drag RSMs"* and *"Use GLA(1) or SCALED(2) or BOX(3)"*. The flag parameters are represented in the code by variables included into the C structure `opt` which have the names, correspondingly: `opt.use_rangeRS, opt.use_dragRS, opt.use_GLA`. The flags are located in the `Optim Control` section of the command file. Here is the portion of the command file illustrating their placement:

```
Optim Control
   26           Starting cycle
   30           Ending cycle
   0.024        Move limits
  175           Number of constraints
   0            Use RS for wing bending material weight
   0            Use Range RSM
   1            Use drag RSMs
   3            Use GLA (1) or SCALED (2) or BOX (3)
```

The flags can assume the following values:

Use Range RSM - flag indicating whether to use or not range RS model:

0 : Range RSM is not used in optimization.
1 : Range RSM is used in optimization.

Use drag RSMs - flag indicating whether to use or not drag RS models:

0 : Drag RSMs are not used in optimization.
1 : Drag RSMs are used in optimization.

Use GLA (1) or SCALED (2) or BOX (3) - mode select flag:

1 : GLA correction of wave drag RS model is used.
2 : SCALED correction of wave drag RS model is used.
3 : "box" constraints are used in optimization.

Note that *GLA* and *SCALED* corrections are applied to wave drag RS model only, so these flag values should be used only when using drag RS models. "Box" optimization can be used with both range and drag RS models.

The values of the main and nose gear lengths have been increased by 1 ft each:

```
Landing Gear
   20.75 Main gear length
   19.75 Nose gear length
   15.00 Tipback angle (deg)
   63.00 Maximum overturn angle (deg)
```

New commands that can be used with the modified code are:

`ANALYZE` - Performs multiple design analyses. Required input file is `analyze.in`. Output is written into `analyze.out`.

`ALPHA6` - Prints out a table of data for making α-plots of exact and RSM predicted values of range and drag components. Output is written into standard output file `hsct.out`.

analyze.in

This file is required when using `ANALYZE` command. The first line of the file should contain the number of designs N_{des} to be processed by the code. Each of the next lines should contain 29 design variables of the designs to be analyzed. All information past the 29 numbers on each line will be ignored by the program. The number of lines with design variables should be equal to or greater than N_{des}.

analyze.out

This is the output file of the case `ANALYZE`. Each line of the file contains 29 design variables of the analyzed design, value of TOGW, exact range and values of drag components (friction drag coefficient $C_{D_{fric}}$, wave drag coefficient $C_{D_{wave}}$, lift curve slope C_{L_α}, LE suction coefficient C_T/C_L^2 and attainable lE suction coefficient LES_{att}). Other data may be printed into the file if required. To do this, the case `ANALYZE` in the `main()` should be modified in the required way and `HSCT` recompiled.

box.in

This file contains the values of side constraints for each design variable. Here is the sample file, that was used in all optimizations with "box" constraints activated:

```
1.6339    2.1378
0.9130    1.3695
3.2564    4.8845
1.3872    1.8831
0.9782    1.4673
1.1709    1.7563
0.7363    1.1045
6.6087    9.9131
4.0915    6.1373
2.0202    3.0302
2.2547    3.3820
1.5208    2.2812
1.5010    2.0457
0.0209    0.0313
0.0373    0.0559
0.1246    0.1589
0.1996    0.2993
```

```
0.8935    1.3402
0.4257    0.6386
1.4953    2.2429
0.4274    0.6411
0.9198    1.3797
2.2697    3.4046
3.7179    5.5769
4.6722    6.4152
0.3038    0.4557
7.3695   11.0543
7.8929   11.8393
4.5817    6.8726
```

A.2 Source Files

aero.c

Subroutine setupAeroAnalysis():

Case RSMODEL was added in the wave drag portion of the subroutine. The case serves to define the values of GLA correction factors when parameter opt.use_GLA is equal to 1, and to define SCALED correction factor when parameter opt.use_GLA is equal to 2.

Subroutine Lift_Drag():

Case RSMODEL was added to the subroutine to call RS model functions for lift curve slope CLa_RS() and LE suction coefficient CToCL2_RS().

Subroutine Wave_Drag():

Case RSMODEL was added to the subroutine to call RS model function for wave drag coefficient wave_RS().

dataio.c

Subroutine writeDesHistory():

The subroutine was modified to print out the value of range predicted by the range RS model.

Subroutine Read_Command_File():

The subroutine was modified to read in the values of the flag parameters (`opt.use_rangeRS, opt.use_dragRS, opt.use_GLA`) and new commands (`ANALYZE` and `ALPHA6`).

main.c

Subroutine main():

Case `OPTIM` was modified to define the type of the approximation for wave drag and lift drag when RS models are used in optimization. Both wave and lift drag approximations are set to `APPROX` when range RSM is used, and to `RSMODEL` when drag RSMs are used in optimization.

Case `ANALYZE` was added. Each design is read in from the `analyze.in` file one at a time, geometry of the aircraft is modified and analysis performed. Data on range and drag components are printed to the `analyze.out` file.

Case `ALPHA6` was added, which sets approximation type of wave and lift drag to `RSMODEL` and sends a specific choice variable to the `doAlpha()` subroutine which performs "alpha" analysis.

Subroutine analys():

Penalty of 10% was added to the objective function value (TOGW) if the fuselage weight is zero. This happens when one of the fuselage design variables assumes negative values. The penalty prevents the optimizer from pushing design variables into the negative domain.

Subroutine `constraints()`:

Simplified range constraint was added for optimizations with range RS model.

Additional 52 constraints defining the reasonable design space (see Table 4.6) were included. The constraints are activated when any of the RS models are used.

"Box" constraints were added, which are activated when flag variable `opt.use_GLA` is equal to 3. The values of the side limits are read in from file `box.in`.

`modify.c`

Subroutine `Modify_with_DV()`:

The call to the function `adjust_Pod()` was moved down to a place after the engine thrust is changed to the current value. This was done to exclude axial placing of the nacelles according to the previous engine size.

`options.c`

Subroutine `doAlpha()`:

A new case "`choice==6`" (`ALPHA6`) was added here. The case serves to print out a table for making α-plots of the exact and RSM predicted values of range and drag components. The output file is `hsct.out`.

`RSM.c`

The file contains all RS model functions. If a different version ("Series") of the RS models needs to be used, the file should be replaced with the corresponding version `RSM.c` file, which has to be compiled and linked to the executable *HSCT* file.

A.3 Include Files

defines.h

Three new parameters were defined:

```
#define RSMODEL         6
#define _ALPHA6_        16
#define _ANALYZE_       40
```

functions.h

Declarations of RSM functions were added:

```
double range_RS(double*);
double wave_RS(double*);
double CToCL2_RS(double*);
double CLa_RS(double*);
double LES_RS(double*);
```

structs.h

In the structure `OptimControl` new integer variables were added (flag parameters for RSM use control):

```
int use_rangeRS, use_dragRS, use_GLA;
```

Appendix B

Comparison of the Final Designs for Optimization Runs with RS Models and "Standard" Optimization

In this section values of all 29 design variables and 68 constraints are listed for the final designs of the three optimization runs: 1) with the range RS model inside a "box"(see Section 5.3.2), 2) with the drag RS models inside a "box" (see Section 5.4.4), and 3) "standard" optimization (Case 29c from [5]). The constraint values were calculated using "exact" analyses of the *HSCT* code. Values of the active constraints for each of the designs are printed in bold font.

Table B.1: Normalized (or scaled) design variables for the final designs of optimization runs with the range RS model, drag RS models, and "standard" optimization. (The values shown here are used in the *HSCT* code. To find the physical values use the multiplier as in Table 2.1.)

#	Range RS model	Drag RS models	"Standard" optimization	Description of the variable
1	1.7923	1.7573	1.8132	Wing root chord
2	1.3598	1.0983	1.1732	LE Break, x
3	4.6531	3.6532	4.2726	LE Break, y
4	1.7757	1.7007	1.6684	TE Break, x
5	1.0242	1.4488	1.6233	TE Break, y
6	1.5635	1.4136	1.3631	LE of wing tip, x
7	1.0989	0.9716	1.0198	Tip chord
8	7.0811	7.6035	7.5067	Wing semi-span
9	4.7594	4.7949	4.9511	Chordwise location of max. t/c
10	2.0308	2.2797	2.9601	Airfoil LE radius parameter, r_t
11	2.2652	2.8452	2.3741	Airfoil t/c at root
12	1.7934	2.0166	1.7514	Airfoil t/c at LE break
13	1.5119	1.9093	1.5700	Airfoil t/c at tip
14	0.0246	0.0263	0.0284	Fuselage restraint 1, x
15	0.0559	0.0435	0.0717	Fuselage restraint 1, r
16	0.1264	0.1385	0.1411	Fuselage restraint 2, x
17	0.2346	0.2433	0.2579	Fuselage restraint 2, r
18	1.1423	1.1114	1.1133	Fuselage restraint 3, x
19	0.5352	0.5330	0.5426	Fuselage restraint 3, r
20	1.8620	1.8751	1.8336	Fuselage restraint 4, x
21	0.5443	0.5269	0.5369	Fuselage restraint 4, r
22	0.9244	0.9456	0.7082	Nacelle 1, y
23	3.3855	3.3559	1.4405	Nacelle 2, y
24	3.9712	4.3359	4.0334	Mission fuel
25	5.9252	5.8488	5.8400	Starting cruise altitude
26	0.3646	0.3876	0.3767	Cruise climb rate
27	8.5204	8.9500	4.5405	Vertical tail area
28	9.5704	8.8070	7.4723	Horizontal tail area
29	5.0411	5.3830	4.9257	Thrust per engine

Table B.2: Values of the constraints for the final designs. Active constraints are in bold font. Formulae used for the constraint functions in the *HSCT* code are listed in Table 2.2.

#	Range RS model	Drag RS models	"Standard" optimization	Description of the constraint
1	**-2.389482e-01***	3.939601e-02†	**-1.641084e-02**	Range $\geq$ 5,500 *n.mi.*
2	2.957566e-01	2.136158e-01	2.882373e-01	Required C_L at landing speed ≤ 1
3	3.197645e+00	3.213137e+00	3.522417e+00	Section $C_\ell \leq 2$
4	2.918982e+00	2.870422e+00	3.144846e+00	Section $C_\ell \leq 2$
5	2.648246e+00	2.535337e+00	2.774682e+00	Section $C_\ell \leq 2$
6	2.383408e+00	2.206352e+00	2.408926e+00	Section $C_\ell \leq 2$
7	2.122486e+00	1.882050e+00	2.064988e+00	Section $C_\ell \leq 2$
8	1.863453e+00	1.559176e+00	1.762765e+00	Section $C_\ell \leq 2$
9	1.604141e+00	1.233227e+00	1.458301e+00	Section $C_\ell \leq 2$
10	1.342097e+00	8.997828e-01	1.148174e+00	Section $C_\ell \leq 2$
11	1.074398e+00	5.540757e-01	8.284381e-01	Section $C_\ell \leq 2$
12	7.973411e-01	4.279630e-01	4.939826e-01	Section $C_\ell \leq 2$
13	5.059438e-01	3.499936e-01	2.356149e-01	Section $C_\ell \leq 2$
14	1.930270e-01	2.741774e-01	1.741863e-01	Section $C_\ell \leq 2$
15	9.273766e-02	2.010787e-01	1.164805e-01	Section $C_\ell \leq 2$
16	4.567058e-02	1.322467e-01	6.464632e-02	Section $C_\ell \leq 2$
17	1.049954e-02	7.185751e-02	2.399245e-02	Section $C_\ell \leq 2$
18	3.664867e-03	3.299176e-02	1.024544e-02	Section $C_\ell \leq 2$
19	9.816412e-02	7.677721e-02	9.388643e-02	Section $C_\ell \leq 2$
20	2.000000e+08	2.000000e+08	2.000000e+08	Section $C_\ell \leq 2$
21	7.692201e-02	8.618597e-02	1.171675e-01	Landing angle of attack $\leq 12^\circ$
22	1.382320e-01	1.990528e-01	1.264447e-01	Fuel volume $\leq$ half of wing volume
23	2.695341e+00	2.238582e+00	2.399419e+00	Spike prevention
24	2.460555e+01	2.410449e+01	2.490317e+01	Wing chord $\geq$ 7.0 *ft.*
25	2.276806e+01	2.193510e+01	2.260853e+01	Wing chord $\geq$ 7.0 *ft.*
26	2.093048e+01	1.976882e+01	2.031389e+01	Wing chord $\geq$ 7.0 *ft.*
27	1.909282e+01	1.761235e+01	1.801927e+01	Wing chord $\geq$ 7.0 *ft.*
28	1.725507e+01	1.547280e+01	1.583708e+01	Wing chord $\geq$ 7.0 *ft.*
29	1.541722e+01	1.334715e+01	1.388568e+01	Wing chord $\geq$ 7.0 *ft.*
30	1.357929e+01	1.122722e+01	1.193533e+01	Wing chord $\geq$ 7.0 *ft.*
31	1.174127e+01	9.108740e+00	9.984980e+00	Wing chord $\geq$ 7.0 *ft.*
32	9.903168e+00	6.990533e+00	8.034629e+00	Wing chord $\geq$ 7.0 *ft.*
33	8.064979e+00	6.046119e+00	6.084278e+00	Wing chord $\geq$ 7.0 *ft.*
34	6.226709e+00	5.338849e+00	4.575323e+00	Wing chord $\geq$ 7.0 *ft.*

*Violated due to the RS model prediction error.

†Active when range is calculated using the RS models.

Table B.3: Values of the constraints for the final designs (contd.). Active constraints are in bold font. Formulae used for the constraint functions in the *HSCT* code are listed in Table 2.2.

#	Range RS model	Drag RS models	"Standard" optimization	Description of the constraint
35	4.388363e+00	4.631579e+00	3.986976e+00	Wing chord ≥ 7.0 *ft.*
36	3.577751e+00	3.924310e+00	3.398629e+00	Wing chord ≥ 7.0 *ft.*
37	2.979080e+00	3.217041e+00	2.810282e+00	Wing chord ≥ 7.0 *ft.*
38	2.380338e+00	2.509772e+00	2.221935e+00	Wing chord ≥ 7.0 *ft.*
39	1.781529e+00	1.802502e+00	1.633588e+00	Wing chord ≥ 7.0 *ft.*
40	1.182654e+00	1.095233e+00	1.045241e+00	Wing chord ≥ 7.0 *ft.*
41	5.837178e-01	3.879637e-01	4.568937e-01	Wing chord ≥ 7.0 *ft.*
42	3.061280e-01	3.678415e-01	2.981176e-01	No engine 1 scrape at landing AOA
43	4.908875e-01	5.491291e-01	5.201925e-01	No engine 2 scrape at landing AOA
44	4.631257e-01	6.851754e-01	5.381563e-01	No engine 1 scrape, with 5° roll
45	2.268788e-01	4.539897e-01	6.347670e-01	No engine 2 scrape, with 5° roll
46	1.620953e+00	2.124359e+00	2.402130e+00	No wing tip scrape at landing
47	1.921682e+00	1.895037e+00	1.656681e+00	Rudder deflection $\leq 22.5°$
48	1.725876e+01	1.754684e+01	2.479281e+01	Bank angle for crosswind landing $\leq 5°$
49	**-4.157332e-03**	**-1.226144e-02**	**-7.947030e-02**	Takeoff rotation to occur ≤ 5 *sec*
50	1.107426e+01	3.864846e+00	6.925842e-01	Tail deflection for approach trim $\leq 22.5°$
51	3.924057e-02	4.804595e-02	**7.402187e-03**	Wing root T.E. $\leq$ horiz. tail L.E.
52	2.498783e-03	4.687047e-04	**-5.498739e-03**	Balanced field length $\leq 11,000$ *ft*
53	4.924014e+00	5.048868e+00	5.290362e+00	T.E. break scrape at landing with 5° roll
54	5.217974e-01	1.081273e+00	7.569386e-01	L.E. break $\leq$ semispan
55	5.913539e+00	4.247864e+00	3.624122e+00	T.E. break $\leq$ semispan
56	5.101904e-01	8.968585e-01	5.827601e-01	Root $t/c \geq 1.5\%$
57	1.956289e-01	3.444476e-01	1.676018e-01	Break $t/c \geq 1.5\%$
58	**7.969036e-03**	2.729149e-01	4.667059e-02	Tip $t/c \geq 1.5\%$
59	2.348009e+00	3.175636e+00	4.205535e+00	Fuselage: $x_{rest_1} \geq 5ft$
60	1.386227e-02	9.673182e-02	9.885750e-02	Fuselage: $x_{rest_1} + 10\text{ft} \leq x_{rest_2}$
61	4.045235e+00	3.658683e+00	3.617592e+00	Fuselage: $x_{rest_2} + 10\text{ft} \leq x_{rest_3}$
62	4.988220e-01	5.478973e-01	5.112270e-01	Fuselage: $x_{rest_3} + 10\text{ft} \leq x_{rest_4}$
63	3.793052e-01	3.749394e-01	3.887960e-01	Fuselage: $x_{rest_4} + 10\text{ft} \leq 300\text{ft}$
64	3.207029e-01	3.509774e-01	1.182460e-02	Nacelle 1, $y \geq$ side-of-body
65	1.904942e+00	1.808542e+00	4.553503e-02	Nacelle 1, $y \leq$ nacelle 2, y
66	**6.062717e-03**	2.078031e-02	1.113034e-02	Engine-out limit with vertical tail design; otherwise 50%
67	**-1.188807e-01**	**9.274703e-02**	**2.988652e-02**	Max thrust required $\leq$ available thrust
68	**-6.360079e-02**	**8.735168e-02**	**1.594607e-02**	Max thrust required $\leq$ available thrust

Appendix C

Description of the Final RS Models for the 29 Design Variable Problem

Detailed description of the final forms of the response surface models for the 29 design variable problem is presented in this appendix. While generating the response surface models, numerical round-off error was minimized by scaling each variable x_i to a value x_i' where

$$\begin{aligned} x_i' &= a x_i - b\,, \\ a &= 2/\left(x_{i_{\max}} - x_{i_{\min}}\right), \\ b &= 1 + 2x_{i_{\min}}/\left(x_{i_{\max}} - x_{i_{\min}}\right)\,, \end{aligned} \tag{C.1}$$

and $-1 \leq x_i' \leq 1$. The terms $x_{i_{\min}}$ and $x_{i_{\max}}$ represent the maximum and minimum values for x_i which occur in the data used to generate the response surface. The *RSG* program was used to generate each response surface model. The x_i variables for all RS models correspond in order to the twenty nine design variables listed in Table 2.1.

Table C.1: Range RS model scaling factors.

Variable	a	b	Variable	a	b
x_1	+3.969e+00	+7.485	x_{16}	+5.831e+01	+8.265
x_2	+4.381e+00	+5.000	x_{17}	+2.006e+01	+5.004
x_3	+1.228e+00	+5.000	x_{18}	+4.477e+00	+5.000
x_4	+4.033e+00	+6.595	x_{19}	+9.394e+00	+4.999
x_5	+4.089e+00	+5.000	x_{20}	+2.675e+00	+5.000
x_6	+3.416e+00	+5.000	x_{21}	+9.359e+00	+5.000
x_7	+5.432e+00	+4.999	x_{22}	+4.349e+00	+5.000
x_8	+6.053e-01	+5.000	x_{23}	+1.762e+00	+5.000
x_9	+9.776e-01	+5.000	x_{24}	+1.076e+00	+5.000
x_{10}	+1.980e+00	+5.000	x_{25}	+1.147e+00	+6.361
x_{11}	+1.774e+00	+5.000	x_{26}	+1.317e+01	+5.000
x_{12}	+2.630e+00	+5.000	x_{27}	+5.428e-01	+5.000
x_{13}	+3.672e+00	+6.511	x_{28}	+5.068e-01	+5.000
x_{14}	+1.923e+02	+5.019	x_{29}	+8.730e-01	+5.000
x_{15}	+1.075e+02	+5.011			

Table C.2: Range RS model coefficient values.

Index	Basis Function	Coefficient	Index	Basis Function	Coefficient
1	*constant*	+1.645e+00	31	$x'_1\ x'_9$	+8.032e-05
2	x'_1	-4.119e-02	32	$x'_1\ x'_{11}$	-1.389e-03
3	x'_2	-1.144e-01	33	$x'_1\ x'_{12}$	-2.329e-04
4	x'_3	+6.718e-02	34	$x'_1\ x'_{21}$	+1.147e-05
5	x'_4	+2.071e-02	35	$x'_1\ x'_{25}$	-2.092e-04
6	x'_5	-1.185e-03	36	$x'_1\ x'_{29}$	+4.932e-04
7	x'_6	+6.608e-02	37	${x'_2}^2$	-3.966e-02
8	x'_7	+4.860e-03	38	$x'_2\ x'_3$	+4.360e-02
9	x'_8	+2.567e-02	39	$x'_2\ x'_4$	+4.824e-02
10	x'_9	-1.558e-03	40	$x'_2\ x'_6$	+2.061e-02
11	x'_{11}	-9.018e-05	41	$x'_2\ x'_9$	-1.153e-03
12	x'_{12}	-3.840e-04	42	$x'_2\ x'_{11}$	+4.005e-03
13	x'_{17}	-8.350e-05	43	$x'_2\ x'_{12}$	+1.528e-03
14	x'_{18}	-2.947e-05	44	$x'_2\ x'_{24}$	-1.083e-03
15	x'_{19}	+2.257e-05	45	$x'_2\ x'_{25}$	+6.567e-04
16	x'_{20}	+1.555e-03	46	$x'_2\ x'_{26}$	-4.600e-04
17	x'_{23}	-1.725e-04	47	$x'_2\ x'_{29}$	-6.758e-04
18	x'_{24}	+4.536e-04	48	${x'_3}^2$	-9.450e-03
19	x'_{25}	-8.755e-04	49	$x'_3\ x'_4$	-2.944e-02
20	x'_{26}	+1.759e-04	50	$x'_3\ x'_6$	+2.535e-03
21	x'_{27}	-1.565e-04	51	$x'_3\ x'_8$	-8.424e-04
22	x'_{28}	-2.906e-05	52	$x'_3\ x'_9$	+1.999e-03
23	x'_{29}	+1.660e-04	53	$x'_3\ x'_{11}$	-4.198e-03
24	${x'_1}^2$	-6.351e-03	54	$x'_3\ x'_{12}$	-2.236e-03
25	$x'_1\ x'_2$	-5.448e-03	55	$x'_3\ x'_{24}$	-3.719e-03
26	$x'_1\ x'_3$	-3.300e-03	56	$x'_3\ x'_{25}$	-4.912e-03
27	$x'_1\ x'_4$	+1.686e-02	57	$x'_3\ x'_{26}$	+1.209e-03
28	$x'_1\ x'_6$	+6.040e-04	58	$x'_3\ x'_{29}$	-4.709e-04
29	$x'_1\ x'_7$	+7.930e-04	59	${x'_4}^2$	-1.819e-02
30	$x'_1\ x'_8$	+1.189e-03	60	$x'_4\ x'_5$	+1.347e-03

Table C.3: Range RS model coefficient values (contd.).

Index	Basis Function	Coefficient	Index	Basis Function	Coefficient
61	$x'_4\ x'_6$	-2.842e-02	91	$x'_8\ x'_{28}$	-8.356e-04
62	$x'_4\ x'_9$	+3.557e-03	92	$x'_8\ x'_{29}$	+7.799e-04
63	$x'_4\ x'_{11}$	-1.531e-03	93	${x'_9}^2$	-4.878e-04
64	$x'_4\ x'_{12}$	+8.724e-04	94	$x'_9\ x'_{11}$	-3.923e-04
65	$x'_4\ x'_{20}$	-3.535e-03	95	$x'_9\ x'_{18}$	-3.864e-05
66	$x'_4\ x'_{22}$	+9.141e-05	96	$x'_9\ x'_{19}$	-2.082e-04
67	$x'_4\ x'_{23}$	+3.821e-04	97	$x'_9\ x'_{20}$	+1.840e-04
68	$x'_4\ x'_{24}$	+3.003e-05	98	$x'_9\ x'_{24}$	+3.229e-04
69	$x'_4\ x'_{25}$	+3.686e-03	99	$x'_9\ x'_{25}$	+3.073e-04
70	$x'_4\ x'_{26}$	+2.989e-05	100	${x'_{10}}^2$	-3.980e-04
71	$x'_4\ x'_{29}$	-5.097e-04	101	$x'_{10}\ x'_{18}$	-2.667e-05
72	${x'_6}^2$	+8.508e-03	102	$x'_{10}\ x'_{20}$	+3.418e-04
73	$x'_6\ x'_7$	+1.958e-03	103	$x'_{10}\ x'_{21}$	-2.224e-05
74	$x'_6\ x'_8$	+7.565e-03	104	${x'_{11}}^2$	-4.289e-04
75	$x'_6\ x'_9$	+1.978e-04	105	$x'_{11}\ x'_{12}$	-8.065e-04
76	$x'_6\ x'_{12}$	-5.793e-04	106	$x'_{11}\ x'_{19}$	+4.770e-04
77	$x'_6\ x'_{19}$	+1.989e-04	107	$x'_{11}\ x'_{20}$	+5.132e-04
78	$x'_6\ x'_{21}$	+1.962e-05	108	$x'_{11}\ x'_{21}$	-5.478e-04
79	$x'_6\ x'_{24}$	+2.688e-03	109	$x'_{11}\ x'_{24}$	-2.621e-04
80	$x'_6\ x'_{25}$	+8.694e-04	110	$x'_{11}\ x'_{25}$	+2.595e-05
81	$x'_6\ x'_{29}$	-1.613e-04	111	$x'_{11}\ x'_{29}$	-1.211e-03
82	$x'_7\ x'_8$	+1.263e-04	112	${x'_{12}}^2$	-1.285e-04
83	$x'_7\ x'_{21}$	-1.182e-04	113	$x'_{12}\ x'_{25}$	-4.455e-04
84	${x'_8}^2$	-1.217e-02	114	$x'_{13}\ x'_{20}$	+1.453e-04
85	$x'_8\ x'_9$	+4.199e-03	115	$x'_{13}\ x'_{21}$	-1.082e-04
86	$x'_8\ x'_{11}$	-6.144e-03	116	${x'_{15}}^2$	-1.957e-04
87	$x'_8\ x'_{18}$	-3.822e-04	117	$x'_{15}\ x'_{20}$	-3.338e-04
88	$x'_8\ x'_{19}$	-2.959e-06	118	$x'_{16}\ x'_{17}$	-2.597e-04
89	$x'_8\ x'_{21}$	-8.680e-04	119	$x'_{16}\ x'_{19}$	-8.176e-05
90	$x'_8\ x'_{25}$	+3.760e-03	120	$x'_{16}\ x'_{20}$	+2.308e-04

Table C.4: Range RS model coefficient values (contd.).

Index	Basis Function	Coefficient	Index	Basis Function	Coefficient
121	$x'_{17}{}^2$	-2.310e-04	136	$x'_{21}{}^2$	-9.631e-05
122	$x'_{17}\ x'_{19}$	+1.126e-04	137	$x'_{21}\ x'_{25}$	+9.057e-05
123	$x'_{17}\ x'_{21}$	-1.678e-04	138	$x'_{22}{}^2$	-2.603e-04
124	$x'_{18}{}^2$	-2.228e-04	139	$x'_{24}{}^2$	-3.261e-04
125	$x'_{18}\ x'_{19}$	-1.803e-04	140	$x'_{24}\ x'_{25}$	-3.022e-04
126	$x'_{18}\ x'_{20}$	-3.460e-04	141	$x'_{24}\ x'_{26}$	-4.930e-04
127	$x'_{18}\ x'_{22}$	+2.336e-04	142	$x'_{24}\ x'_{29}$	-2.215e-05
128	$x'_{18}\ x'_{25}$	+1.388e-04	143	$x'_{25}{}^2$	-1.077e-05
129	$x'_{18}\ x'_{27}$	-4.084e-05	144	$x'_{25}\ x'_{26}$	-5.557e-04
130	$x'_{19}{}^2$	+1.703e-05	145	$x'_{25}\ x'_{28}$	-3.662e-05
131	$x'_{19}\ x'_{21}$	+1.655e-04	146	$x'_{25}\ x'_{29}$	+5.488e-04
132	$x'_{19}\ x'_{25}$	-2.663e-04	147	$x'_{26}{}^2$	-1.055e-04
133	$x'_{20}{}^2$	+5.160e-06	148	$x'_{27}{}^2$	-4.229e-04
134	$x'_{20}\ x'_{21}$	+2.961e-04	149	$x'_{28}{}^2$	-1.895e-04
135	$x'_{20}\ x'_{25}$	-1.421e-04	150	$x'_{29}{}^2$	-1.604e-04

Table C.5: Leading edge thrust term (C_T/C_L^2) RS model scaling factors.

Variable	a	b	Variable	a	b
x_1	+3.969e+00	+7.485	x_{16}	+5.831e+01	+8.265
x_2	+4.381e+00	+5.000	x_{17}	+2.006e+01	+5.004
x_3	+1.228e+00	+5.000	x_{18}	+4.477e+00	+5.000
x_4	+4.033e+00	+6.595	x_{19}	+9.394e+00	+4.999
x_5	+2.336e+00	+3.285	x_{20}	+2.675e+00	+5.000
x_6	+3.416e+00	+5.000	x_{21}	+9.359e+00	+5.000
x_7	+5.432e+00	+4.999	x_{22}	+3.442e+00	+3.750
x_8	+5.953e-01	+4.901	x_{23}	+1.249e+00	+3.834
x_9	+9.776e-01	+5.000	x_{24}	+8.706e-01	+3.855
x_{10}	+1.577e+00	+3.778	x_{25}	+1.147e+00	+6.361
x_{11}	+1.614e+00	+4.459	x_{26}	+1.317e+01	+5.000
x_{12}	+2.590e+00	+4.907	x_{27}	+5.428e-01	+5.000
x_{13}	+2.383e+00	+4.576	x_{28}	+5.068e-01	+5.000
x_{14}	+1.594e+02	+4.331	x_{29}	+7.653e-01	+4.260
x_{15}	+2.162e+01	+1.806			

Table C.6: Leading edge thrust term (C_T/C_L^2) RS model coefficient values.

Index	Basis Function	Coefficient	Index	Basis Function	Coefficient
1	*constant*	+5.628e-02	21	$x'_2\ x'_{25}$	+8.765e-04
2	x'_1	-4.277e-04	22	${x'_3}^2$	-3.320e-03
3	x'_2	+5.713e-02	23	$x'_3\ x'_4$	+8.524e-03
4	x'_3	-2.950e-02	24	$x'_3\ x'_6$	+2.460e-03
5	x'_4	-7.022e-03	25	$x'_3\ x'_7$	+9.488e-04
6	x'_6	-8.463e-03	26	$x'_3\ x'_8$	+2.313e-03
7	x'_7	-9.097e-04	27	$x'_3\ x'_{25}$	+3.409e-03
8	x'_8	-6.261e-03	28	${x'_4}^2$	+3.574e-03
9	x'_{15}	-1.160e-03	29	$x'_4\ x'_5$	-1.006e-03
10	x'_{24}	-7.516e-04	30	$x'_4\ x'_6$	+4.393e-03
11	${x'_1}^2$	+5.290e-04	31	$x'_4\ x'_8$	-2.327e-03
12	$x'_1\ x'_2$	+7.146e-04	32	$x'_4\ x'_{15}$	+4.191e-03
13	$x'_1\ x'_3$	+4.581e-04	33	$x'_4\ x'_{24}$	+2.238e-03
14	${x'_2}^2$	+8.312e-03	34	${x'_6}^2$	+2.728e-04
15	$x'_2\ x'_4$	-1.977e-02	35	$x'_6\ x'_8$	-2.743e-03
16	$x'_2\ x'_6$	-8.511e-03	36	$x'_7\ x'_8$	-1.009e-03
17	$x'_2\ x'_7$	-9.103e-04	37	${x'_8}^2$	-3.764e-03
18	$x'_2\ x'_8$	-2.049e-03	38	$x'_8\ x'_{14}$	-1.197e-03
19	$x'_2\ x'_{11}$	+1.116e-03	39	$x'_8\ x'_{25}$	+1.490e-03
20	$x'_2\ x'_{24}$	-2.130e-03	40	$x'_8\ x'_{27}$	-6.705e-04

Table C.7: Wave drag coefficient ($C_{D_{wave}}$) RS model scaling factors.

Variable	a	b	Variable	a	b
x_1	+3.969e+00	+7.485	x_{16}	+5.831e+01	+8.265
x_2	+4.381e+00	+5.000	x_{17}	+2.006e+01	+5.004
x_3	+1.228e+00	+5.000	x_{18}	+4.477e+00	+5.000
x_4	+4.033e+00	+6.595	x_{19}	+9.394e+00	+4.999
x_5	+2.336e+00	+3.285	x_{20}	+2.675e+00	+5.000
x_6	+3.416e+00	+5.000	x_{21}	+9.359e+00	+5.000
x_7	+5.432e+00	+4.999	x_{22}	+3.442e+00	+3.750
x_8	+5.953e-01	+4.901	x_{23}	+1.249e+00	+3.834
x_9	+9.776e-01	+5.000	x_{24}	+8.706e-01	+3.855
x_{10}	+1.577e+00	+3.778	x_{25}	+1.147e+00	+6.361
x_{11}	+1.614e+00	+4.459	x_{26}	+1.317e+01	+5.000
x_{12}	+2.590e+00	+4.907	x_{27}	+5.428e-01	+5.000
x_{13}	+2.383e+00	+4.576	x_{28}	+5.068e-01	+5.000
x_{14}	+1.594e+02	+4.331	x_{29}	+7.653e-01	+4.260
x_{15}	+2.162e+01	+1.806			

Table C.8: Wave drag coefficient ($C_{D_{wave}}$) RS model coefficient values.

Index	Basis Function	Coefficient	Index	Basis Function	Coefficient
1	*constant*	+1.530e-03	31	$x'_2\ x'_{10}$	-1.240e-05
2	x'_2	+4.881e-05	32	$x'_2\ x'_{11}$	-2.762e-05
3	x'_3	+1.058e-04	33	$x'_2\ x'_{12}$	-3.361e-05
4	x'_5	+9.926e-05	34	$x'_2\ x'_{18}$	-2.725e-05
5	x'_9	+1.005e-04	35	$x'_2\ x'_{19}$	-3.984e-05
6	x'_{11}	+2.801e-04	36	$x'_2\ x'_{20}$	+1.120e-05
7	x'_{14}	-3.935e-06	37	$x'_2\ x'_{27}$	+8.763e-06
8	x'_{18}	-1.077e-04	38	${x'_3}^2$	+5.482e-05
9	x'_{19}	-3.382e-05	39	$x'_3\ x'_4$	-9.907e-06
10	x'_{21}	-1.405e-05	40	$x'_3\ x'_6$	+1.990e-05
11	x'_{25}	-4.630e-06	41	$x'_3\ x'_7$	-2.302e-05
12	x'_{27}	+9.137e-06	42	$x'_3\ x'_8$	-1.042e-05
13	${x'_1}^2$	+3.747e-05	43	$x'_3\ x'_9$	-8.882e-05
14	$x'_1\ x'_2$	-3.211e-05	44	$x'_3\ x'_{11}$	+1.287e-04
15	$x'_1\ x'_3$	+9.111e-05	45	$x'_3\ x'_{21}$	+2.501e-05
16	$x'_1\ x'_4$	+5.490e-04	46	$x'_3\ x'_{22}$	+6.317e-06
17	$x'_1\ x'_5$	+2.925e-04	47	$x'_3\ x'_{23}$	-2.849e-05
18	$x'_1\ x'_6$	+5.643e-05	48	${x'_4}^2$	+1.215e-04
19	$x'_1\ x'_8$	+6.035e-05	49	$x'_4\ x'_6$	-8.155e-06
20	$x'_1\ x'_9$	-3.205e-05	50	$x'_4\ x'_7$	+1.186e-05
21	$x'_1\ x'_{11}$	+6.335e-05	51	$x'_4\ x'_9$	-1.764e-05
22	$x'_1\ x'_{21}$	+3.353e-05	52	$x'_4\ x'_{11}$	-3.316e-05
23	$x'_1\ x'_{28}$	-2.943e-06	53	$x'_4\ x'_{12}$	+1.853e-04
24	$x'_1\ x'_{29}$	-2.303e-05	54	$x'_4\ x'_{13}$	+4.991e-05
25	${x'_2}^2$	+8.431e-05	55	$x'_4\ x'_{14}$	+2.188e-05
26	$x'_2\ x'_3$	-1.199e-04	56	$x'_4\ x'_{16}$	-4.187e-06
27	$x'_2\ x'_4$	-8.768e-05	57	$x'_4\ x'_{18}$	+2.670e-05
28	$x'_2\ x'_6$	-5.470e-05	58	$x'_4\ x'_{19}$	-1.378e-05
29	$x'_2\ x'_8$	+1.771e-05	59	$x'_4\ x'_{20}$	-6.012e-05
30	$x'_2\ x'_9$	+1.218e-04	60	$x'_4\ x'_{22}$	+1.186e-05

Table C.9: Wave drag coefficient ($C_{D_{wave}}$) RS model coefficient values (contd.).

Index	Basis Function	Coefficient	Index	Basis Function	Coefficient
61	$x'_4\ x'_{23}$	-1.753e-05	91	$x'_9\ x'_{19}$	-8.206e-05
62	$x'_4\ x'_{28}$	-6.760e-06	92	$x'_9\ x'_{20}$	+3.548e-05
63	$x'_4\ x'_{29}$	-4.776e-05	93	$x'_{10}\ x'_{14}$	-2.935e-06
64	$x'_5\ x'_7$	+7.212e-06	94	$x'_{10}\ x'_{15}$	+5.466e-06
65	$x'_5\ x'_{14}$	-1.238e-06	95	$x'_{10}\ x'_{20}$	+1.797e-05
66	$x'_5\ x'_{15}$	-5.824e-06	96	$x'_{10}\ x'_{23}$	-1.660e-05
67	$x'_5\ x'_{23}$	-1.378e-06	97	${x'_{11}}^2$	+4.342e-05
68	${x'_6}^2$	+1.535e-05	98	$x'_{11}\ x'_{12}$	+4.861e-05
69	$x'_6\ x'_8$	+6.542e-05	99	$x'_{11}\ x'_{16}$	+2.789e-06
70	$x'_6\ x'_9$	-2.112e-05	100	$x'_{11}\ x'_{19}$	+3.601e-05
71	$x'_6\ x'_{12}$	+1.338e-05	101	$x'_{11}\ x'_{20}$	+2.260e-05
72	$x'_6\ x'_{14}$	+2.094e-05	102	$x'_{11}\ x'_{21}$	+6.588e-05
73	$x'_6\ x'_{19}$	+4.047e-05	103	$x'_{11}\ x'_{24}$	-1.787e-05
74	$x'_6\ x'_{20}$	-1.965e-05	104	$x'_{11}\ x'_{29}$	-2.224e-05
75	$x'_6\ x'_{21}$	-1.829e-05	105	${x'_{12}}^2$	+1.499e-05
76	$x'_7\ x'_9$	-1.647e-05	106	$x'_{12}\ x'_{14}$	-5.281e-05
77	$x'_7\ x'_{13}$	+1.732e-05	107	$x'_{12}\ x'_{24}$	+6.435e-05
78	$x'_7\ x'_{14}$	+2.272e-06	108	$x'_{13}\ x'_{24}$	-1.154e-05
79	$x'_7\ x'_{28}$	+9.067e-06	109	$x'_{14}\ x'_{24}$	+2.478e-06
80	${x'_8}^2$	+4.334e-05	110	$x'_{14}\ x'_{28}$	-5.298e-06
81	$x'_8\ x'_9$	-2.450e-05	111	$x'_{15}\ x'_{20}$	-1.257e-04
82	$x'_8\ x'_{11}$	-4.783e-05	112	${x'_{16}}^2$	-5.045e-06
83	$x'_8\ x'_{12}$	+1.219e-05	113	$x'_{16}\ x'_{17}$	-3.340e-05
84	$x'_8\ x'_{14}$	+4.054e-05	114	$x'_{16}\ x'_{20}$	-1.084e-05
85	$x'_8\ x'_{18}$	+2.160e-05	115	${x'_{17}}^2$	+2.272e-05
86	$x'_8\ x'_{19}$	+2.356e-05	116	$x'_{17}\ x'_{20}$	-1.354e-05
87	$x'_8\ x'_{28}$	-1.836e-05	117	$x'_{17}\ x'_{21}$	+2.598e-05
88	${x'_9}^2$	+1.999e-04	118	${x'_{18}}^2$	+4.332e-05
89	$x'_9\ x'_{11}$	-2.875e-05	119	$x'_{18}\ x'_{19}$	+1.237e-04
90	$x'_9\ x'_{18}$	-2.167e-05	120	$x'_{18}\ x'_{20}$	-1.665e-05

Table C.10: Wave drag coefficient ($C_{D_{wave}}$) RS model coefficient values (contd.).

Index	Basis Function	Coefficient	Index	Basis Function	Coefficient
121	$x'_{18}\ x'_{21}$	+3.563e-05	131	$x'_{21}\ x'_{28}$	+1.219e-05
122	$x'_{18}\ x'_{22}$	-2.469e-05	132	${x'_{22}}^2$	-8.178e-06
123	${x'_{19}}^2$	+1.027e-04	133	$x'_{22}\ x'_{23}$	-9.549e-06
124	$x'_{19}\ x'_{20}$	-1.711e-05	134	$x'_{22}\ x'_{28}$	+1.282e-05
125	$x'_{19}\ x'_{21}$	+1.150e-04	135	${x'_{23}}^2$	+1.347e-05
126	$x'_{19}\ x'_{28}$	+1.358e-05	136	$x'_{23}\ x'_{24}$	-3.692e-06
127	${x'_{20}}^2$	+3.942e-05	137	$x'_{23}\ x'_{28}$	-2.179e-05
128	$x'_{20}\ x'_{21}$	-1.084e-04	138	${x'_{24}}^2$	-5.462e-06
129	$x'_{20}\ x'_{25}$	-2.238e-05	139	$x'_{24}\ x'_{25}$	+4.878e-06
130	${x'_{21}}^2$	+1.074e-04	140	${x'_{29}}^2$	-3.389e-06

Table C.11: Lift curve slope (C_{L_α}) RS model scaling factors.

Variable	a	b	Variable	a	b
x_1	+3.969e+00	+7.485	x_{16}	+5.831e+01	+8.265
x_2	+4.381e+00	+5.000	x_{17}	+2.006e+01	+5.004
x_3	+1.228e+00	+5.000	x_{18}	+4.477e+00	+5.000
x_4	+4.033e+00	+6.595	x_{19}	+9.394e+00	+4.999
x_5	+2.336e+00	+3.285	x_{20}	+2.675e+00	+5.000
x_6	+3.416e+00	+5.000	x_{21}	+9.359e+00	+5.000
x_7	+5.432e+00	+4.999	x_{22}	+3.442e+00	+3.750
x_8	+5.953e-01	+4.901	x_{23}	+1.249e+00	+3.834
x_9	+9.776e-01	+5.000	x_{24}	+8.706e-01	+3.855
x_{10}	+1.577e+00	+3.778	x_{25}	+1.147e+00	+6.361
x_{11}	+1.614e+00	+4.459	x_{26}	+1.317e+01	+5.000
x_{12}	+2.590e+00	+4.907	x_{27}	+5.428e-01	+5.000
x_{13}	+2.383e+00	+4.576	x_{28}	+5.068e-01	+5.000
x_{14}	+1.594e+02	+4.331	x_{29}	+7.653e-01	+4.260
x_{15}	+2.162e+01	+1.806			

Table C.12: Lift curve slope (C_{L_α}) RS model coefficient values.

Index	Basis Function	Coefficient	Index	Basis Function	Coefficient
1	*constant*	+1.643e+00	26	$x'_3\ x'_6$	+2.691e-03
2	x'_1	-4.186e-02	27	$x'_3\ x'_8$	+1.424e-03
3	x'_2	-1.165e-01	28	$x'_3\ x'_{11}$	-2.393e-03
4	x'_3	+6.628e-02	29	$x'_3\ x'_{12}$	-9.335e-04
5	x'_4	+2.104e-02	30	$x'_3\ x'_{16}$	-1.394e-03
6	x'_6	+6.517e-02	31	$x'_3\ x'_{24}$	-5.149e-03
7	x'_7	+5.611e-03	32	$x'_3\ x'_{25}$	-4.932e-03
8	x'_8	+1.823e-02	33	${x'_4}^2$	-1.695e-02
9	x'_{25}	-1.331e-03	34	$x'_4\ x'_6$	-2.686e-02
10	${x'_1}^2$	-5.821e-03	35	$x'_4\ x'_7$	-2.180e-03
11	$x'_1\ x'_2$	-5.766e-03	36	$x'_4\ x'_8$	+2.531e-02
12	$x'_1\ x'_3$	-3.054e-03	37	$x'_4\ x'_{25}$	+3.745e-03
13	$x'_1\ x'_4$	+1.742e-02	38	${x'_5}^2$	+1.995e-03
14	$x'_1\ x'_5$	-8.253e-04	39	${x'_6}^2$	+8.477e-03
15	$x'_1\ x'_7$	+1.001e-03	40	$x'_6\ x'_7$	+1.986e-03
16	$x'_1\ x'_8$	+1.231e-03	41	$x'_6\ x'_8$	+7.309e-03
17	${x'_2}^2$	-3.643e-02	42	$x'_6\ x'_{14}$	-2.323e-03
18	$x'_2\ x'_3$	+3.974e-02	43	$x'_6\ x'_{24}$	+2.391e-03
19	$x'_2\ x'_4$	+4.454e-02	44	$x'_6\ x'_{27}$	-2.061e-03
20	$x'_2\ x'_6$	+1.753e-02	45	${x'_8}^2$	-1.207e-02
21	$x'_2\ x'_8$	-1.163e-02	46	$x'_8\ x'_{13}$	-8.591e-06
22	$x'_2\ x'_{25}$	+2.574e-03	47	$x'_8\ x'_{14}$	+3.322e-03
23	${x'_3}^2$	-8.451e-03	48	$x'_8\ x'_{25}$	+2.521e-03
24	$x'_3\ x'_4$	-2.825e-02	49	$x'_8\ x'_{27}$	+2.282e-03
25	$x'_3\ x'_5$	-4.695e-03	50	${x'_{10}}^2$	-3.102e-04

Vita

Oleg Golovidov was born on August 7th, 1971 in Stepnogorsk, Kazakhstan (former USSR). He entered Moscow Aviation Institute in September, 1987 and graduated in April, 1995, Cum Laude with the Engineer of Aircraft Design degree. He entered the graduate program at Virginia Polytechnic Institute and State University, department of Aerospace and Ocean Engineering in August, 1995. He completed his Master of Science in Aerospace Engineering degree in June, 1997 and began a career with the Engineous Software Inc.